Coordination Chemistry Reviews, 13 (1974) 173–278

THE DETERMINATION OF STRUCTURAL PROPERTIES OF DIMERIC TRANSITION METAL ION COMPLEXES FROM EPR SPECTRA

T.D. SMITH

Chemistry Department, Monash University, Clayton, Victoria, 3168 (Australia)

and

J.R. PILBROW

Physics Department, Monash University, Clayton, Victoria, 3168 (Australia)

(Received July 9th, 1973)

CONTENTS

A. Introduction 174
B. General interaction between pairs of spin ½ ions 177
(i) The interaction tensor 177
(ii) The dipole-dipole interaction 179
(iii) Spin Hamiltonian in the Zeeman representation 183
C. Similar ion dimers 185
(i) Perturbation theory 185
(a) Introduction 185
(b) $|J| \leq 30$ cm^{-1} 186
(c) The effect of the magnitude of $|J|$ 192
(d) Triplet case in terms of D and E 195
(e) Results for axial dimers 196
(f) Computer simulation of spectra 197
(g) Reliability of simulated spectra 199
(h) The effect of dimer symmetry on EPR spectra 200
(ii) Computer diagonalisation procedure when exchange coupling is strong 205
(a) Introduction 205
(b) Solution of the spin Hamiltonian 207
D. Dissimilar ions 212
(i) Introduction 212
(ii) Dissimilar ion dimers represented by coordinates of ion 1 213
(iii) Dissimilar ion dimers represented by separate spin quantisation for ions 1 and 2 214
(iv) Computer simulation using the results in Section D (iii) 216
E. Identification and interpretation of dimer spectra 219
F. Copper(II) and vanadyl complexes of known structure 220
G. Copper(II) and vanadyl porphyrins and phthalocyanines 228
(i) Porphyrins 228
(ii) Phthalocyanines 230

H. Hydroxycarboxylic acid chelates 232
I. Aminopolycarboxylic acid chelates 242
J. Amine, amino acid and peptide chelates 244
K. Chelates of thio ligands 257
L. Copper(II) in natural products 264
M. Dimeric chelates with significant exchange 265
Acknowledgements 266
Appendix 266
References 274

A. INTRODUCTION

The occurrence of metal ion dimer units in many inorganic compounds is a well-known phenomenon[1-7]. X-ray crystallographic studies on a variety of metal ion compounds have indicated some of the possible packing arrangements[8-18]. Magnetic susceptibility measurements, particularly on copper(II) compounds, showed a large number of examples where the paramagnetic ions were antiferromagnetically coupled[1]. In fact, before about 1965, it is hard to find any reports which indicate exchange interactions smaller than about 100K! But in view of the fact that most of these susceptibility measurements were carried out only down to 77°K, this apparently large exchange coupling phenomenon is not particularly surprising. To establish the occurrence of exchange coupling of ~30K or smaller has necessitated measurements at helium temperatures[18-36].

There is a good deal of interest in studies of complexing in solution and some of the interest lies in studies of dimers. On the whole, electron paramagnetic resonance (EPR) studies, even of frozen solutions of a wide range of copper(II) systems, do not show any evidence of pair formation, though EPR triplet spectra had been observed in a number of copper compounds as long ago as 1952 when Bleaney and Bowers published their classic work on copper(II) acetate[37]; see also refs. 6, 7.

The major thrust of the work to be reviewed herein is the identification and interpretation of EPR spectra due to copper(II), vanadyl and titanium(III) dimers, in just those situations which could not have been recognised on the basis of magnetic susceptibility or even X-ray studies on their own. Of particular interest are cases in which exchange coupling is small ($\lesssim 30$ cm^{-1}) and where the dominant interaction which brings about the characteristic shape of the EPR dimer spectra is dipole–dipole in origin[18,38-65]. For a copper(II) – copper(II) separation of ~2.6 Å, which represents the minimum value likely, the zero field splitting parameter $D \sim 0.2$ cm^{-1} is the maximum one should expect, very much smaller than the exchange coupling determined from magnetic susceptibility measurements.

Previous reviews of paramagnetic dimers discussing copper(II) compounds have concentrated on mechanisms of exchange coupling between the metal ions in single crystal and powder samples mostly with reference to magnetic susceptibility results

and to a lesser extent EPR[1-7]. The purpose of this review is to concentrate particularly on the newer phenomenon, dipole–dipole coupled dimers of spin-½ ion pairs of copper(II), vanadyl and titanium(III). Results reviewed cover powders of isomorphous diamagnetic compounds doped with small amounts of the appropriate paramagnetisation, or frozen solutions. Theoretical developments thus far have been confined to pairs of spin-½ ions, and the theory is presented in some detail, including some more general results not previously published. It will be seen that the authors' approach leans heavily upon the ability to produce computer-simulated EPR dimer spectra, which may then be compared with the appropriate experimental results. When the dipole–dipole coupling dominates the zero field splitting of the energy levels, one may determine the metal ion–metal ion separation from the EPR data[18-36,37-65]. The value of this piece of information from the point of view of structure needs hardly to be emphasised! More than this, in certain ideal cases where the structure is known, it is possible to obtain significant confirmation of the dipole–dipole dimer model[60]. When, however, exchange coupling is significant, account is taken of the pseudo-dipolar terms arising from exchange and spin–orbit coupling which then may dominate the zero-field splitting within the states[46]. In the latter situation, it is impossible to deduce the metal ion separation reliably.

For interacting pairs of spin-½ ions, the problem is a variation on the well-known singlet–triplet phenomenon found in other branches of physics and chemistry. Perhaps one of the best known areas of EPR in which singlet–triplet states are found is in the field of free radicals. Through the work particularly of van der Waals and de Groot[66,67], Kottis and Lefebvre[68,69] and Wasserman et al.[70], a great deal of progress has been made in the interpretation of EPR triplet spectra. In fact some of the work on copper(II) and vanadyl dimer compounds has been interpreted using results for what is a simpler free radical case[18-22,24,25,27,36,61,65]. The major objection to this approach for metal ion dimers is that they do not have such sharp powder (or frozen solution) lines in their EPR spectra as do the free radicals. Also there is considerable g anisotropy, particularly for copper(II), and large and very anisotropic hyperfine interactions for both copper(II) and vanadyl systems. It is the authors' view that by far the most helpful and satisfactory way to proceed with an analysis and interpretation of the EPR spectra of these systems is to simulate the spectra by computer, using an appropriate symmetry model. Only then, when all features of the spectra have been accounted for, may one begin to draw conclusions about the structural details of the dimer.

There is an even more important consideration which makes computer simulation methods even more appropriate. The presence of dipolar and hyperfine terms mix the "singlet" and "triplet" states so that the states are, therefore, no longer "pure" singlet–triplet in character, unless, of course, there is appreciable exchange. Thus, in general, "singlet"–"triplet" transitions must be allowed for*[71-74].

* We will continue to use the terms singlet and triplet as it will be clear from the context what is meant.

When exchange coupling is sufficiently weak that pseudo-dipolar terms can be neglected, and the zero-field splitting within the "triplet" is due to the dipole–dipole interaction alone, we can satisfactorily account for experimental results by means of a perturbation theory analysis. Computer diagonalisation methods as a means of producing computer-simulated curves are out of the question when hyperfine interactions are important, as in copper(II) and vanadyl systems, in view of the large matrices involved (64 × 64 for copper(II), 256 × 256 for vanadyl pairs). However, the computer diagonalisation approach is appropriate for titanium(III) axial dimers, and also for copper(II) when there is large exchange coupling and no resolved hyperfine structure. Until quite recently, detailed theoretical models were mostly based upon an axial dimer model, partly in the interests of simplicity[38,39,52,53,56]. However, crystallographic studies of dimeric metal chelates, for example, clearly indicated that other symmetry arrangements of the paramagnetic ion pairs do in fact occur[8–18]. Also, stereochemical requirements of certain ligands suggest that low symmetry dimers ought to be quite common. With this in mind, recent work has been directed towards an examination of the effect of symmetry on the magnetic interactions within dimers, as a means of arriving at a more satisfactory interpretation of EPR data[60a,99]. Recently, Hatfield and Lund[60b] have carried out similar calculations based on a complementary approach to the problem. In certain ideal cases, it has been the aim to compare structural conclusions based on EPR results with those from X-ray data.

Most of the attention in this field has been given to copper(II) dimer systems consisting of pairs of identical (similar) ions; however, dimers consisting of dissimilar ion pairs have received spasmodic attention from the earliest days of EPR until the present[75–79]. In Section B we shall be concerned with the form of the interaction between metal ion pairs with spin ½, as well as details of the Zeeman and hyperfine interactions of the ions. The problems associated with the choice of a suitable basis for the use of perturbation theory are also discussed. Section C is in two parts and deals with the theory of similar ion dimers. The first part gives the derivation of the perturbation theory applicable to weakly exchange-coupled dimers and for which the dominant interactions producing the characteristic EPR spectra are due to dipolar coupling alone. In the second part the method of attack in strongly exchange coupled systems is outlined, based on the computer diagonalisation of the triplet state energy matrix. In Section D the theory of the EPR due to dissimilar spin ½ ion pairs is outlined, perturbation theory being applicable only when $J = 0$, except perhaps for certain simple cases and then only along principal axes of the Zeeman and dipolar tensors. Dissimilar ion dimers can arise in several ways. They will occur whenever two similar ions have sites with non-parallel principal axes (e.g. planar configurations in which the two planes are non-parallel), but also when two different ions occupy similar or different sites in close proximity irrespective of whether or not their axes are parallel. Abragam and Bleaney have given an excellent and lucid discussion of the basic physics of the situation for a simple example[79]. A related problem of a spin-

label in the neighbourhood of a paramagnetic metal ion has been discussed from a relaxation point of view by Leigh[80]. In Section E we consider the experimental criteria used in analysing spectra due to dimers before presenting a review of the results for different chemical systems in Sections F and following.

B. GENERAL INTERACTION BETWEEN PAIRS OF SPIN ½ IONS

(i) The interaction tensor

It is well-known that most $3d$ transition metal ion coordination compounds have approximately spin-only magnetism. The orbital magnetic moment is said to be quenched by the ligand field, and the resulting angular momentum of the ground state, called the effective spin, turns out to be the same as the true spin angular momentum for d^1, d^3, d^5 and d^9 configurations. However, the consequence of a small amount of mixing to excited energy levels by the spin–orbit coupling causes the ground state g values to deviate from the free electron value of 2.0023. In the case of $3d^1$ and $3d^9$ configurations, which are the subject of discussion in this article, the effective spin is one-half ($S = ½$).

In discussing the interpretation of EPR spectra due to dimer or binuclear complexes of spin one-half ions, we shall be concerned with the "magnetic" interactions such as exchange, dipole–dipole or pseudo-dipolar but *not* with the forces which actually bind the molecules together. Dimer molecules are held together in practice by a variety of forces, e.g. electric dipole forces in asymmetric porphyrins. Further discussion of the chemical binding occurs in sections F–M. Binding energies will always be very large compared with the magnetic interaction when it is realised that exchange lies in the range $0 - 300$ cm^{-1} in typical cases and the dipole–dipole interaction may be as large as 0.2 cm^{-1}, as in copper acetate[60a]. However, it is the "magnetic" interactions which couple the energy levels of the metal ion pairs in the dimer or binuclear complexes, that determine the detailed nature of the EPR spectra. It is the purpose of this paper to describe these relevant features, as well as to show how to develop appropriate theoretical models to describe the magnetic properties of such systems. In particular we shall be concerned to show not only how one simulates spectra by computer, but to make specific comparisons between experiment and theory to illustrate the general validity of this approach.

We now discuss the various "magnetic" couplings between pairs of paramagnetic ions in dimer molecules as are appropriate for d^1 and d^9 systems. The best known and most widely popular interaction is the isotropic exchange. This arises through the combined effect of the electrostatic repulsion of the electrons (e^2/r_{12}) and the Pauli exclusion principle. It has the effect of coupling the states to give a singlet and triplet. Since the individual ions have spins of one-half, ($S_1 = S_2 = ½$) it can be shown that exchange may be represented very conveniently by the expression

$$\mathcal{H}_{ex} = -J\,\mathbf{S}_1 \cdot \mathbf{S}_2 \tag{1a}$$

The convention regarding the sign in eq. (1a) is arbitrary and unfortunately many authors use one or more of the alternative conventions $\pm 2J$ or $+J$ in writing down the exchange interaction. Because eqn. (1a) is of the form $\mathbf{S}_1 \cdot \mathbf{S}_2$, which is just the vector scalar product of the two spin vector operators $\mathbf{S}_1$ and $\mathbf{S}_2$, isotropic exchange is frequently described as a scalar coupling. It can easily be shown that singlet and triplet energy levels differ in energy by an amount J. The singlet is lowest when J is negative (antiferromagnetic) while the triplet is lowest in energy when J is positive (ferromagnetic).

In passing note that antiferromagnetic coupling is usually the case for copper dimers[1-7]; however, Hatfield and co-workers have reported triplet ground states in a number of cases[19-22,24,27,28,34,35]. The bulk of the results so far published[1], based upon magnetic susceptibility measurements down to 77°K, have yielded large values of $J \sim -300\ \mathrm{cm}^{-1}$. The studies by Hatfield and co-workers suggest that there are many cases where $|J| \lesssim 30\ \mathrm{cm}^{-1}$. It is the view of the present authors that indeed there are significant numbers of cases where $|J| \simeq 0$.

A magnetic interaction between pairs of paramagnetic ions which will always be present is the familiar dipole–dipole interaction.

$$\mathcal{H}_{dip} = \frac{\boldsymbol{\mu}_1 \cdot \boldsymbol{\mu}_2}{r^3} - \frac{3(\boldsymbol{\mu}_1 \cdot \mathbf{r})(\boldsymbol{\mu}_2 \cdot \mathbf{r})}{r^5} \tag{1b}$$

where $\boldsymbol{\mu}_1$ and $\boldsymbol{\mu}_2$ are the magnetic dipole moments of the two interacting ions 1 and 2 and r the internuclear separation of the ions. This interaction will be examined in more detail in Section B(ii) but we note that it can be re-expressed in terms of the spins $\mathbf{S}_1$ and $\mathbf{S}_2$ and written in the form of a second-rank tensor interaction.

$$\mathcal{H}_T = \mathbf{S}_1 \cdot \mathbf{J} \cdot \mathbf{S}_2 \tag{1c}$$

The coupling tensor, $\mathbf{J}$, has nine components in general and is not necessarily symmetric.

As explained originally by Bleaney and Bowers[37], the combined effect of spin–orbit coupling and isotropic exchange on the assembly of ground and excited energy levels of the two interacting ions can lead to an additional contribution to the interaction energy. This is variously called anisotropic exchange or pseudo-dipolar coupling[60a]. Actually anisotropic exchange as defined by Erdos[81] includes both pseudo-dipolar and dipolar coupling[82,83]. The pseudo-dipolar coupling as introduced by Bleaney and Bowers[37] has precisely the same form as ordinary dipolar coupling and is further discussed in Section C(ii) (a).

It has previously been pointed out by the authors and their colleagues that pseudo-dipolar coupling can be neglected when $|J| \lesssim 30\ \mathrm{cm}^{-1}$ or thereabouts. The effective upper limit on $|J|$ is not known for certain, largely because of the predictive unreliability of theories of pseudo-dipolar coupling[37,84,85].

In the most general situation, in which the dimer does not possess inversion symmetry, the tensor J will be asymmetric and the expression (1c) may be re-written as the sum of two terms

$$\mathcal{H}_T = \mathbf{S}_1 \cdot \mathbf{J}_s \cdot \mathbf{S}_2 + J_a \mathbf{S}_1 \times \mathbf{S}_2 \tag{1d}$$

where $\mathbf{J}_s$ is the symmetric part of tensor J and $J_a \mathbf{S}_1 \times \mathbf{S}_2$ represents the skew symmetric or so-called asymmetric exchange[81]. Asymmetric exchange involves the vector cross product of the spin vector operators $\mathbf{S}_1$ and $\mathbf{S}_2$, and will have a contribution from the ordinary magnetic dipole–dipole term.

To summarise, the interaction Hamiltonian is written as

$$\mathcal{H}_{int} = \mathcal{H}_{ex} + \mathcal{H}_T = -J\,\mathbf{S}_1 \cdot \mathbf{S}_2 + \mathbf{S}_1 \cdot \mathbf{J} \cdot \mathbf{S}_2 \tag{2}$$

(ii) The dipole–dipole interaction

We now consider what is generally the most important of the interactions for the interpretation of the EPR of a wide range of dimers observed in powders and frozen solutions, viz. the dipole–dipole term.

For ions which possess orbital, as well as spin, angular momentum, higher order multipole contributions to the interaction, eq. (1b), may be required. The examples discussed herein are all from the iron group, where the orbital moment is quenched, there being relatively small *g*-shifts from 2.0023 due to spin–orbit coupling. As pointed out by Abragam and Bleaney[86], the general interactions between such ions can always be expressed as a multipole expansion, of which eqn. (1b) is the leading term. The next highest term varies as r^{-5} and it will be neglected in what follows. High order terms may sometimes, however, be important and measureable in the case of rare earth ions[87].

The point dipole approach may conceivably break down when there is significant overlap of the electron distributions of the two ions, e.g. when $r \lesssim 3$ Å, or when there is considerable delocalisation of the unpaired electron density onto the ligands. Since eqn. (1b) is part of a multipole expansion based on the static internuclear separation of the metal ions, the value of r deduced from EPR results should be the true internuclear separation. As already indicated, one's ability to do this is restricted to those cases in which "pseudo"-dipolar terms are negligible. A final justification for the determination of r from EPR data will depend on how well the value agrees with that based on X-ray data when both types of information are, in fact, available.

We digress to describe the principles underlying the subsequent derivations so that it may become clear where the calculations are heading. The first part is to consider the dimer energy levels in a d.c. magnetic field, and to determine where the EPR transitions occur as a function of molecular orientation within the dimer or binuclear complex. The objective is to use the resulting EPR transition field values and intensity information to simulate, by computer, dimer spectra based on suitable

symmetry models for comparison with experimental data, and for the elucidation of structural information on dimer and binuclear complexes. Except for the discussion in Section C(ii), relating to cases with significant pseudo-dipolar interactions, in which the energies, and, therefore, EPR transitions are obtained by computer diagonalisation of the energy matrix, we shall be concerned with those solutions of dimer energy levels and wavefunctions which can be obtained by the logical and straightforward application of the formulae of time-independent, non-degenerate perturbation theory, as can be found in standard texts in quantum mechanics. As always in perturbation theory calculations, one attempts to choose as the basis or starting wavefunctions, those which are as close as possible to being the eigenfunctions of the energy. Using these basic functions, one calculates the matrix elements of the total energy of the dimer. The energy Hamiltonian consists of the interaction of the spins $\mathbf{S}_1$ and $\mathbf{S}_2$ with the magnetic field, $\mathcal{H}_{int}$, as well as the metal-ion hyperfine interaction. The details are described in Section (iii) following, and for dissimilar ion pairs, in Section D.

The interaction between the spins $\mathbf{S}_1$ and $\mathbf{S}_2$ and the magnetic field is the Zeeman interaction and it is assumed that this provides the dominant splitting of the energy levels under ordinary conditions. Thus the Zeeman interaction is taken to be the zero order interaction for the perturbation theory calculation, and therefore the basis states are chosen to be simple products of the Zeeman interaction eigenstates of the two separate ions. For this reason the calculations are said to be carried out in the Zeeman representation. Since $\mathcal{H}_{Zeeman} \simeq 0.3\ cm^{-1}$ at X-band frequencies while $\mathcal{H}_{dip} \simeq 0.13\ cm^{-1}$ when $r = 3$ Å, $\mathcal{H}_{dip}$ is taken to be the perturbation interaction. There is also the nuclear hyperfine interaction in the cases of copper(II) or vanadyl and this, being about $0.01 - 0.02\ cm^{-1}$, is also included in the perturbation operator. The question arises, however, about how isotropic exchange fits into the theory. Interestingly enough, $-J\,\mathbf{S}_1 \cdot \mathbf{S}_2$ can be treated on an equal footing with $\mathcal{H}_{dip}$ for similar ion dimers, in principle, whatever the size of J, though one must add pseudo-dipolar terms when $|J| \gtrsim 30\ cm^{-1}$. There are difficulties in the case of dissimilar ion dimers, as explained in Section D. The general procedure is outlined in Table 1.

It turns out that the dimer energies of the two states of total spin zero (S_1 ↑ and S_2 ↓ and vice versa) are approximately equal in the Zeeman representation. So there is one subtlety, in that part of the energy matrix has to be diagonalised first before proceeding with the perturbation theory treatment. For this reason we talk of the coupled and uncoupled representations later on. The uncoupled representation consists of the simple single ion Zeeman wavefunction products, and the coupled representation takes into account a redefinition of the total spin zero wavefunctions. This point will be made clear in Section C.

Thus it is now necessary to choose a suitable representation for the perturbation calculations, and this is done in the following pages.

We allow for the most general arrangement of the ion pair as in Fig. 1, except that

TABLE 1

Flow diagram for calculations in Section C(i)

Consider dipole–dipole exchange terms for triclinic dimer symmetry

↓

Energy matrix in a magnetic field

↓

Diagonalise part of energy matrix → "singlet", "triplet"

(Ignore least important hyperfine terms at this stage)

↓

Assume Zeeman interaction ≫ dipolar; include *all* hyperfine terms

Calculate energy levels to *second* order, wavefunctions to *first* order in dipolar and hyperfine effects.

↓

Derive transition fields and intensities for $\Delta M_s = 1$ and 2 transitions.

↓

Consider effect of size of J:

$|J| \ll h\nu$ (microwave energy): require all energy levels

$|J| \approx h\nu$: complication discussed

$30\ \text{cm}^{-1} \gtrsim |J| \gg h\nu$: ESR "triplet" problem only

↓

Simulation of theoretical spectra

↓

Comparison of simulated and experimental spectra

↓

Comparison of ESR and X-ray data

we assume the principal axes of **g** and **A** for each ion coincide*. However, the dipolar principal axes do not generally coincide with the **g** and **A** tensors of either ion, except in certain high symmetry limits of the model[88,89]. It is convenient to transform $\mathcal{H}_{\text{dip}}$ into the coordinate frame of ion 1 (the coordinates of ion 2 would do as well!), but first $\boldsymbol{\mu}_1$ and $\boldsymbol{\mu}_2$ must be suitably represented. Thus[90,91] the connection between $\boldsymbol{\mu}_1$ and the components of $\mathbf{S}_1$ in the coordinate frame of ion 1 is written as

$$\boldsymbol{\mu}_1 = \beta \sum_{\alpha = x_1, y_1, z_1} g_{1\alpha} S_{1\alpha} \boldsymbol{\alpha} \qquad (3a)$$

* For low symmetry sites, **g** and **A** principal axes need not necessarily coincide.

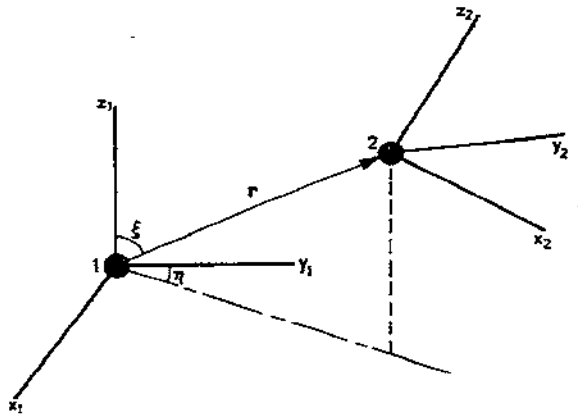

Fig. 1. Orientation of g tensor principal axes and internuclear axis for general low symmetry dimer formed by ions 1 and 2.

where x_1, y_1 and z_1 are the principal axes of $\mathbf{g}_1$ and the $\boldsymbol{\mu}$ are unit vectors along these axes; β is the Bohr magneton. An exactly analogous expression may be written down for $\boldsymbol{\mu}_2$ in the coordinate frame of ion 2. It is a simple matter to show that[90,91] $\boldsymbol{\mu}_2$, expressed in the coordinate frame of ion 1, is given by

$$\boldsymbol{\mu}_2 = \beta \sum_{\substack{\zeta,\gamma=x_1,y_1,z_1 \\ \xi=x_2,y_2,z_2}} d_{\zeta\xi}\, d_{\gamma\xi}\, S_{2\gamma}\, g_{2\xi}\, \boldsymbol{\xi} \tag{3b}$$

where the $d_{\zeta\xi}$ are the direction cosines connecting the ζ axis (z_1, y_1 or z_1) and ξ (x_2, y_2 or z_2). By direct substitution of eqns. (3a) and (3b) into eqn. (1b), we find that

$$\mathcal{H}_{\mathrm{dip}} = \sum_{\alpha,\gamma=x_1,y_1,z_1} J_{\alpha\gamma}\, S_{1\alpha}\, S_{2\gamma} \tag{4}$$

where

$$J_{\alpha\gamma} = g_{1\alpha} \left\{ \sum_{\xi=x_2,y_2,z_2} g_{2\xi}\, d_{\gamma\xi} \left(d_{\alpha\xi} - 3\sigma_\alpha \sum_{\zeta=x_1,y_1,z_1} d_{\zeta\xi}\, \sigma_\zeta\right)\right\} \beta^2/r^3 \tag{5}$$

In eqn. (5), σ_α and σ_ζ are direction cosines of $\mathbf{r}$ with respect to x_1, y_1 and z_1. One immediate deduction from eqn. (5) is that $J_{\alpha\gamma} = J_{\gamma\alpha}$ only when the dimer consists of similar ions[81]. We should say that $\mathbf{J}$ is symmetric only for centrosymmetric dimers, but this can lead to confusion. Strictly, all that is required for $\mathbf{J}$ to be symmetric is that the ion sites be what has been defined to be similar. In a compound, such similar sites will possess inversion symmetry. On the other hand, when considering complexes

in solution, we do not claim that the dimer molecule as a whole necessarily be centrosymmetric, only that the immediate environments of the two ions be similar. This distinction is not just a matter of semantics.

(iii) Spin Hamiltonian in the Zeeman representation

In order to set up the perturbation theory in Sections C and D, the total spin Hamiltonian for the pair of ions is transformed into a representation in which the Zeeman interactions for the individual ions are both diagonal. This is in the Zeeman representation referred to in the previous section. Section C is concerned with similar ion pairs when x_1, y_1 and z_1 and x_2, y_2 and z_2 axes are parallel. The spin Hamiltonian may be written

$$\mathcal{H} = \mathcal{H}_1 + \mathcal{H}_2 + \mathcal{H}_{\text{int}} \tag{6}$$

where

$$\mathcal{H}_i = \sum_{j=x_i,y_i,z_i} (\beta g_j S_{ij} H_j + A_j S_{ij} I_{ij}), \quad i = 1, 2 \tag{7}$$

$\mathcal{H}_1$ and $\mathcal{H}_2$ are the separate spin Hamiltonians of ions 1 and 2 including hyperfine interactions ($\mathcal{H}_{\text{hfi}}$).

Here H_j, A_j and I_{ij} ($j = x_i, y_i, z_i$) are, respectively, the j-components of the applied field, the hyperfine interaction and the nuclear spin respectively of ion i with respect to the x_i, y_i and z_i axes. To avoid unnecessary subscripts we do not use i in g_j, A_j or H_j since the particular ion site is referenced via x_i, y_i or z_i in eqns. (3) and (7). $\mathcal{H}_i$ is now transformed into the representation in which the Zeeman interaction is diagonal for general orientations of the magnetic field. To achieve this one replaces the spin and nuclear spin operator components in eqn. (7) with respect to the x_i, y_i, z_i axes by those in terms of the $'$ and $''$ axes respectively as shown in Fig. 2. Let the direction cosines between the electron spin axes ($'$) and nuclear spin axes ($''$) with x_i, y_i and z_i be $l^i_{p'q}$ and $\lambda^i_{p''q}$ respectively. To arrive at eqn. (8)

$$S_q = \sum l^i_{p'q} S_{ip'} \text{ and } I_q = \sum \lambda^i_{p''q} I_{ip''},$$

where $p' = x'_i, y'_i, z'_i$, $p'' = x''_i, y''_i, z''_i$ and $i = 1, 2$. Then[100],

$$\begin{aligned}\mathcal{H}_i = {} & g_i \beta H S_{iz_i'} + K_i S_{iz_i'} I_{iz_i''} + \tau_{i1} S_{ix_i'} I_{ix_i''} + \tau_{i2} S_{iy_i'} I_{iy_i''} \\ & + \tau_{i3} S_{iy_i'} I_{ix_i''} + \tau_{i4} S_{ix_i'} I_{iz_i''} + \tau_{i5} S_{iy_i'} I_{iz_i''}\end{aligned} \tag{8}$$

Various quantities in eqn. (8) are defined as follows

$$g_i^2 = \sum_{j=x_i,y_i,z_i} g_j^2 \, l_j^2$$

$$K_i^2 g_i^2 = \sum_{j=x_i,y_i,z_i} A_j^2 \, g_j^2 \, l_j^2 \tag{9a}$$

$$\tau_{i1} = g_i A_{z_i} [(\alpha_{x_i}^2 + \alpha_{y_i}^2)/(g_{x_i}^2 l_{x_i}^2 + g_{y_i}^2 l_{y_i}^2)]^{1/2}$$

$$\tau_{i2} = A_{x_i} A_{y_i} [(g_{x_i}^2 l_{x_i}^2 + g_{y_i}^2 l_{y_i}^2)/(\alpha_{x_i}^2 + \alpha_{y_i}^2)]^{1/2}/(K_i g_i)$$

$$\tau_{i3} = \alpha_{x_i} g_{x_i} l_{x_i} g_{y_i} l_{y_i} [A_{y_i}^2 - A_{x_i}^2] / \{ [(\alpha_{x_i}^2 + \alpha_{y_i}^2)(g_{x_i}^2 l_{x_i}^2 + g_{y_i}^2 l_{y_i}^2)]^{1/2} K_i g_i \}$$

$$\tau_{i4} = g_{z_i} l_{z_i} (K_i^2 - A_{z_i}^2)/\{K_i [g_{x_i}^2 l_{x_i}^2 + g_{y_i}^2 l_{y_i}^2]^{1/2}\}$$

$$\tau_{i5} = (A_{y_i}^2 - A_{x_i}^2) g_{x_i} l_{x_i} g_{y_i} l_{y_i} / \{K_i g_i [g_{x_i}^2 l_{x_i}^2 + g_{y_i}^2 l_{y_i}^2]^{1/2}\}$$

$$\alpha_k = A_k g_k l_k / K_i g_i \mid k = x_i, y_i, z_i \tag{9b}$$

In eqn. (9), l_{x_i}, l_{y_i} and l_{z_i} are the direction cosines of **H** with respect to the x_i, y_i and z_i axes.

To achieve the particular results in eqns. (8) and (9) it is necessary to note first of all that the Zeeman interaction reduces to the single form $g_i \beta H S_{iz_i'}$ and we say it is diagonal. This result fixes the orientation of the Oz_i' axis but not the Ox_i' and Oy_i' axes. Therefore we are free for example to set Oy_i' in the $x_i y_i$ plane (see Fig. 2). Similarly, to obtain the terms in k_i in eqns. (8) and (9), only the Oz_i'' axis is specified and the Oy_i'' axis may also be arranged in the $x_i y_i$ plane. Incidentally there is no physical consequence of this arbitrary choice of axes, but the form of eqn. (9b)

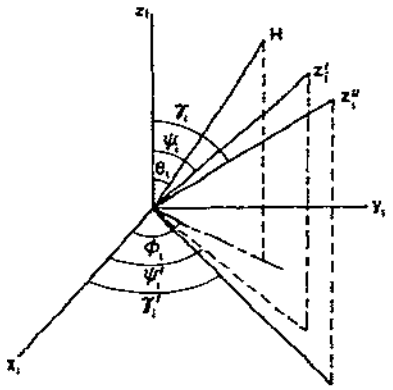

Fig. 2. Orientation of magnetic field (H), electron and nuclear quantisation axes (x_i', y_i', z_i' and x_i'', y_i'', z_i'' respectively, $i = 1, 2$) for ions 1 and 2 in the Zeeman representation. See eqns. (16a) and (16b) for relationships between the angles. In general subscripts 1 and 2 should be used for all angles. For similar ion dimers $\psi_1 = \psi_2 = \psi$ etc.

depends upon it. To obtain the actual form of eqn. (9) in terms of l_{x_i}, l_{y_i} and l_{z_i}, the direction cosines of H with respect to the x_i, y_i, z_i axes, one must exploit the various orthogonality relations between the $l^i_{p'q}$ and also the $\lambda^i_{p''q}$, as well as the conditions which diagonalise the Zeeman term.

In terms of the Zeeman representation of each ion separately,

$$\mathcal{H}_{\text{int}} = \sum_{\substack{p'_1=x'_1,y'_1,z'_1 \\ p'_1=x'_2,y'_2,z'_2}} (D_{p'_1p'_2} + J_{p'_1p'_2})\, S_{1p'_1}\, S_{2p'_2} \tag{10}$$

where

$$D_{p'_1p'_2} = \sum_{\substack{\alpha,\gamma=x_1,y_1,z_1 \\ r=x_2,y_2,z_2}} J_{\alpha\gamma}\, l^1_{\alpha p'_1}\, l^2_{rp'_2}\, d_{\gamma r} \tag{11}$$

and

$$J_{p'_1p'_2} = -J \sum_{\substack{q_1=x_1,y_1,z_1 \\ q_2=x_2,y_2,z_2}} l^1_{q_1p'_1}\, l^2_{q_2p'_2}\, d_{q_1q_2} \tag{12}$$

For similar ions with parallel principal axes, $d_{q_1q_2} = \delta_{q_1q_2}$ and, therefore, $J_{p'_1p'_2} = -J$. But in general, in this particular representation, isotropic exchange behaves as if it were anisotropic. In Section D we discuss the problems raised by this question for dissimilar ion pairs and suggest an alternative formulation of the theory. However, even when that has been done it is found that perturbation theory can only be applied when $J = 0$.

C. SIMILAR ION DIMERS

(i) Perturbation theory

(a) Introduction

Perturbation theory solutions to eqn. (6) will be developed subject to the restrictions $\mathcal{H}_i$ (Zeeman) $\gg \mathcal{H}_{\text{dip}}$ when $|J| \lesssim 30\ \text{cm}^{-1}$. It may seem surprising that J can be considerably larger than $\mathcal{H}_{\text{dip}}$ or $\mathcal{H}_i$ (Zeeman), but it turns out that isotropic exchange can be treated on an equal footing with $\mathcal{H}_{\text{dip}}$ in the calculations. The crucial limitation to the size of J is set by the onset of "pseudo"-dipolar contributions to J in which case the EPR data cannot be interpreted simply in terms of dipolar splittings, nor can r be deduced. There are good reasons to suppose that for $|J| \lesssim 30\ \text{cm}^{-1}$, "pseudo"-dipolar terms should not be important. Were it not for the "pseudo"-dipolar effect, the calculations presented could also apply to much larger values of J.

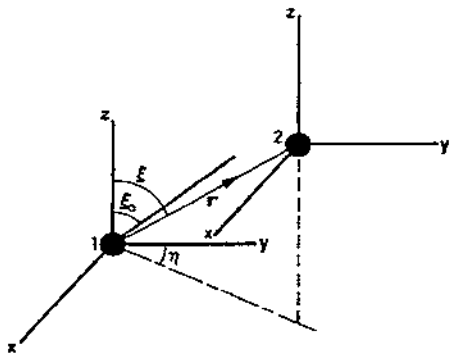

Fig. 3. Orientation of tensor principal axes and internuclear axis for similar dimers. (When $\eta = 0$, zero field splitting tensor has major principal direction at angle ξ_0 to z axis in zy plane. $\xi_0 = \xi$ only when $g_y = g_z$.)

When $|J| \ll h\nu$, the microwave quantum of energy, all possible states must be considered, whereas if $|J| \gg h\nu$ the EPR spectrum may be considered as arising simply within the triplet state, the singlet state being removed in energy by an amount J. In the latter case, the major effect of the condition $|J| \gg h\nu$ is to ensure that the states have pure "singlet" and "triplet" character. From the computer results, $|J| \gtrsim 3h\nu$ appears to satisfy this criterion, leading to triplet state EPR.

Because of the onset of "pseudo"-dipolar terms when $|J| \gtrsim 30\ \text{cm}^{-1}$, (or in the vicinity $|J| \sim 30 - 100\ \text{cm}^{-1}$), it becomes necessary to abandon perturbation theory, and to resort to computer diagonalisation of the energy matrix before computing a theoretical EPR spectrum. In Section C(ii) we discuss such a diagonalisation approach for axial dimers in some detail. In some cases, the procedure developed by Wasserman et al.[70] for free radical triplet spectra can be used without difficulty.

In the course of the development of the perturbation theory for lower than axial symmetry, it was noted that when $|J| \approx h\nu$, at least one perturbation energy denominator approaches zero. This problem is discussed briefly in Section C(i)(b).

To assist the reader in following the steps in the argument, a summary flow diagram is given in Table I. The essential method followed is the same as that used previously[38,39,52,53,56,60a]. An alternative formulation of this problem has been reported by Hatfield and Lund[60b], but their results contain a fundamental error as is discussed in Section F.

(b) $|J| \lesssim 30\ cm^{-1}$ [56,60a]

For similar ion pairs, we have already noted that $d_{ij} = \delta_{ij}$ and the x_1, y_1, z_1 and x_2, y_2, z_2 axis sets are parallel (see Fig. 3). Thus, from eqn. (5) we may write

$$J_{\alpha\gamma} = g_{1\alpha} \left\{ \sum_{\xi=x,y,z} g_{2\xi} (1 - 3 \sum_{\xi=x,y,z} \sigma_\xi \sigma_\alpha \right\} \beta^2/r^3 \qquad (13)$$

Subscripts 1 or 2 on x, y and z are dropped for the remainder of Section C. Also we put $g_{1\alpha} = g_{2\alpha} = g_\alpha$. In terms of the angles ξ and η in Fig. 3 we can write the components of J as follows where we have used the relations $\sigma_x = \sin\xi \sin\eta$, $\sigma_y = \sin\xi \cos\eta$ and $\sigma_z = \cos\xi$.

$$
\begin{aligned}
J_{xx} &= g_x^2(1-3\sin^2\eta \sin^2\xi)\beta_r \\
J_{yy} &= g_y^2(1-3\cos^2\eta \sin^2\xi)\beta_r \\
J_{zz} &= g_z^2(1-3\cos^2\xi)\beta_r \\
J_{xy} &= J_{yx} = -3g_x g_y \sin^2\xi \sin\eta \cos\eta\, \beta_r \\
J_{xz} &= J_{zx} = -3g_z g_x \sin\xi \cos\xi \sin\eta\, \beta_r \\
J_{yz} &= J_{zy} = -3g_z g_y \sin\xi \cos\xi \cos\eta\, \beta_r
\end{aligned}
\tag{14}
$$

where $\beta_r = \beta^2/r^3$. The various symmetry types covered by this model are listed in Table 2. Monoclinic symmetry (C_2, C_{2h} or C_s) requires $g_x \neq g_y$ and/or $A_x \neq A_y$. Equations (9) may be simplified by using the polar angles θ and ϕ made by **H** with x, y and z (Fig. 2). Thus noting that $l_{x_1} = l_{x_2} = l_x = \sin\theta \cos\phi$, $l_y = \sin\theta \sin\phi$ and $l_z = \cos\theta$

$$g^2 = g_z^2 \cos^2\theta + g_\perp^2 \sin^2\theta$$

where

$$g_\perp^2 = g_x^2 \cos^2\phi + g_y^2 \sin^2\phi$$

$$K^2 g^2 = A_z^2 g_z^2 \cos^2\theta + A_\perp^2 g_\perp^2 \sin^2\theta$$

TABLE 2

Symmetries for similar ion dimers

ξ°	η°	**g** tensor	**A** tensor	Symmetry	θ_m°	ϕ_m°
0	0	Axial	Axial	Axial	90	0
0	0	Orthorhombic	Orthorhombic	Orthorhombic	90	90
90	0		Axial or orthorhombic	Orthorhombic	90	90
$\neq 0$	0		Axial or orthorhombic	Monoclinic	180	90
$\neq 0$	$\neq 0$	Orthorhombic[a]	Orthorhombic[a]	Triclinic	180	180

[a] At least one of **g** or **A** must be orthorhombic for distinction to be made.

and where

$$g_\perp^2 A_\perp^2 = A_x^2 g_x^2 \cos^2\phi + A_y^2 g_y^2 \sin^2\phi \tag{15}$$

also[52]

$$\tau_1 = A_z A_\perp / K$$

$$\tau_2 = A_x A_y / A_\perp$$

$$\tau_3 = [A_z(A_y^2 - A_x^2) g_x g_y g_z \sin\phi \cos\phi \cos\theta]/(KgA_\perp g_\perp^2)$$

$$\tau_4 = g_z g_\perp (A_\perp^2 - A_z^2)\sin\theta \cos\theta/(Kg^2)$$

$$\tau_5 = \tau_3 A_\perp g_\perp \tan\theta/(A_z g_z)$$

By means of the conditions imposed in diagonalising the Zeeman interaction, we may obtain relationships between the sines and cosines of the various angles in Fig. 2 ($\psi_i = \psi$ etc.). Note also that $l_{ij}^1 = l_{ij}^2 = l_{ij}$.

$$\begin{aligned}
\cos\psi &= g_z \cos\theta/g \\
\sin\psi &= g_\perp \sin\theta/g \\
\cos\psi' &= g_x \cos\phi/g_\perp \\
\sin\psi' &= g_y \sin\phi/g_\perp
\end{aligned} \tag{16a}$$

$$\begin{aligned}
\cos\gamma &= A_z g_z \cos\theta/(Kg) \\
\sin\gamma &= A_\perp g_\perp \sin\theta/(Kg) \\
\cos\gamma' &= A_x g_x \cos\phi/(A_\perp g_\perp) \\
\sin\gamma' &= A_y g_y \sin\phi/(A_\perp g_\perp)
\end{aligned} \tag{16b}$$

Equation (10) may now be rewritten as

$$\mathcal{H}_{\text{int}} = -J\,\mathbf{S}_1' \cdot \mathbf{S}_2' + \sum_{p_1', p_2' = x', y', z'} D_{p_1' p_2'}\, S_{1p_1'}\, S_{2p_2'} \tag{17}$$

where

$$D_{p_1' p_2'} = \sum_{\gamma, \alpha = x, y, z} l_{\alpha p_1'}\, l_{\gamma p_2'}\, J_{\alpha\gamma} \tag{18}$$

and

$$(l_{ij}) \equiv \begin{pmatrix} \cos\psi\cos\psi' & -\sin\psi' & \sin\psi\cos\psi' \\ \cos\psi\sin\psi' & \cos\psi' & \sin\psi\sin\psi' \\ -\sin\psi & 0 & \cos\psi \end{pmatrix} \tag{19}$$

To develop the necessary perturbation theory, the states are described in the first instance as simple product functions in an uncoupled representation using the notation

$$|\pm\pm m_1 m_2\rangle \equiv |M_1 = \pm, M_2 = \pm\tfrac{1}{2}, m_1 m_2\rangle \equiv |M_1\rangle |m_1\rangle |M_2\rangle |m_2\rangle \tag{20}$$

M_i and m_i are the effective spin and nuclear quantum numbers for ion i. Since $S_i = \frac{1}{2}$, $M_i = \pm\frac{1}{2}$ and we simplify the notation to $\pm$ as in eqns. (20). Also we put $M_s = M_1 + M_2$.

The energy matrix, along with some definitions, and excluding terms in τ_1, τ_2 and τ_3, is given in Table 3. In passing note that the correspondence with D_1, D_2 and D_3 as used in earlier discussions of the axial case and the terms used herein

$$D_1 = \tfrac{1}{4} D_{zz}, D_2 = \tfrac{1}{4}(D_{xx} + D_{yy}), D_3 = \tfrac{1}{4}(D_{xx} - D_{yy})$$
$$D_2' = D_2 - \tfrac{1}{2} J \tag{21a}$$

TABLE 3

Energy Matrix for similar ion dimers – uncoupled representation

	$\|++m_1m_2\rangle$ $\|\psi_1\rangle$	$\|+-m_1m_2\rangle$	$\|-+m_1m_2\rangle$	$\|--m_1m_2\rangle$ $\|\psi_3\rangle$
$\langle++m_1m_2\|$	$g\beta H$ $+D'_{zz}/4$ $+\frac{1}{2}K(m_1+m_2)$	G_1^* $+\frac{1}{2}(\tau_4 - i\tau_5)m_2$	G_2^* $+\frac{1}{2}(\tau_4 - i\tau_5)m_1$	G_3^*
$\langle+-m_1m_2\|$	c.c.	$-D'_{zz}/4$ $+\frac{1}{2}K(m_1-m_2)$	$G_4^* - \frac{1}{2}J$	$-G_2^*$ $+\frac{1}{2}(\tau_4 - i\tau_5)m_1$
$\langle-+m_1m_2\|$	c.c.	c.c.	$-D'_{zz}/4$ $-\frac{1}{2}K(m_1-m_2)$	$-G_1^*$ $+\frac{1}{2}(\tau_4 - i\tau_5)m_2$
$\langle--m_1m_2\|$	c.c.	c.c.	c.c.	$-g\beta H$ $+D'_{zz}/4$ $-\frac{1}{2}K(m_1+m_2)$

c.c. denotes complex conjugate.

$G_1 = \frac{1}{4}(D_{zx} + iD_{zy})$

$G_2 = \frac{1}{4}(D_{xz} + iD_{yz})$

$G_3 = \frac{1}{4}(D_{xx} - D_{yy}) + \frac{i}{4}(D_{xy} + D_{yx})$

$G_4 = \frac{1}{4}(D_{xx} + D_{yy}) + \frac{i}{4}(D_{yx} - D_{xy}) = D_2 - iD_5$

We define the quantity

$$D_6 = (D_{yx} - D_{xy})/4 \tag{21b}$$

Inspection of Table 3 shows that, apart from the terms in K, the diagonal energies for the $|+-m_1m_2>$ and $|-+m_1m_2>$ states are equal. Therefore in order to remove this near degeneracy so as to be able to apply perturbation theory, the inner 2×2 part of the energy matrix must first be diagonalised. This 2×2 matrix has energy eigenvalues and eigenfunctions

$$E_2 = -\frac{D'_{zz}}{4} + \Phi, \; |\psi_2> = (U + iV)\,|+-m_1m_2> + b\,|-+m_1m_2> \tag{22}$$

and

$$E_4 = -\frac{D'_{zz}}{4} - \Phi, \; |\psi_4> = (W + iX)\,|+-m_1m_2> + d\,|-+m_1m_2>$$

where $D'_{zz} = D_{zz} - J$ and Φ, U, V, W, X, b and d are all defined in eqns. (23) and (24). Thus

$$\Phi = [D'^2_2 + D_6^2 + \tfrac{1}{4}K^2 (m_1 - m_2)^2]^{\frac{1}{2}} \tag{23}$$

and

$$\begin{aligned} &U = D'_2/f_1, \; V = -D_6/f_1, \; b = [\Phi - \tfrac{1}{2}K(m_1 - m_2)]/f_1 \\ &f_1 = \{D'^2_2 + D_6^2 + [\Phi - \tfrac{1}{2}K(m_1 - m_2)]^2\}^{\frac{1}{2}} \\ &W = D'_2/f_2, \; X = -D_6/f_2, \; d = [-\Phi - \tfrac{1}{2}K(m_1 - m_2)]/f_2 \\ &f_2 = \{D'^2_2 + D_6^2 + [-\Phi - \tfrac{1}{2}K(m_1 - m_2)]^2\}^{\frac{1}{2}} \end{aligned} \tag{24}$$

Since we are dealing in this section with similar ions, $D_6 = 0$ and therefore $V = X = 0$. However, we leave V and X in the expressions which follow, for then as we shall see in Section D, the corresponding expressions for dissimilar ions can be written down by inspection, taking necessary precautions to ensure that correct forms for D_{ij} and $J_{\alpha\gamma}$ are used.

This procedure leads to the coupled representation defined by the states

$$|\psi> \equiv |++m_1m_2>, \; |\psi_2>, \; |\psi_3> \equiv |--m_1m_2> \text{ and } |\psi_4> \tag{25}$$

The energy matrix in the coupled representation is given in full in Table 4, and the S_i are defined as follows.

$$S_1 = (UD_{zx} + VD_{zy} + bD_{xz})/4 + ((U\tau_4 + V\tau_5)m_2 + b\tau_4 m_1)/2$$

$$S_2 = (VD_{zx} - UD_{zy} - bD_{yz})/4 + ((-U\tau_5 + V\tau_4)m_2 - b\tau_5 m_1)/2$$

TABLE 4

Energy matrix for similar ion dimers -- coupled representation

	$\|\psi_1>$ $\|++m_1m_2>$	$\|\psi_2>$ [a]	$\|\psi_3>$ $\|--m_1m_2>$	$\|\psi_4>$ [a]
$<\psi_1\|$	$g\beta H$			
$\|$	$+D'_{zz}/4$	$S_1 + iS_2$	$S_3 + iS_4$	$S_7 + iS_8$
	$+\frac{1}{2}K(m_1+m_2)$			
$\|\psi_2>$	c.c.	$-\frac{D'_{zz}}{4}+\Phi$	$S_5 + iS_6$	0
			$-g\beta H$	
$\|\psi_3>$	c.c.	c.c.	$+D'_{zz}/4$	$S_9 + iS_{10}$
			$-\frac{1}{2}K(m_1+m_2)$	
$\|\psi>$	c.c.	c.c.	c.c.	$-D'_{zz}/4-\Phi$

[a] See eqn. (17) for definitions of $|\psi_2>$ and $|\psi_4>$.

$$
\begin{aligned}
S_3 &= (D_{xx} - D_{yy})/4 = D_3 \\
S_4 &= -(D_{xy} + D_{yx})/4 \\
S_5 &= (-UD_{xz} + VD_{yz} - bD_{zx})/4 + ((U\tau_4 - V\tau_5)m_1 + b\tau_4 m_2)/2 \\
S_6 &= (VD_{xz} + UD_{yz} + bD_{zy})/4 - ((V\tau_4 + U\tau_5)m_1 + b\tau_5 m_2)/2 \\
S_7 &= (WD_{zx} + XD_{zy} + dD_{xz})/4 + ((W\tau_4 + X\tau_5)m_2 + d\tau_4 m_1)/2 \\
S_8 &= (XD_{zx} - WD_{zy} - dD_{yz})/4 + ((-W\tau_5 + X\tau_4)m_2 - d\tau_5 m_1)/2 \\
S_9 &= (-WD_{xz} + XD_{yz} - dD_{zx})/4 + ((W\tau_4 - X\tau_5)m_1 + d\tau_4 m_2)/2 \\
S_{10} &= (-XD_{xz} - WD_{yz} - dD_{zy})/4 + ((W\tau_5 + X\tau_4)m_1 + d\tau_5 m_2)/2
\end{aligned}
\tag{26}
$$

The energy levels, correct to second order in the perturbations, are

$$E_1 = g\beta H + D'_{zz}/4 + \tfrac{1}{2}K(m_1+m_2) + \frac{S_1^2+S_2^2}{\Delta_{12}^0} + \frac{S_3^2+S_4^2}{\Delta_{13}^0} + \frac{S_7^2+S_8^2}{\Delta_{14}^0}$$

$$E_2 = -D'_{zz}/4 + \Phi - \frac{S_1^2+S_2^2}{\Delta_{12}^0} + \frac{S_5^2+S_6^2}{\Delta_{23}^0}$$

$$E_3 = -g\beta H + D'_{zz}/4 - \tfrac{1}{2}K(m_1+m_2) - \frac{S_3^2+S_4^2}{\Delta_{13}^0} - \frac{S_5^2+S_6^2}{\Delta_{23}^0} - \frac{S_9^2+S_{10}^2}{\Delta_{43}^0} \qquad (27)$$

$$E_4 = -D'_{zz}/4 - \Phi - \frac{S_7^2+S_8^2}{\Delta_{14}^0} + \frac{S_9^2+S_{10}^2}{\Delta_{43}^0}$$

Similarly, the wave functions to first order, apart from small normalisation corrections, are

$$|\psi_1>' = |\psi_1> + \frac{S_1 - iS_2}{\Delta_{12}^0}|\psi_2> + \frac{S_3 - iS_4}{\Delta_{13}^0}|\psi_3> + \frac{S_7 - iS_8}{\Delta_{14}^0}|\psi_4>$$

$$|\psi_2>' = |\psi_2> - \frac{S_1 + iS_2}{\Delta_{12}^0}|\psi_1> + \frac{S_5 - iS_6}{\Delta_{23}^0}|\psi_3>$$

$$|\psi_3>' = |\psi_3> - \frac{S_3 + iS_4}{\Delta_{13}^0}|\psi_1> - \frac{S_5 + iS_6}{\Delta_{23}^0}|\psi_2> - \frac{S_9 - iS_{10}}{\Delta_{43}^0}|\psi_4> \qquad (28)$$

$$|\psi_4>' = |\psi_4> - \frac{S_7 + iS_8}{\Delta_{14}^0}|\psi_1> + \frac{S_9 + iS_{10}}{\Delta_{43}^0}|\psi_3>$$

where the Δ_{ij}^0 are the zero order energy differences between states i and j.

(c) The effect of the magnitude of J

When $|J| \ll h\nu$, the states $|\psi_1>$, $|\psi_2>$ and $|\psi_3>$ do not constitute a "pure" triplet, nor is $|\psi_4>$ a "pure" singlet. Therefore all four states must be retained in the calculations. The results in eqns. (27) and (28) are used to calculate transition positions and intensities for the *four* $\Delta M_s = \pm 1$ and the *single* $\Delta M_s = \pm 2$ transitions for *each* pair of values of m_1 and m_2. They are as follows: $\Delta M_s = \pm 1$.

$$1 \rightarrow 2 \quad H_1 = H_0 + H_0\,(-D'_{zz}/2 - K(m_1+m_2)/2 + \Phi - [2V_{12} + \tfrac{1}{2}V_{34} + V_{78} - V_{56}])/W_0$$

$$2 \rightarrow 3 \quad H_2 = H_0 + H_0\,(D'_{zz}/2 - K(m_1+m_2)/2 - \Phi - [-V_{12} + \tfrac{1}{2}V_{34} + 2V_{56} + V_{9,10}])/W_0$$

$$1 \rightarrow 4 \quad H_3 = H_0 + H_0\,(-D'_{zz}/2 - K\,(m_1+m_2)/2 - \Phi - [V_{12}+\tfrac{1}{2}V_{34}+2V_{78}-V_{9,10}])/W_0$$

$$4 \rightarrow 3 \quad H_4 = H_0 + H_0\,(D'_{zz}/2 - K\,(m_1+m_2)/2 + \Phi - [-V_{78}+2V_{9,10}+\tfrac{1}{2}V_{34}+V_{56}])/W_0$$

where

$$W_0 = h\nu = g\beta H_0,\ V_{ij} = (S_i^2+S_j^2)/W_0 \text{ (N.B. } V_{9,10} = (S_9^2+S_{10}^2)/W_0) \tag{29}$$

The corresponding transition intensities to first order are

$$P_{1,2} = \tfrac{1}{4}\,[(U+b)^2+V^2]\,(1 \pm S_3/W_0)$$

$$P_{3,4} = \tfrac{1}{4}\,[(W+d)^2+X^2]\,(1 \pm S_3/W_0) \tag{30}$$

Second order corrections to eqns. (30) were found to be unnecessary in the computer simulations.

$\Delta M_s = 2$

$$H(\Delta M_s=2) = H_0/2 - H_0\,[K(m_1+m_2)/2 + V_{12}+V_{34}+V_{56}+V_{78}+V_{9,10}]/W_0 \tag{31}$$

The transition probability to second order, there being no first order contribution, is

$$P(\Delta M_s=2) = \{[(U+b)\,(S_1-S_5)+V(S_2+S_6)+(W+d)\,(S_7-S_9)+X(S_8-S_{10})]^2$$
$$+\,[(U+b)\,(S_2-S_6)-V\,(S_1+S_5)+(W+d)\,(S_8+S_{10})-X(S_7+S_9)]^2\}/W_0^2 \tag{32}$$

To obtain eqns. (29)—(32) the perturbation denominators are defined in the following way. For $\Delta M_s = 1$ transitions $\Delta_{13}^0 = 2g\beta H_0 = 2W_0$ and the other $\Delta_{ij}^0 = W_0$ whereas for $\Delta M_s = 2$ transitions, $\Delta_{13}^0 = W_0$ and the other $\Delta_{ij}^0 = W_0/2$ since the latter transitions occur at about half the magnetic field of the former. H_0, which is defined in eqns. (29), is the magnetic field at which transitions occur in the absence of dipolar and hyperfine interactions.

To eqns. (27), we may add energy shifts to second order in the $\tau_1 - \tau_3$ terms, so far neglected in the analysis, which couple states with different m_1 and m_2 values. In the small exchange limit, they produce energy shifts, evaluated using the ordinary perturbation formulae,

$$\Delta E_1 = \{\tfrac{1}{2}[2I\,(I+1)-m_1^2-m_2^2]\,(\tau_1+\tau_2+\tau_3) - \tau_1\tau_2(m_1+m_2)\}/(4W_0)$$

$$\Delta E_2 = \{\tfrac{1}{2}(a^2-b^2)\,(m_2^2-m_1^2)\,(\tau_1^2+\tau_2^2+\tau_3^2) - \tau_1\tau_2\,(m_1+m_2)\}/(4W_0)$$

$$\Delta E_3 = \{-\tfrac{1}{2}[2I\,(I+1)-m_1^2-m_2^2]\,(\tau_1^2+\tau_2^2+\tau_3^2) - \tau_1\tau_2\,(m_1+m_2)\}/(4W_0)$$

$$\Delta E_4 = \{-\tfrac{1}{2}(a^2-b^2)\,(m_2^2-m_1^2)\,(\tau_1^2+\tau_2^2+\tau_3^2) - \tau_1\tau_2\,(m_1+m_2)\}/(4W_0)$$

where $I_1 = I_2 = I$.
The corrections to the magnetic fields for the various transitions are thus

$$\Delta H_{1,2} = -H_0 \{I(I+1) - m_{1,2}^2 b^2 - m_{2,1} a^2\}(\tau_1^2 + \tau_2^2 + \tau_3^2)/(4W_0{}^2)$$

$$\Delta H_{3,4} = -H_0 \{I(I+1) - m_{1,2}^2 a^2 - m_{2,1}^2 b^2\}(\tau_1^2 + \tau_2^2 + \tau_3^2)/(4W_0{}^2)$$

and

$$\Delta H(\Delta M_s = 2) = -H_0 \{I(I+1) - m_1^2 - m_2^2\}(\tau_1^2 + \tau_2^2 + \tau_3^2)/(4W_0{}^2) \tag{34}$$

where

$$a^2 = U^2 + V^2 = d^2 \text{ and } c^2 = W^2 + X^2 = b^2 \tag{35}$$

a and c are entirely analogous to the same symbols used in previous publications[38, 39,52,53,56,60a].

When we consider the effect of the number of allowed pairs of m_1 and m_2 values, it can be seen that there are *not* four $\Delta M_s = \pm 1$ transitions, but $4(2I_1+1)(2I_2+1)$, i.e. 64 for copper(II) pairs and 256 for vanadyl pairs. Also there are $(2I_1+1)(2I_2+1)\Delta M_s = 2$ transitions, i.e. 16 for copper(II) pairs and 64 for vanadyl pairs. It is important to realise that $\Delta M_s = \pm 2$ transitions have maximum intensity away from principal axes.

We turn now to the situation described by $h\nu \ll |J| \lesssim 30\ \text{cm}^{-1}$. Here J is restricted to values sufficiently small that pseudo-dipolar corrections are not required in the D_{pq}, but sufficiently large that the four pair states split into a singlet and a triplet, separated in energy by J. If J is retained in the calculation, from eqn. (24) it can be shown that $U \to \pm b = 2^{-\frac{1}{2}}$ and $V \to d = 2^{-\frac{1}{2}}$, where the upper sign refers to $J < 0$ and the lower sign, $J > 0$. Then EPR is due to the triplet state alone and so the calculations can be simplified by eliminating those terms which depend on the singlet state. Thus there are now therefore $2(2I_1+1)(2I_2+1)$ transitions of $M = \pm 1$ type, namely half of those before.

The modifications necessary to characterise the problem by means of a triplet state when $|J| \gg h\nu$ are as follows. When $J < 0$, the triplet levels are $|\psi_1\rangle$, $|\psi_2\rangle$ and $|\psi_3\rangle$. Calculation of the EPR spectrum requires the use of only H_1, H_2 and $H(\Delta M = 2)$. Thus we may set to zero the variables $S_7 = S_8 = S_9 = S_{10} = V_{78} = V_{9,10} \equiv 0$. For $J > 0$, $|\psi_1\rangle$, $|\psi_4\rangle$ and $|\psi_3\rangle$ are now the triplet levels and therefore only H_3 and H_4 are needed along with $H(\Delta M_s = 2)$. Thus $S_1 = S_2 = S_5 = S_6 = V_{12} = V_{56} \equiv 0$. In these two special cases, some modification may be required in eqns. (33) and (34) but in any case these corrections are small enough not to matter.

A particular difficulty arises if $|J| \simeq h\nu$. Suppose that $J = -h\nu$. In this case it is more correct to regard the zero-order Hamiltonian as arising from both the Zeeman and exchange terms. Then in the eqns. (27) and (28) we have modified perturbation denominators, $\Delta_{14}^0 \simeq 2g\beta H_0$ and $\Delta_{43}^0 \approx 0$. Thus as they stand eqns. (27) and (28) cannot be used. What this really means is that $|\psi_3\rangle$ and $|\psi_4\rangle$ are no longer close to being eigenstates of the system. But the situation may be explored by diagonalising

the 2 × 2 matrix involving states $|\psi_3>$ and $|\psi_4>$ followed by a binomial expansion about $|J| \simeq h\nu$ of the resulting expressions for the eigenvalues. The new basis states are $|\psi_1>$, $|\psi_2>$ and the linear combinations of $|\psi_3>$ and $|\psi_4>$ resulting from the 2 × 2 diagonalisation. Perturbation theory can then be carried through as before. Preliminary computer-simulated spectra based on this procedure gave results which were different from those when $|J| \ll h\nu$ or $|J| \gg h\nu$. This matter need be investigated further only if appropriate practical examples come to light. Of course, the only way of being sure about the situation is to diagonalise the total energy matrix by computer, but this has not been done.

(d) Triplet case in terms of D and E

If we ignore the hyperfine interaction, it is certainly possible to treat the EPR as being due to a state with $S = 1$, where $|J| \gg h\nu$, and to describe the ground state splitting within the triplet by means of the usual D and E terms in the spin Hamiltonian,

$$D(S_z^2 - \frac{1}{3}S(S+1)) + E(S_x^2 - S_y^2), S = S_1 + S_2 = 1$$

This approach was used by Bleaney and Bowers in their classic paper on copper acetate[37] as well as by Hatfield and co-workers[18–36,60b], Belford and co-workers[61,65], Cowsik et al.[88] and Buluggiu et al.[89]. It is also the approach used in studies of free radical triplets[66–70].

For low symmetry cases, e.g. monoclinic or triclinic, the fine structure tensor represented by D and E, will not, in general, have its principal axes along the g principal axes, or, for that matter, along the internuclear axis. In particular for the monoclinic case, where $\eta = 0$ (Fig. 3), and using eqn. (14), it can readily be shown that[91]

$$\begin{aligned} D &= \frac{3}{4}[C_{yy}\sin^2\xi_0 + C_{zz}\cos^2\xi_0 + 2J_{yz}\sin\xi_0\cos\xi_0] \\ E &= \frac{1}{4}[C_{xx} - C_{zz}\sin^2\xi_0 - C_{yy}\cos^2\xi_0 + 2J_{yz}\sin\xi_0\cos\xi_0] \end{aligned} \tag{36}$$

where

$$\tan 2\xi_0 = \frac{2\frac{g_y}{g_z}\tan\xi}{\left(\frac{2}{3}+\frac{1}{3}\frac{g_y^2}{g_z^2}\right) - \left(\frac{2}{3}\frac{g_y^2}{g_z^2}+\frac{1}{3}\right)\tan^2\xi} \tag{37}$$

and

$$C_{zz} = \frac{1}{3}(2J_{zz} - J_{xx} - J_{yy}) \tag{38}$$

C_{xx} and C_{yy} are obtained by cyclic permutation of eqn. (38). Unless $g_y = g_z$, $\xi_0 \neq \xi$ so the major principal direction of the dipolar tensor is *not* along **r**. In this case $\eta = 0$ since one principal axis is always along the x axis.

Equations (36) – (38) are only of academic interest as far as computer simulation of the spectra is concerned when there is hyperfine interaction to consider. They do not enable more efficient computations to be made and offer no advantage in consideration of the problem when J is small, when all energies must be considered. There is a more serious objection to their use in transition metal dimers. To describe the hyperfine interaction the individual ion effective spins must be used and it is therefore much more sensible to proceed as outlined in Section C(i)(b). However, we shall use D (and E) in Section C(ii) when the computer simulation of triplet state spectra is described for large exchange. In that case the hyperfine interaction is not explicitly taken into account.

*(e) Results for axial dimers**[52,53,56]

The results corresponding to eqns. (29) – (32) for axial dimers where $\xi = 0$ are as follows

$$H_{1,2} = H_0 \{1-(2D_4^2+\tfrac{1}{2}D_3^2)/(g\beta H_0)^2 \mp 2D_1/(g\beta H_0)$$
$$-[\tfrac{1}{2}K(m_1+m_2) \mp \Phi]/(g\beta H_0) \mp 2D_4 R(m_1+m_2)(1+ab)/(g\beta H_0)^2$$
$$-\tfrac{1}{2}R^2(a^2 m_{2,1}^2 + b^2 m_{1,2}^2)/(g\beta H_0)^2$$
$$-\frac{B^2(A^2+K^2)}{4K^2}[I(I+1) - (m_{1,2}^2 b^2 + m_{2,1}^2 a^2)]/(g\beta H_0)^2\}$$

$$H_{3,4} = H_0 \{1-(2D_4^2+\frac{1}{2}D_3^2)/(g\beta H_0)^2 \mp 2D_1/(g\beta H_0)$$
$$-[\tfrac{1}{2}K(m_1+m_2) \pm \Phi]/(g\beta H_0) \mp 2D_4 R(m_1+m_2)(1+cd)/(g\beta H_0)^2$$
$$-\tfrac{1}{2}R^2(c^2 m_{2,1}^2 + d^2 m_{1,2}^2)/(g\beta H_0)^2$$
$$-\frac{B^2(A^2+K^2)}{4K^2}[I(I+1) - (m_{2,1}^2 b^2 + m_{1,2}^2 a^2)]/(g\beta H_0)^2\} \qquad (29)$$

and ignoring second and higher order terms

$$\mathcal{P}_{1,2} = \tfrac{1}{4}(a+b)^2\left(1 \pm \frac{D_3}{g\beta H_0}\right)$$

* The equations in this section involve removal of some small sign inconsistencies which crept into our earlier publications[38,39,52,53,56]. These were not sufficient to cause any material change in computed spectra.

$$P_{3,4} = \tfrac{1}{4}(c+d)^2\left(1 \mp \frac{D_3}{g\beta H_0}\right) \qquad (30)'$$

and

$$H(\Delta M_s = 2) = H_0\{\tfrac{1}{2} - (2D_4^2 + \tfrac{1}{2}D_3^2)/(g\beta H_0)^2 - \tfrac{1}{2}K(m_1 + m_2)/(g\beta H_0) - R^2(m_1^2 + m_2^2)/(2g\beta H_0)^2 - \frac{B^2}{4}\frac{(A^2+K^2)}{K^2}[2I(I+1) - m_1^2 - m_2^2]/(g\beta H_0)^2\} \qquad (31)'$$

and

$$P(\Delta M_s = 2) \simeq \frac{4D_4^2}{(g\beta H_0)^2} \qquad (32)'$$

The various variables in these equations are defined as follows.

$$\left.\begin{aligned} D_1 &= \beta^2[(g_\perp^4 \sin^2\theta - 2g_\parallel^4\cos^2\theta)/g^2]/(4r^3)\\ D_2 &= \beta^2[\{2g_\parallel^2(1-2\sin^2\theta) + g_\perp^2\sin^2\theta\}g_\perp^2/g^2]/(4r^3)\\ D_3 &= -\beta^2[g_\perp^2(g_\perp^2 + 2g_\parallel^2)\sin^2\theta/g^2]/(4r^3)\\ D_4 &= \beta^2[\{(g_\perp^2 + 2g_\parallel^2)g_\parallel g_\perp \sin\theta\cos\theta\}g^2]/(4r^3)\\ R &= (B^2 - A^2)g_\parallel g_\perp \sin\theta\cos\theta/(Kg^2) \end{aligned}\right\} \qquad (21)'$$

$$\left.\begin{aligned} K^2g^2 &= A^2g_\parallel^2\cos^2\theta + B^2g_\perp^2\sin^2\theta\\ g^2 &= g_\parallel^2\cos^2\theta + g_\perp^2\sin^2\theta\\ \Phi &= [D_2^2 + \tfrac{1}{4}K^2(m_1 - m_2)^2]^{\frac{1}{2}} \end{aligned}\right\} \qquad (15)'$$

and

$$D = -(g_\parallel^2 + \tfrac{1}{2}g_\perp^2)\beta^2/r^3 \qquad (36)'$$

The prime notation for equation numbers indicates that these expressions are all derived from the equations bearing the same number.

(f) Computer simulation of spectra[39,60a,92]

In frozen solutions or powder samples, it is assumed that all orientations of the

metal ion pair complexes with respect to the applied magnetic field are possible. Thus a general expression for the ESR lineshape may be written

$$f(H) = \sum_{n=1}^{N} \int_{\phi=0}^{\phi_m} \int_{\theta=0}^{\theta_m} P(n,\theta,\phi)\, G(H,n,\theta,\phi)\, \mathrm{d}\cos\theta\, \mathrm{d}\phi \tag{39}$$

where N = the number of transitions, θ_m and ϕ_m the upper values of the polar angles θ and ϕ. $P(n,\theta,\phi)$ is the transition probability of the nth transition for a complex for which H makes polar angles θ and ϕ with respect to the x, y and z axes as defined in Fig. 2. $P(n,\theta,\phi)$ consists of two factors, the P_i of eqn. (30) or $P(\Delta M_s = 2)$, eqn. (31), and the powder value of the g-anisotropy transition probability factor[93].

$$[g_x^2 g_y^2 \sin^2\theta + g_y^2 g_z^2 (\sin^2\phi + \cos^2\theta \cos^2\phi) + g_z^2 g_x^2 (\cos^2\phi + \cos^2\theta \sin^2\phi)]/2g^2 \tag{40}$$

The expression (40) applies when $\mathbf{H} \perp \mathbf{H}_{rf}$.

Since experimental results are usually in the form of the first derivative of absorption, the shape function, G, in eqn. (39) must be expressed as the first derivative of whatever lineshape is used. The Gaussian first derivative lineshape at a magnetic field, H, is

$$G(H,n,\theta,\phi) = -\{[H-H(n,\theta,\phi)]/\sigma^3\} \exp\{-[H-H(n,\theta,\phi)]^2/2\sigma^2\} \tag{41}$$

where $H(n,\theta,\phi)$ is the centre of the nth transition of a dimer complex for which H makes polar angles θ and ϕ with the x, y and z axes. $H(n,\theta,\phi)$ is one of $H_1 \ldots H_4$ or $H(\Delta M_s = 2)$ in eqns. (29) or (31). σ is the Gaussian half-width. The corresponding Lorentzian first derivative is

$$G(H,n,\theta,\phi) = -\sigma[H-H(n,\theta,\phi)]/\{\sigma^2 + [H-H(n,\theta,\phi)]^2\}^2 \tag{42}$$

In both eqns. (41) and (42) numerical normalisation factors have been left out. It is important to note the presence of σ^{-3} in eqn. (41) and σ in eqn. (42) since they ensure proper normalisation in the event of linewidth anisotropy.

Evaluation of the integrals in eqn. (39) is unfortunately not possible by analytic methods. The simplest approximation is the trapezoidal rule whereby the integrals are replaced by summations over finite intervals. Other approaches such as Gaussian quadrature would require much more computer time. Therefore

$$f(H) \simeq \sum_{n=1}^{N} \sum_{\phi=0}^{\phi_m} \sum_{\theta=0}^{\theta_m} P(n,\theta,\phi)\, G(H,n,\theta,\phi)\, \Delta\cos\theta\, \Delta\phi \tag{43}$$

To ensure smoothness in the final output, $f(H)$ vs. H, one must find, by trial and error, a sufficient number of orientations of θ and ϕ so that computer noise is eliminated. For θ between 0° and 90°, our practice is to take equal increments $\Delta\theta$ up to 43.6° followed by equal increments in $\Delta\cos\theta$. This precaution provides a small advantage over completely equal increments $\Delta\theta$ over the whole range in view of the

rapid change in $\cos\theta$ as $\theta \to 90^\circ$ from above or below. Equal increments of ϕ were used.

Equation (43) was evaluated using a FORTRAN program, GNDIMER*, on the CDC 3200 computer at the Monash University Computer Centre. The program evaluates the analytical expressions for $H(n,\theta,\phi)$ and $P(n,\theta,\phi)$ for a given orientation (θ,ϕ) and sums the contributions to $f(H)$ at specific output values of H. To save computer time, only $f(H)$ is stored; contributions to $f(H)$ are calculated and added in transition by transition. It is worth noting that approaches to this problem which involve storing $H(n,\theta,\phi)$ and $P(n,\theta,\phi)$ as arrays first, and then calculating $f(H)$ will be somewhat slower. To save further computer time, we usually cut off Gaussian lines at $\pm 3\sigma$ and Lorentzian lines at $\pm 4\sigma$, though these cut-offs can easily be varied to check the reliability of the approach.

The final curve is thus an array of points $(f(H), H)$ printed by the computer line printer as well as a continuous curve or some convenient scale drawn by an off-line CALLCOMP graph plotter.

Appropriate values of θ' and ϕ' for the various symmetries are given in Table 2.

Peaks in spectra from randomly oriented complexes in powders or frozen solutions arise from those orientations for which $\partial H/\partial\theta = 0$ or $\partial H/\partial\phi = 0$. Such conditions occur along major principal directions, but in the case of non-coincident principal directions for the various spin Hamiltonian tensors, the extrema will not necessarily occur for *all* possible principal directions. In the absence of an actual component linewidth, $\partial H/\partial\theta = 0$ or $\partial H/\partial\phi = 0$ should yield an infinite intensity. However, this does not occur, though one does obtain a peak in the resulting spectrum. Whether all, or only some, of the peaks will actually be resolved is dependent upon the actual nature of the energy levels as a function of orientation. Sometimes $\partial H/\partial\theta = 0$ or $\partial H/\partial\phi = 0$ for orientations away from principal directions, and additional peaks may be observed in the spectrum[46,92,94,95]. For this reason, sometimes one must be very cautious in assigning some peaks in powder or frozen solution spectra.

(g) Reliability of simulated spectra[60a]

It has proved difficult to obtain an exact match between experimental and computer simulated curves in every detail of line position or lineshape. Least squares fitting is out of the question at the present time and would only be feasible if there were some way of speeding up the present programs by a factor of 100. It is generally satisfactory to rely upon visual fitting of the results. Wherever possible we aim to fit $\Delta M_s = \pm 2$ peaks to ± 5 gauss and those for $\Delta M_s = \pm 1$ to ± 10 gauss. Experimental peaks are measured to an accuracy of ± 5 gauss. Variation of the results outside these ranges by means of adjustment of the spin Hamiltonian and structural parameters

* GNDIMER, and the other two programs mentioned later, ALLSYM and EXCHANGE, are available upon request to the authors.

gives an indication of what we may regard as errors in final results. This does not represent a statistical best fit analysis.

There is one slight difficulty in presenting the experimental results and theoretical curves produced by the CALLCOMP graph plotter on the same diagram. The magnetic field sweep of some of our spectrometers is not quite linear throughout the entire field range 1200–4000 gauss and, therefore, the field sweep assumed for the CALLCOMP plots is taken to be an average value for the particular field range required. However, our fits are primarily judged on how well the various peaks match, not on how well a particular CALLCOMP spectrum overlays the experimental one.

In addition, some of the experimental results show a certain amount of baseline drift as well as superposition of residual copper(II) monomer spectra. No correction has been made for these effects, and so in judging the goodness of fit from our results it is best to be guided by overall peak positions.

From a study of our results, it is clear that the spectra are most sensitive to the values of r, ξ, g_z, A_z, g_x and g_y. In no case has it been possible to determine values of A_x or A_y for copper(II) dimers with any certainty.

In some cases better results were obtained with an anisotropic linewidth, but we do not claim to have determined the linewidths to high precision in any case. Linewidth anisotropy is included by means of the equation[92]

$$\sigma = \{(g_x^2 W_x^2 \cos^2\phi + g_y^2 W_y^2 \sin^2\phi)\sin^2\phi + g_z^2 W_z^2 \cos^2\theta\}^{1/2}/g \qquad (44)$$

W_x, W_y and W_z are the principal linewidth components which are taken to be parallel to the x, y and z axes (in general with reference to ion 1 (Fig. 1)).

We must be reminded that the present treatment is based on the use of perturbation theory to second order in $\mathcal{H}_{dip}$ and the hyperfine interaction. In practice there are sometimes discrepancies between the $\Delta M_s = \pm 1$ and $\Delta M_s = \pm 2$ results when computed and experimental spectra are compared. Second order corrections are expected to be most reliable for $\Delta M_s = \pm 2$ spectra and the high field end of $\Delta M_s = \pm 1$ spectra. It often proves difficult, therefore, to match simultaneously both high and low field $\Delta M_s = \pm 1$ peaks as well as $\Delta M_s = \pm 2$ spectra to the previously mentioned tolerances. In particular this problem may in part be compensated for by small errors in the g values. However, r and ξ (and η where relevant) are not particularly sensitive to this problem. Some of these discrepancies may also partly originate in an inadequate symmetry model.

(h) The effect of dimer symmetry on EPR spectra

To gain some appreciation of the kinds of results which can occur, some illustrative examples are presented in this section, laying the foundation for subsequent interpretation. First the variations expected for axial copper dimers for $r = 3.5$ and 5 Å are illustrated. Figure 4 shows both $\Delta M_s = \pm 1$ and $\Delta M_s = \pm 2$ spectra when $J = 0$ whereas Fig. 5 shows only the $\Delta M_s = \pm 1$ spectra for $J = -24$ cm^{-1} since $\Delta M_s = \pm 2$

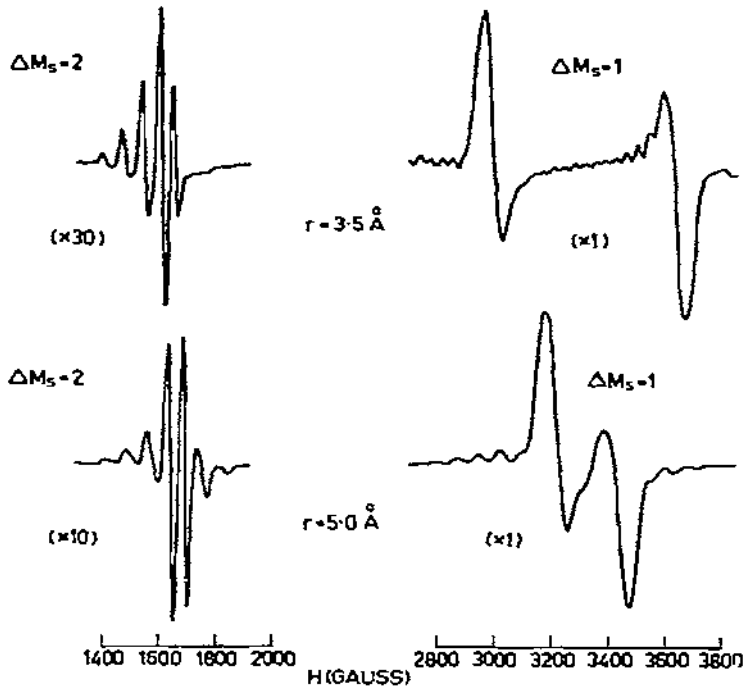

Fig. 4. Theoretical EPR spectra due to axial copper(II) dimers when $J = 0$, $g_{\parallel} = 2.07$, $g_{\perp} = 2.02$, $A_z = A_{\parallel} = 0.0148\ \text{cm}^{-1}$, $A_{\perp} = 0.0027\ \text{cm}^{-1}$ for $r = 3.5$ Å and 5.0 Å. Linewidth 10 gauss ($\Delta M_s = \pm 2$) and 18 gauss ($\Delta M_s = \pm 1$). Microwave frequency 9450 MHz.

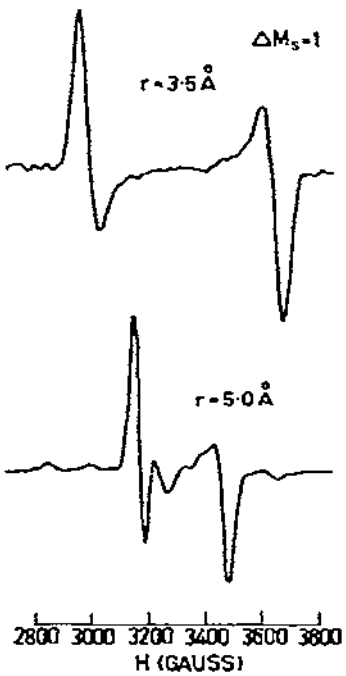

Fig. 5. Theoretical EPR spectra due to axial copper(II) dimers when $J = -24\ \text{cm}^{-1}$, $\Delta M_s = \pm 1$ spectrum only. All other parameters as in Fig. 4.

spectra are almost completely identical with those for $J = 0$ in Fig. 4. Other illustrations of variations in spectra using different g values have been given previously[39]. For these calculations 45 orientations of θ from 0 to 90° were found to be quite adequate. In the case of the corresponding $\Delta M_s = \pm 2$ spectra up to 90 orientations of θ were used though in fact $\Delta M_s = \pm 2$ spectra can be very satisfactorily obtained as few as 30 orientations of θ. Some general comments about the appearance of the spectra occur near the end of this section.

When the symmetry is lower than axial, i.e. orthorhombic, monoclinic or triclinic, we begin by showing a series of computer-simulated curves obtained in the absence of hyperfine structure, a situation entirely appropriate to titanium(III) dimers. For monoclinic symmetry ($\eta = 0$), variation in the spectra as ξ is varied[60a] from one orthorhombic limit ($\xi = 0$) to another ($\xi = 90°$) is shown in Fig. 6. In this result, 180 orientations of θ between 0 and 180° and 8 orientations of ϕ from 0 to 90° were sufficient to avoid computer noise in the output. As has already been stated, monoclinic and triclinic cases are only distinguishable when $g_x \neq g_y$ (and/or $A_x \neq A_y$). For the same set of parameters as in Fig. 6, the variation in the triclinic case[60a] as η runs from 0 to 45° when $\xi = 45°$ is shown in Fig. 7. In Figs. 6 and 7 only small anisotropy in $\mathbf{g}$ is assumed in the xy plane.

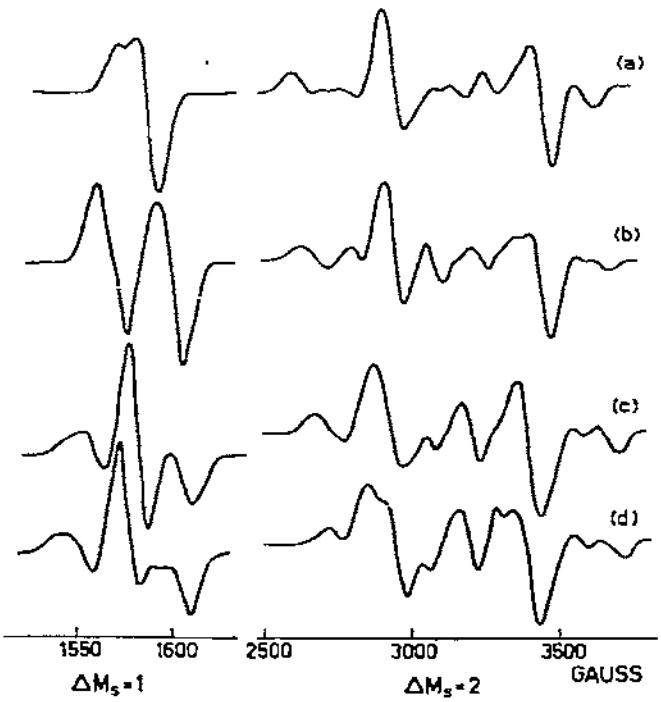

Fig. 6. Theoretical ESR spectra due to *monoclinic* dimer as ξ is varied. (a) $\xi = 0°$ (orthorhombic), (b) $\xi = 30°$, (c) $\xi = 60°$, (d) $\xi = 90°$ (orthorhombic). Other parameters are $r = 3.8$ Å, $g_x = 2.02$, $g_y = 2.015$, $g_z = 2.08$, $A_x = A_y = A_z = 0$, $W_x = W_y = W_z = 30$ gauss, $J = -20$ cm^{-1}, microwave frequency 9081 MHz.

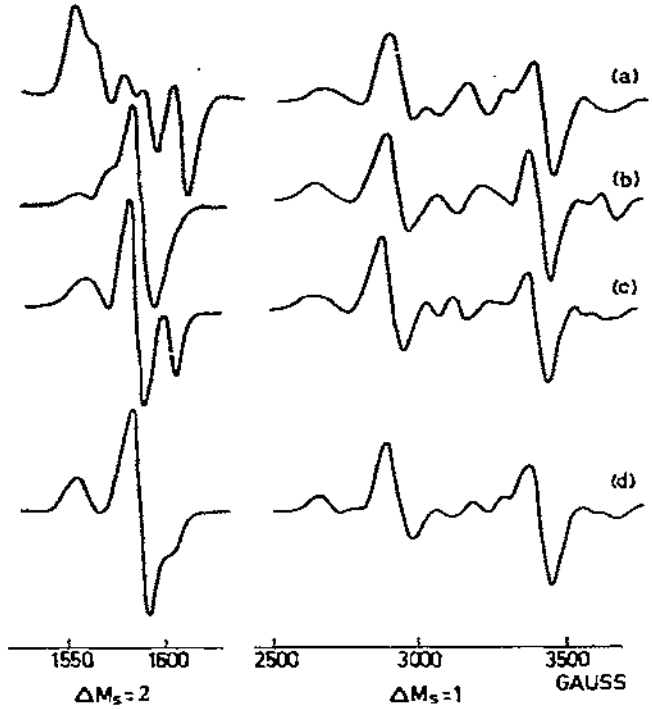

Fig. 7. Theoretical ESR spectra due to triclinic dimer as η is varied, $\xi = 30°$. (a) $\eta = 0°$ (monoclinic), (b) $\eta = 15°$, (c) $\eta = 30°$, (d) $\eta = 45°$. Other parameters are $r = 3.8$ A, $g_x = 2.02$, $g_y = 2.015$, $g_z = 2.08$, $A_x = A_y = A_z = 0$, $W_x = W_y = W_z = 30$ gauss, $J = -20$ cm^{-1}, microwave frequency 9081 MHz.

The effect of the hyperfine interaction is as follows. In the limit in which the triplet lies well away from the singlet state, the sixteen-line hyperfine structure for copper(II) dimers, present on each $\Delta M_s = \pm 1$ or ± 2 transition, simplifies to a seven-line pattern with intensities 1 : 2 : 3 : 4 : 3 : 2 : 1. The hyperfine spacing is *one-half* that of the spectrum due to each individual copper(II) ion. When the hyperfine coupling between the ions is weak, i.e. $|J| \ll h\nu$, the hyperfine pattern, while it may approximate to a seven-line pattern, will generally be more complicated. (For vanadyl dimers, instead of a seven-line hyperfine structure in the strong exchange limit, fifteen lines are found.)

We may identify the various observed features of the EPR spectra as follows. In the $\Delta M_s = \pm 1$ spectrum, characteristically there are two very strong peaks spaced about 600 gauss on either side of $g \approx 2$ when $r \approx 3.5$ Å (they will be further apart if r is smaller and vice versa). On the low field side of the lower of these peaks, frequently there is a resolved seven-line group (for copper(II)), intensities approximating 1 : 2 : 3 : 4 : 3 : 2 : 1, while some additional further structure is often found near the strong high-field peak.

In the axial limit, the resolved structure with the seven-line pattern of which not all lines are seen in Fig. 5 arises from those dimers for which H is along the z axis ("z" lines). In Fig. 4, when $J = 0$, the hyperfine pattern is obviously not as simple as a seven-line group. The strong lines, with generally *no* hyperfine structure, arise from those molecules for which H is aligned in the xy plane ("x" or "y" lines). The lack of hyperfine structure is a result of the smaller hyperfine component in the xy plane compared with that along the z axis for copper(II). In the case of vanadyl dimers, as we shall see, the x-lines also show resolved h.f.s. Figure 8 illustrates these conclusions with a simplified schematic representation[60a]. The effect of the size of J is indicated for $J < 0$.

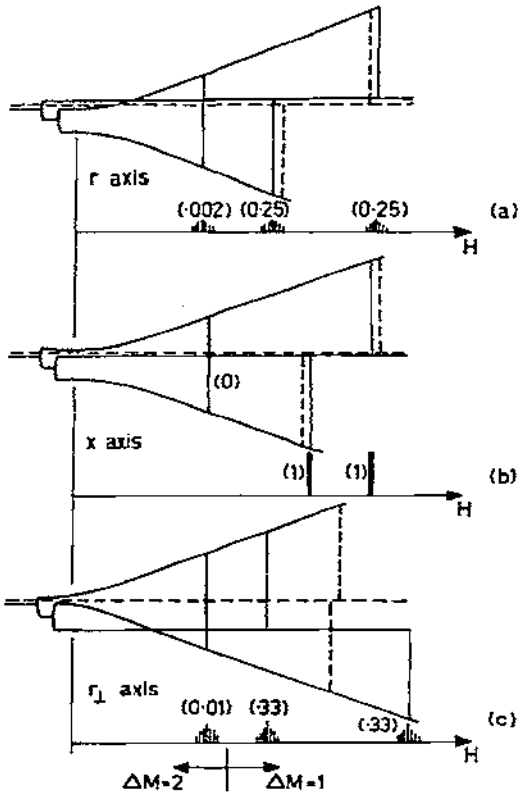

Fig. 8. Schematic energy level diagrams showing origin of peaks in powder (or frozen solution) dimer spectra when $J = 0$ (not to scale). - - - -, "singlet" level. (a) H along r axis, (b) H along x axis, (c) H in zy plane normal to r axis ($r_\perp$). $\Delta M_s = \pm 1$ and ± 2 transitions within triplet shown by |. Hyperfine structure is depicted underneath each energy level diagram. ⋮ indicates "singlet" – "triplet" transitions weakly allowed when $J \ll h\nu$. When $J \neq 0$, "singlet" moves away from "triplet" and the additional lines cannot occur at normal fields. Numbers in parentheses are relative intensities. Resulting spectral intensities in powder modified by angular distribution of dimers.

In the monoclinic case, where r is at an angle ξ to z, the aforementioned seven-line pattern for copper(II) will arise basically from those molecules for which H is close to the internuclear axis ("r" lines). The strong pair of lines will arise most probably from those molecules for which H is parallel to the x axis. There may also be structure in certain cases from those molecules for which H is at an angle $\xi + 90°$ to z, i.e. close to the third dipolar principal direction. Spectra calculated for specific orientations in various planes indicate that z and y direction will normally not be turning directions, except when $\xi = 0°$ or $90°$ and hence will not in general lead to observable peaks or features in powder or from solution spectrum. It is quite possible that there may be other orientations of the molecules, different from g or dipolar principal directions where the transitions either minimise or maximise with respect to H, and which may, therefore, give rise to additional observable peaks in the spectrum.

(ii) Computer diagonalisation procedure when exchange coupling is strong

(a) Introduction

Of all the dimers or binuclear complexes of copper(II) which have been studied[1–7], by far the majority are antiferromagnetically coupled and $-J > 100\ cm^{-1}$. These cases may have their EPR described in terms of the triplet state alone. Perhaps the best-known example is copper(II) acetate[37], which in fact turned out to be structurally relatively simple[96]. The situation discussed in Section (i), where exchange coupling was assumed sufficiently weak to avoid complications caused by "pseudo"-dipolar terms, perturbation theory is adequate to describe the results. Now consider the changes which occur in the spectra when J is large and pseudo-dipolar contributions to the zero-field splitting of the energy levels occur. At X-band frequencies it is not uncommon for EPR transitions for copper(II) dimers to extend from zero to several thousands of gauss, indicating that perturbation theory cannot account for the results.

In this review we are principally concerned with powder or frozen solution spectra, and for the case being considered, the transitions are not only spread over a large field range, but also occur as a number of discrete sharp peaks, occasionally with some hyperfine structure.

In those cases where $|J|$ is large, not only is the triplet state well above the singlet in energy, the zero field splitting within the triplet may in some cases be comparable to $h\nu$. In such situations, the zero field splitting within the triplet has a large pseudo-dipolar contribution as well as the dipolar contribution.

In practice, how may the situation in Section (i) for low J values, and that in the present case when J is assumed large, be distinguished? When J is small and antiferromagnetic, there should be no change in dimer signal intensity, except perhaps due to relaxation effects, as the temperature is lowered from room temperature to 77°K or even 4°K. But when J is large, as Bleaney and Bowers[37] noticed for copper acetate, the triplet state becomes depopulated as the temperature is lowered and so

the signal intensity drops. In that case, being a pure compound, a quite marked linewidth change occurred. As the temperature was lowered, the linewidth decreased to a limiting value below 100°K. That part of the linewidth due to dipolar interactions between neighbouring pairs was reduced as the number of ions in the triplet state decreased. Of course if susceptibility data are available a priori, then one knows what temperature dependence to expect.

The discussion in this section will be restricted to dimers of axial symmetry ($\xi = 0$) and hyperfine interactions will not be included[46]. It follows ref. 46 very closely. Sometimes the characteristic seven-line hyperfine pattern is observed for copper(II) dimers, particularly for the $\Delta M_s \pm 2$ transition. As will be seen, the method which used computer diagonalisation of the energy matrix including hyperfine coupling, would be prohibitive for powder or frozen solution spectra.

The Spin-Hamiltonian for the pair may be written

$$\mathcal{H} = g_{\parallel}\beta H_z S_z + g_{\perp}\beta(H_x S_x + H_y S_y) + D(S_z^2 - \tfrac{1}{3}S(S+1)) + E(S_x^2 - S_y^2) \qquad (45)$$

where $S = S_1 + S_2 = 1$. For axial symmetry, $E = 0$ and it will not be considered further. D consists of a pseudo-dipolar contribution which, according to the simple theory put forward by Bleaney and Bowers, is[37]

$$D_{ex} = -\tfrac{1}{8}J\,[\tfrac{1}{4}(g_{\parallel} - 2)^2 - (g_{\perp} - 2)^2] \qquad (46)$$

and a dipolar part (eqns. (36)–(38))[46]

$$D_{dip} = -(g_{\parallel}^2 + \tfrac{1}{2}g_{\perp}^2)\frac{\beta^2}{r^2} \qquad (47)$$

Since exchange is antiferromagnetic in all known strongly exchange coupled cases, J is negative (as defined) and, therefore, $D_{ex} > 0$. However, D_{dip} is always negative. So herein lies an immediate difficulty. In general we cannot easily separate out the two contributions to D from a single experimental measurement. Ideally if we know r, $g_{\parallel}$ and g, we can calculate D_{dip} very accurately. Then from the experimental value of D we may arrive at a value for D_{ex}. In the case of copper acetate, Bleaney and Bowers[37] initially assumed that the dipolar contribution was negligible. The zero field splitting parameter, D, was determined experimentally to be 0.34 cm^{-1} and was assumed to be positive on the basis of eqn. (46), since J was known to be negative. The interionic distance was later found by X-ray methods to be $r = 2.64$ Å, which implies a negative contribution to the zero field splitting of ca. 0.2 cm^{-1} from the dipolar interaction. Hence $D_{ex} = 0.54$ cm^{-1}, if D is regarded as positive. So comparison of eqn. (46) or the similar result of Ross and Yates[85] should be made with the value $D_{ex} = 0.54$ cm^{-1} and not the measured value $D = 0.34$ cm^{-1}. It is noted that Bleaney subsequently pointed out that the two terms in D have opposite sign when the exchange is antiferromagnetic[97].

A particularly interesting example[46] is that of a copper(II) adenine derivative for which $|D|$ (measured) $\simeq 0.10\ cm^{-1}$ but $D_{dip} = -0.12\ cm^{-1}$ and therefore $D_{ex} \simeq 0.22\ cm^{-1}$. Here $|D_{dip}| \simeq |D\ (measured)|$ and one could easily have drawn the wrong conclusion about the system. The fact that, even when these precautions have been taken, D_{ex} as calculated is two or three times larger than the experimental value, suggests that one should not use the ground state value of J, as determined from susceptibility measurements, but a lower excited state exchange integral. In fact Ross and Yates[84,85] developed a theory in which there were two exchange integrals. But since quantitative agreement between theory and experiment is so poor, one should be less than hasty in predicting the value of D_{ex} a priori.

(b) Solution of the spin Hamiltonian

Because the two interactions mentioned above both give rise to a "triplet" spin Hamiltonian with D and E terms, the following treatment applies, generally to triplet states. Hyperfine effects are not considered explicitly.

The spin Hamiltonian written in the representation in which S_z is diagonal, and where the magnetic fields makes spherical polar angles θ and ϕ with the x, y and z axes is

$$H = g_{\parallel}\beta H S_z \cos\theta + g_{\perp}\beta (H \sin\theta \cos\phi\, S_x + H \sin\theta \sin\phi\, S_y) + D\,[S_z^2 - \tfrac{1}{3} S(S+1)] + E\,(S_x^2 - S_y^2) \tag{48}$$

Since the cases with which we are concerned appear to involve axial symmetry we put $E = 0$ for convenience and $\phi = 0$. Thus we obtain

$$H = g_{\parallel}\beta H S_z \cos\theta + g_{\perp}\beta H S_x \sin\theta + D\,[S_z^2 - \tfrac{1}{3} S(S+1)] \tag{49}$$

and the problem is then two-dimensional in the zx plane. The matrix of H in this representation is

	$\lvert 1>$	$\lvert 0>$	$\lvert -1>$
$<1\rvert$	$\frac{D}{3} + g_{\parallel}\beta H \cos\theta$	$\frac{g_{\perp}\beta H \sin\theta}{2}$	0
$<0\rvert$	$\frac{g_{\perp}\beta H \sin\theta}{2}$	$\frac{-2D}{3}$	$\frac{g_{\perp}\beta H \sin\theta}{2}$
$<-1\rvert$	0	$\frac{g_{\perp}\beta H \sin\theta}{2}$	$\frac{D}{3} - g_{\parallel}\beta H \cos\theta$

(50)

Unfortunately, there is no analytical solution to the secular equation and so in general it is necessary to diagonalize the Hamiltonian for each value of θ.

To understand the features of the spectra from randomly oriented dimers in

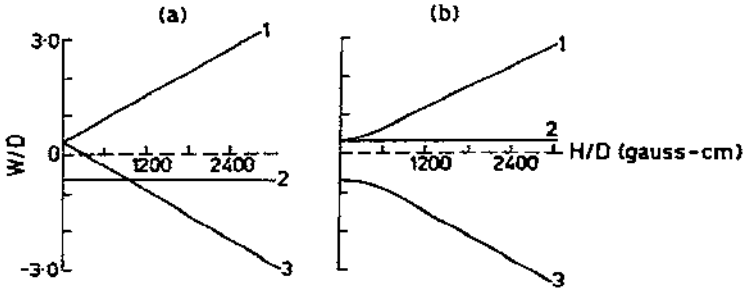

Fig. 9. Energy level diagrams for axial dimers. (a) For H//z axis, (b) H//x axis, H in gauss; zero field splitting parameter D in gigahertz.

powders or frozen solutions, it is important to appreciate the behaviour of the energy levels as a function of orientation. In particular, these are shown in Fig. 9 for the two principal axes of the interaction.

Levels are labelled in accordance with the output order in eigenvalues produced by the computer. Transitions are described as in Table 5. Those transitions marked with an asterisk are "forbidden", or $\Delta M_s = \pm 2$, transitions whilst the others are allowed ($\Delta M_s = \pm 1$). A linear iterative process is used to find the field value corresponding to a given transition for each particular orientation. The $(n+1)$th approximation is given by

$$H_{n+1} = \frac{(h\nu - \Delta W_{n-1})}{\Delta W_n - \Delta W_{n-1}} \times (H_n - H_{n-1}) + H_{n-1} \tag{51}$$

where $h\nu$ is the microwave quantum. ΔW_n is the difference in energy for the appropriate energy levels when $H = H_n$. In the case $D > h\nu$ we must exercise care in the choice of the arbitrary starting values H_1 and H_2, because there are two transitions between the levels 2 and 3. For all transitions this iterative procedure, involving re-

TABLE 5

Transitions occurring along principal axes for axial dimers[a,46]

(i) $D < \frac{1}{2}h\nu$: between levels	1–2, 1–3[b], 2–3 for H parallel to z axis
	1–2, 1–3[b], 2–3 for H parallel to x axis
(ii) $\frac{1}{2}h\nu < D < h\nu$: between levels	1–2[b], 1–3, 2–3 for H parallel to z axis
	1–2, 1–3[b], 2–3 for H parallel to x axis
(iii) $D > h\nu$: between levels	1–2[b], 2–3, 2–3 for H parallel to z axis
	1–2 for H parallel to x axis

[a] D assumed to be positive.
[b] "Forbidden" or $\Delta M_s = \pm 2$ transitions.

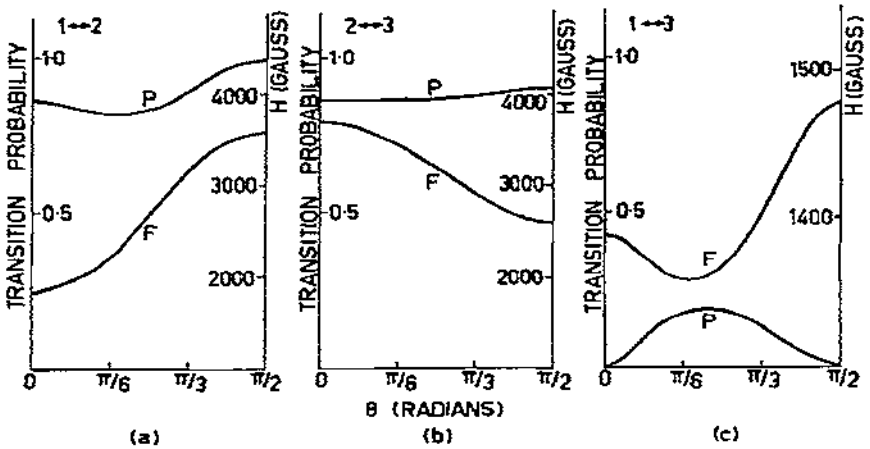

Fig. 10. Angular dependence of field position (F) and transition probability (P) for axial dimer. (a) For transition 1 ↔ 2, (b) for transition 2 ↔ 3, and (c) for transition 1 ↔ 3; $D = 0.1\ \text{cm}^{-1}$; $g_{\parallel} = 2.36; g_{\perp} = 2.09; \nu = 9160$ MHz.

peated diagonalisation of the representative matrix, enables one to converge rapidly on the appropriate field values.

The transition probability for a given transition $i \leftrightarrow j$ is a function of θ, and is proportional to the modulus squared of the matrix element $\langle\psi(i)|S_x|\psi(j)\rangle$ where $\psi(i)$ and $\psi(j)$ are the eigenvectors corresponding to the ith and jth eigenvalues.

Figures 10—12 show the angular behaviour of the transition probabilities and

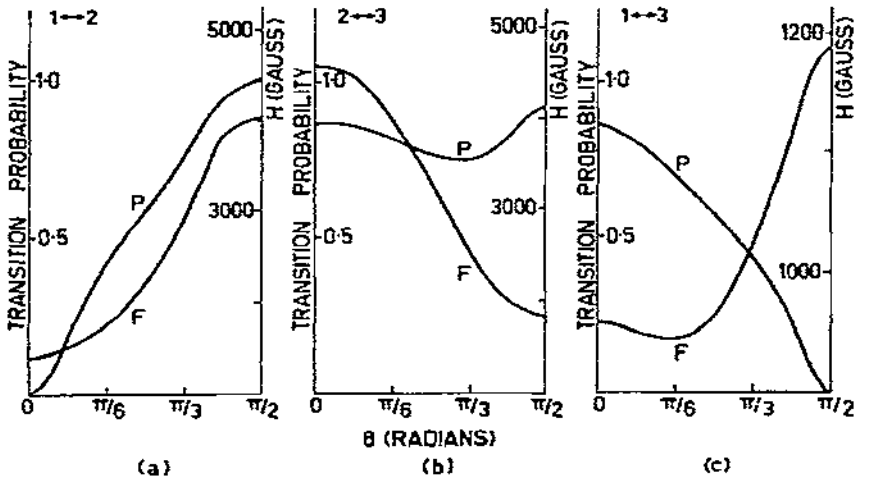

Fig. 11. Angular dependence of field position (F) and transition probability (P) for axial dimer. (a) For transition 1 ↔ 2, (b) for transition 2 ↔ 3, and (c) for transition 1 ↔ 3; $D = 0.2\ \text{cm}^{-1}$; $g_{\parallel} = 2.36; g_{\perp} = 2.09; \nu = 9160$ MHz.

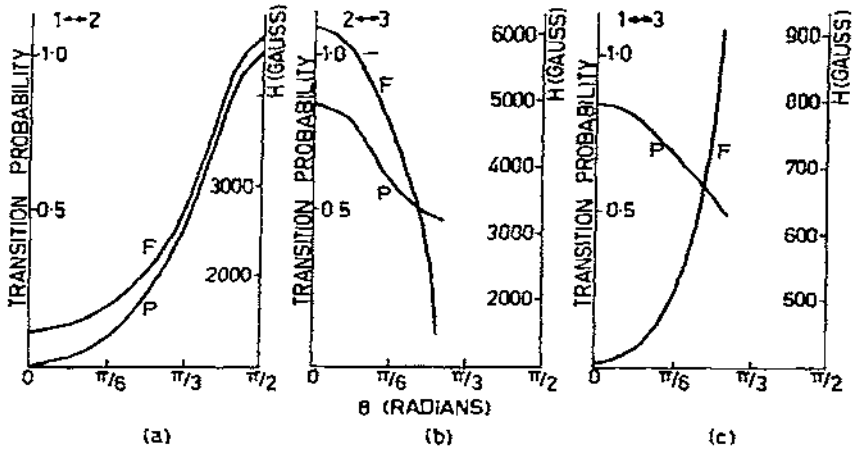

Fig. 12. Angular dependence of field position (F) and transition probability (P) for axial dimer. (a) For transition 1 ↔ 2, (b) for transition 2 ↔ 3, and (c) for transition 2 ↔ 3; $D = 0.35\ \text{cm}^{-1}$; $g_{\parallel} = 2.36$, $g_{\perp} = 2.09$; $\nu = 9160$ MHz.

the field positions for the various transitions for representative values of D in each of the three distinguishable cases mentioned above. Class (i) is of interest because of the relatively limited field spread of the "forbidden" transition components (Fig. 10(c)). The probability of these transitions is zero at the axes and for this value of D maximum at about $\theta = 45°$. This maximum increases as D approaches $h\nu/2$ (i.e. ca. $D = 0.15\ \text{cm}^{-1}$ for X-band ESR). When $|D| \gg h\nu$ (Fig. 12), two transitions occur between levels 2 and 3, one at high field and the other at low field for H parallel to the z axis. These transitions cease to occur at a certain value of θ for which the quantum no longer fits between the levels. The precise angle depends on the value of D and in this case θ is about 52°. The transition 1 ↔ 2 is "forbidden" along the z axis but allowed on the x axis.

The computer simulation of spectra from this point is the same as described in Section (i)(e) using $\theta' = 90°$ and $\phi' = 0$. To investigate some of the properties of the observed spectra in detail, some of the previous arguments in relation to Figs. 10–12 are reiterated. The computer program used here, EXCHANGE, is available upon request to the authors.

In order to identify how particular lines in the observed spectra arise, it is helpful to consider the angular dependence of the spectra intensity for particular transitions. The intensity is proportional to $P_{ij}(H) \sin\theta/(\partial H_{ij}/\partial\theta)$, where $P_{ij}(H)$ is the unweighted transition probability for transition from state i to state j. From Figs. 10–12 for the allowed transitions, $\partial H/\partial\theta = 0$ at the z and x axes; in other words the lines go through field extremes. Because of this the contribution to the intensity is infinite along the principal axes. The introduction of a linewidth effectively reduces $\partial H/\partial\theta$ to $\Delta H/\Delta\theta$. $\Delta H/\Delta\theta$ will not be zero but will be small at these points.

From these considerations it will be seen that, for this kind of problem, the technique applied by Wasserman et al.[70] of identifying spectral lines as arising basically from transitions along the principal axes of the D and g tensors, and thereby simplifying the solution of the spin Hamiltonian, is appropriate. However, this method relies on the unstated assumption that $\partial H/\partial\theta = 0$ only at the axes, i.e. $\theta = 0°$ and $\theta = 90°$. As Fig. 10 shows, $\partial H/\partial\theta$ can be zero off-axis under some circumstances, and in this case for θ = ca. 32°. Fortunately the field position of this maximum is not greatly different from the field position of the contribution due to the direction $\theta = 0$. Hence with the linewidths required in our problems the two are not resolved. However, in cases for which a small linewidth would be appropriate, partial resolution of the line should be apparent. In any event this contribution will lead to a broadening of the low-field line which could not be explained by use of the otherwise satisfactory method of Wasserman et al.

A further consideration arising from Figs. 10–12 is that for $D > \frac{1}{2}h\nu$ the contribution to the spectra from "forbidden" transitions will be negligible. But for $D < \frac{1}{2}h\nu$ this is not so. As D approaches $\frac{1}{2}h\nu$ the transition probability increases considerably. Further, the angular variation of the "forbidden" lines is relatively small and so the peak height of the derivative of the absorption is effectively enhanced. Because of this the peak heights of the $\Delta M_s = \pm 2$ line and the $\Delta M_s = \pm 1$ lines can be comparable

A series of computed spectra which illustrate the behaviour of the spectra from $D = 0.05$ cm^{-1} to $D = 0.5$ cm^{-1} are shown in Fig. 13. The g values chosen are typical

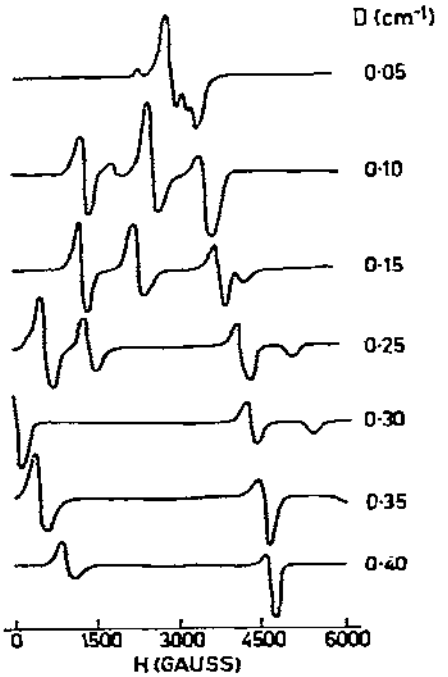

Fig. 13. Calculated EPR spectra for $g_\parallel = 2.36$, $g_\perp = 2.09$, $\sigma = 80$ gauss, $\nu = 9160$ MHz for axial dimer. (Hyperfine interaction not included.)

for this type of problem ($g_{\parallel} = 2.36, g_{\perp} = 2.09$). Initially the lines are all quite close to $g = 2$ and poorly resolved. As D increases the lines spread to higher and lower fields.

As a check on the validity of the method we obtained identical results using the representation in which the Zeeman interaction was diagonal.

All our results can be explained on the basis of the axial spin Hamiltonian (eqn. (49)). However, in the case of orthorhombic symmetry this treatment would not be adequate. The matrix of the spin Hamiltonian in the representation in which S_z is diagonal, must be supplemented by terms in E, and hence the second polar angle ϕ. This introduces complex matrix elements which complicate the diagonalisation of the matrix.

The copper hyperfine interaction has not been included explicitly, though it could be if required for cases in which resolved structure was observed. However, the existence of copper(II) hyperfine structure, especially if it is not resolved, will produce an anisotropy in the linewidth.

D. DISSIMILAR IONS

(i) Introduction

The EPR behaviour of coupled pairs of dissimilar ions was in fact first studied[75,77] as long ago as 1948 and was concerned with two different copper(II) sites in copper sulphate single crystals[75,78,79]. An excellent general discussion of the underlying theory is given by Abragam and Bleaney[79]. In order to envisage the situation, refer back to Fig. 1 where the principal axes of g and A for ions 1 and 2 are non-aligned. This is not the only way to obtain dissimilar ion pairs. We could, for example, have two different ions, which would make a dissimilar ion pair irrespective of whether or not the principal axes of the two ions were parallel. In this connection, an interesting example consists of a spin-label–metal ion pair[80].

Of particular interest in our later discussion are the results for a spiro amine complex in which there are two copper(II) sites, otherwise identical except for a rotation of one site with respect to the other of 90° about the common y axis (Fig. 14)[62,98,99]. It is also alleged that the considerations of this section are relevant to binuclear complexes of egta[98,99], see section (I).

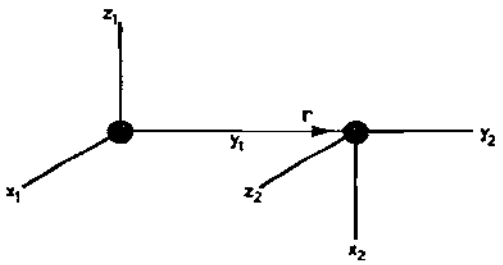

Fig. 14. Orientation of g tensor principal axes for dissimilar ion dimer, special case appropriate to spiro amine complex (see ref. 62 and later discussion).

Development of the necessary dimer theory for dissimilar ions is more difficult than for similar ions. It turns out that it is possible to develop perturbation theory solutions only when $J = 0$, as is explained later in Section D(iii). There are two fairly obvious approaches to this problem. The first is to represent the spin Hamiltonian, eqn. (6), in terms of the Zeeman representation of ion 1. Secondly, eqn. (6) may be represented in terms of the Zeeman representations of both ions as outlined in Section B(iii), and as given explicitly in eqns. (10) – (12). The use of these equations is discussed in detail in Section D(iii).

(ii) Dissimilar ion dimers represented by coordinates of ion 1 (ref. 100)

For H_1, the spin Hamiltonian of ion 1, we may take eqn. (8) as it stands by putting $i = 1$, whereas in terms of the quantisation axes of ion 1, we may write

$$\begin{aligned}\mathcal{H}_2(\text{Zeeman}) &= \beta H \sum_{j=x_2,y_2,z_2} g_j l_j S_{2j} \\ &= \beta H \sum_{q'=x_1',y_1',z_1'} g_{2q'} S_{2q'}\end{aligned} \tag{52}$$

where

$$g_{2q'} = \sum_{r_1,r_2=x_1',y_1',z_1'} g_{r_2} l_{r_2} d_{r_1 r_2} l^1_{r_1 q'} \tag{53}$$

In this representation $\mathcal{H}_2$ is *not* diagonal, and this is the first difficulty. What one has to contend with is substantial off-diagonal matrix elements in the Zeeman interaction, and this will certainly make the reliability of perturbation theory hard to assess.

In this same representation we may express the isotropic exchange interaction as

$$\begin{aligned}-J\mathbf{S}_1 \cdot \mathbf{S}_2 = -J \sum_{r=x_1,y_1,z_1} S_{1r} S_{2r} &= -J \sum_{\substack{r=x_1,y_1,z_1 \\ p'q'=x_1',y_1',z_1'}} l^1_{rp'} l^1_{rq'} S_{1p'} S_{2q'} \\ &= -J\mathbf{S}_1' \cdot \mathbf{S}_2''\end{aligned} \tag{54}$$

where orthogonality relationships among the l^1_{ij} have been used. S_2'' is the effective spin operator for ion 2 in this representation. Similarly the dipolar term is

$$\mathcal{H}_{\text{dip}} = \sum_{\alpha,\gamma=x_1,y_1,z_1} J_{\alpha\gamma} S_{1\alpha} S_{2\gamma} = \sum_{p',q'} D_{p'q'} S_{1p'} S_{2q'} \tag{55a}$$

where

$$D_{p'q'} = \sum_{\alpha,\gamma=x_1,y_1,z_1} J_{\alpha\gamma}\, l^1_{\alpha p'}\, l^1_{\gamma q'} \tag{55b}$$

Neither isotropic exchange nor $\mathcal{H}_{dip}$ cause any perturbation difficulties if one follows the procedure of Section C(i) for similar ions. We must reject this approach from the point of view of perturbation theory since there is no easy way to accommodate off-diagonal Zeeman matrix elements of ion 2. Additionally, the hyperfine structure of ion 2 will be rather complicated.

We turn instead to the alternative representation in which separate spin quantisation for ions 1 and 2 is used, thus ensuring that the Zeeman interactions for each ion are separately diagonal.

(iii) Dissimilar ion dimers represented by separate spin quantisation for ions 1 and 2 (ref. 100)

We may proceed as in Section B(iii) and use all the equations (1) – (12). The only difficulty is applying perturbation theory comes about through eqn. (12) for the isotropic exchange interaction, for

$$-J\mathbf{S}_1 \cdot \mathbf{S}_2 \neq -J\mathbf{S}'_1 \cdot \mathbf{S}'_2$$

where now $\mathbf{S}'_2$ refers to the Zeeman quantisation axes of ion 2. Thus $\mathcal{H}_{ex}$ behaves in this representation as if it were in fact anisotropic! Therefore there will be off-diagonal matrix elements of $\mathcal{H}_{ex}$ in the energy matrix in even the uncoupled representation in other than the $<+-|H_{ex}|-+>$ positions. Since $\mathcal{H}_{ex}$ may be considerably greater than $\mathcal{H}_{dip}$, perturbation theory cannot be used in general.

When $J = 0$ we may of course proceed much as in Section C(i). Because the two ions in general have differently aligned principal directions, we must distinguish between g_1 and g_2 etc. throughout the calculations. In the next paragraphs a number of the equations are rewritten, and in Tables 6 and 7 we give amended versions of Tables 3 and 4 respectively appropriate for dissimilar ions with $J = 0$.

Some of the expressions in eqns. (22) – (26) are modified as follows: Equation (23) becomes

$$\Phi = [D_2^2 + D_6^2 + \tfrac{1}{4}\{(K_1 m_1 - K_2 m_2) + (g_1 - g_2)\beta H\}^2]^{\frac{1}{2}} \tag{56}$$

The expressions in eqns. (24) which are modified are

$$\begin{aligned} b &= [\Phi - \tfrac{1}{2}(K_1 m_1 - K_2 m_2)]/f_1 \\ f_1 &= \{D_2^2 + D_6^2 + [\Phi - \tfrac{1}{2}(K_1 m_1 - K_2 m_2)]^2\}^{\frac{1}{2}} \\ d &= [-\Phi - \tfrac{1}{2}(K_1 m_1 - K_2 m_2)]/f_2 \\ f_2 &= D_2^2 + D_6^2 + [-\Phi - \tfrac{1}{2}(K_1 m_1 - K_2 m_2)]^2\}^{\frac{1}{2}} \end{aligned} \tag{57}$$

TABLE 6

Energy matrix for dissimilar ion dimers – uncoupled representation[a,b]

	$\|++m_1m_2\rangle$ $\|\psi_1\rangle$	$\|+-m_1m_2\rangle$	$\|-+m_1m_2\rangle$	$\|--m_1m_2\rangle$ $\|\psi_3\rangle$
$<++m_1m_2\|$	$\frac{1}{2}(g_1+g_2)\beta H$ $+D_{zz}/4$ $+\frac{1}{2}(K_1m_1+K_2m_2)$	G_1^* $+\frac{1}{2}(\tau_{24}-i\tau_{25})m_2$	G_2^* $+\frac{1}{2}(\tau_{14}-i\tau_{15})m_1$	G_3^*
$<+-m_1m_2\|$	c.c.	$-D_{zz}/4$ $+\frac{1}{2}(g_1-g_2)\beta H$ $+\frac{1}{2}(K_1m_1-K_2m_2)$	G_4^*	$-G_2^*$ $+\frac{1}{2}(\tau_{14}-i\tau_{15})m_1$
$<-+m_1m_2\|$	c.c.	c.c.	$-D_{zz}/4$ $-\frac{1}{2}(g_1-g_2)\beta H$ $-\frac{1}{2}(K_1m_1-K_2m_2)$	$-G_1^*$ $+\frac{1}{2}(\tau_{24}-i\tau_{25})m_2$
$<--m_1m_2\|$	c.c.	c.c.	c.c.	$-\frac{1}{2}(g_1+g_2)\beta H$ $+D_{zz}/4$ $-\frac{1}{2}(K_1m_1+K_2m_2)$

[a] Corresponds to Table 3 for similar ion dimers.
[b] $J = 0$ assumed throughout calculations.

TABLE 7

Energy matrix for dissimilar ion dimers – coupled representation[a,b]

	$\|\psi_1\rangle$ $\|++m_1m_2\rangle$	$\|\psi_2\rangle$[c]	$\|\psi_3\rangle$ $\|--m_1m_2\rangle$	$\|\psi_4\rangle$[c]
$<\psi_1\|$	$g\beta H$ $+D_{zz}/4$ $+\frac{1}{2}(K_1m_1+K_2m_2)$	S_1+iS_2	S_3+iS_4	S_7+iS_8
$<\psi_2\|$	c.c.	$-D_{zz}/4+\Phi$	S_5+iS_6	0
$<\psi_3\|$	c.c.	c.c.	$-g\beta H$ $+D_{zz}/4$ $-\frac{1}{2}(K_1m_1+K_2m_2)$	S_9+iS_{10}
$<\psi_4\|$	c.c.	c.c.		$-D_{zz}/4-\Phi$

[a] Corresponds to Table 4 for similar ion dimers.
[b] $J = 0$ assumed in calculations.
[c] See eqn. (57) for definitions of b, d, f_1 and f_2 and eqn. (56) for Φ.
[d] S_1–S_{10} defined in eqns. (26) subject to modifications in Section D(iii).

In eqns. (26) for the S_i the following changes are made:

$$\tau_4 m_2, \tau_5 m_2 \rightarrow \tau_{24} m_2, \tau_{25} m_2$$

and

$$\tau_4 m_1, \tau_5 m_1 \rightarrow \tau_{14} m_1, \tau_{15} m_1$$

In Tables 6 and 7 write D_{zz} and D_2 rather than D'_{zz} and D'_2 since $J = 0$. To relate to our earlier results in Section C we put

$$g = (g_1 + g_2)/2 \tag{58}$$

Further, the modifications to eqns. (27), (29) and (31) are

$$\tfrac{1}{2}K(m_1 + m_2) \rightarrow \tfrac{1}{2}(K_1 m_1 + K_2 m_2)$$

There is one very important point in connection with the use of Φ in eqns. (29) for $\Delta M_s = \pm 1$ field positions. For dissimilar ions, Φ contains the expression $(g_1 - g_2)\beta H$ and so depends on the magnetic field. There are two ways we can overcome this. The first is to begin by putting $H = H_0$ in Φ and then iterating once $H_1 - H_4$ have been calculated by using the actual value of H_i calculated on that basis. As long as $(g_1 - g_2)/g$ does not become too large, for copper it may be ~15% at most, we assume the simple replacement of H by H_0 in Φ will be sufficient. It is just this point which receives detailed discussion by Abragam and Bleaney[79].

Finally eqns. (33) must be modified, and they become

$$\begin{aligned}
\Delta E_1 &= \{[I_1(I_1+1) - m_1^2]T_1 + [I_2(I_2+1) - m_2^2]T_2 - T_3\}/(8W_0) \\
\Delta E_2 &= \{(a^2-b^2)(T_2 m_2^2 - T_1 m_1^2) - T_3\}/(8W_0) \\
\Delta E_3 &= \{-[I_1(I_1+1) - m_1^2]T_1 + [I_2(I_2+1) - m_2^2]T_2 - T_3\}/(8W_0) \\
\Delta E_4 &= \{-(a^2-b^2)(T_2 m_2^2 - T_1 m_1^2) - T_3\}/(8W_0)
\end{aligned} \tag{59a}$$

where

$$T_i = \tau_{i1}^2 + \tau_{i2}^2 + \tau_{i3}^2 \qquad i = 1, 2$$

and (59b)

$$T_3 = 2(\tau_{11}\tau_{12} m_1 + \tau_{21}\tau_{22} m_2)$$

(iv) Computer simulation using the results in Section D(iii)

For purposes of computer simulation, we can define the orientation of H with respect to the dimer by means of θ and ϕ, the polar angles in terms of x_1, y_1 and

z_1. Thus we may write g_1, K_1 and τ_{1i} as in eqns. (15), in general remembering to use the subscript 1 on all g and A components. In eqns. (15), the expressions are all in rather simpler form than in eqns. 9(b). However, although we could similarly express g_2, K_2 and T_{2i} in an entirely analogous form to eqn. (15) using the polar angles of H with respect to x_2, y_2 and z_2, this does not offer any computational advantage. It is far simpler for all practical purposes to express the direction cosines of H with respect to x_2, y_2 and z_2 in terms of those with respect to x_1, y_1 and z_1 (hence in terms of θ and ϕ), and then to use those results in the expressions for g_2, K_2 and τ_{2i} given in eqn. (9). Thus we have

$$l_{i_2} = \sum_{j_1 = x_1, y_1, z_1} d_{j_1 i_2} l_{j_1} \quad i_2 = x_2, y_2, z_2 \tag{60}$$

Only when the principal axes of ions 1 and 2 are parallel does

$$l_{i_1} = l_{i_2} = l_i \; (i_1 = x_1, y_1, z_1, \; i_2 = x_2, y_2, z_2, \; i = x, y, z)$$

And in that case, $g_1 = g_2, K_1 = K_2$ and $\tau_{1i} = \tau_{2i}$ only when, in addition, the two ions are similar and in identical sites.

In general, the dissimilar ion dimers will have no symmetry elements and so $\theta_m = \phi_m = 180°$ (triclinic). The computer simulation is carried out as described in Section C(i)(e) using a program ALLSYM. We note, however, that the calculation of the anisotropy in the transition probabilities is rather complicated[99]. The necessary details are given in the Appendix. It turns out that as a result of this more complete treatment, a small correction is necessary in the first-order terms in eqns. (30) and (30)' for the similar ion dimers. However, the error is of no apparent consequence in the computed spectra for $r \gtrsim 3$ Å.

Some representative spectra, based on a particular dissimilar-ion model, Fig. 14, are shown in Fig. 15. It is clear that the spectra are more complicated in shape than in the similar-ion case, and, for that reason, the correct anisotropic transition probabilities are required to ensure that subtleties in lineshape are faithfully obtained in general. A feature of the general dissimilar-ion problem was the significant amount of consistency checking of the program ALLSYM to establish its reliability.

For the symmetry represented in Fig. 14, appropriate to the copper(II) spiro amine complex[62,98,99] and the binuclear egta examples[98,99] to be discussed later, it is found that in the x_1, y_1, z_1 frame of axes

$$\begin{aligned} J_{xx} &= g_{x_1} g_{x_2} \beta_r \\ J_{yy} &= -2 g_{y_1} g_{y_2} \beta_r \\ J_{zz} &= g_{z_1} g_{x_2} \beta_r \end{aligned} \tag{61}$$

and the other components are all zero. In this situation we may include isotropic

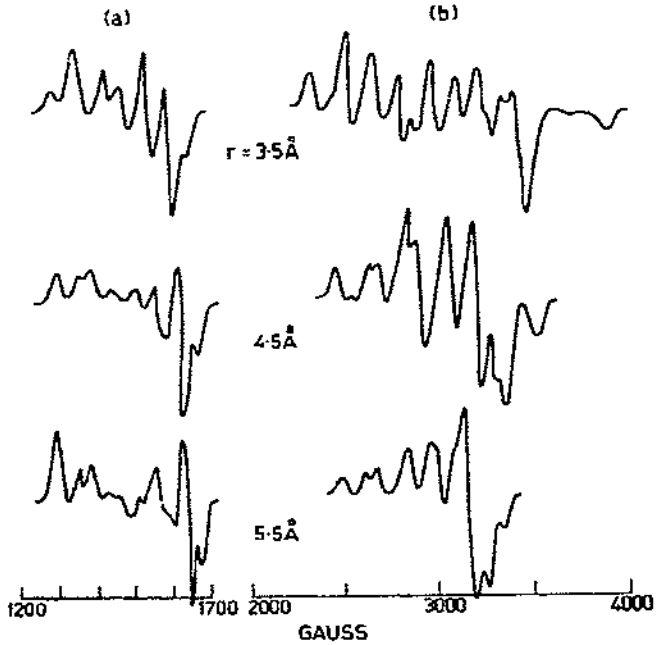

Fig. 15. Representative computer spectra due to dissimilar copper(II) ion pairs for symmetry model Fig. 14 and using program ALLSYM. $g_{1x} = g_{1y} = g_{2x} = g_{2y} = 2.06$, $g_{1z} = g_{2z} = 2.30$, $\xi = 90°$, $\eta = 0°$, $\nu = 9.140$ GHz, $A_z = 0.0180$ cm^{-1}, $A_x = A_y = 0.0010$ cm^{-1}. (a) $\Delta M_s = \pm 2$, $\sigma = 10$ gauss, (b) $\Delta M_s = \pm 1$, $\sigma = 20$ gauss.

exchange in perturbation theory only along the x, y and z axes. If further, as was assumed in analysing the spiro amine case[62], $g_{x_1} = g_{x_2} = g_\perp = g_{y_1} = g_{y_2}$ and $g_{z_1} = g_{z_2} = g_\parallel$,

$$J_{xx} = J_{zz} = g_\parallel g_\perp \beta_r$$
$$J_{yy} = -2g_\perp{}^2 \beta_r \tag{62}$$

Now

$$l_{x_1} = \sin\theta\cos\phi,\ l_{y_1} = \sin\theta\sin\phi \text{ and } l_{z_1} = \cos\theta \tag{63a}$$

so therefore

$$l_{x_2} = \cos\theta,\ l_{y_2} = \sin\theta\sin\phi \text{ and } l_{z_2} = \sin\theta\cos\phi \tag{63b}$$

Thus

$$g_1^2 = (g_x^2 \sin^2\theta\cos^2\phi + g_y^2 \sin^2\theta\sin^2\phi + g_z^2\cos^2\theta)$$
$$= g_\parallel^2 \cos^2\theta + g_\perp{}^2 \sin^2\theta \tag{64}$$

$$g_2^2 = g_\perp^2(\cos^2\theta + \sin^2\theta\sin^2\phi) + g_\parallel^2\sin^2\theta\cos^2\phi$$

The hyperfine expressions (eqn. (9a)) may be similarly worked out. We may note that for ion 1, using eqn. (15) we have

$$\begin{aligned} &\tau_{11} = A_\perp^2/K \quad \tau_{12} = A_\perp \quad \tau_{13} = \tau_{15} \equiv 0 \\ &\tau_{14} = g_\parallel g_\perp \sin\theta\cos\theta\,(A_\perp^2 - A_\parallel^2)/(Kg^2) \end{aligned} \tag{65}$$

In terms of previous publications, $\tau_{14} = R$ (refs. 39, 52, 53, 56) and E (ref. 38).

E. IDENTIFICATION AND INTERPRETATION OF DIMER SPECTRA

A necessary condition for obtaining EPR spectra due to dimers is that the paramagnetic ion pair systems are magnetically isolated from one another so as to keep experimental linewidths small[60a]. Copper acetate is an exception[37]. This is achieved in powders and single crystals by dilution in a diamagnetic host lattice, which could affect the structural relationship between the units comprising the dimer molecule. The change of host lattice could be of critical importance particularly in cases where the relationship between the molecules in the pure state is controlled by packing considerations. Provided that the change of environment brought about by diamagnetic dilution is not critical in deciding the structural alignment in copper(II), vanadyl or even titanium(III) complexes, a reasonable starting point in accounting for the spectra is to take a symmetry model based on known crystallographic data on the pure paramagnetic compound. For solution studies, dilution is achieved in practice by using small concentrations of the metal ion compounds dissolved in suitable solvents. When dimer formation is incomplete, as is frequently the case, dimer $\Delta M_s = \pm 1$ spectra are often considerably obscured by residual monomeric spectra in the $g \approx 2$ region of the spectrum. This situation is often the case in powders containing small concentrations of the paramagnetic metal ion. In order to make any progress at all in the case of dimers observed in frozen solution, it is usually best to begin by taking the simplest possible dimer symmetry model commensurate with either single crystal X-ray data of the pure compound or a related system. In many of the cases to be described in subsequent sections, however there are no suitable structural data available, and one must be guided by intuition and any help molecular models can provide.

Before one can decide whether the perturbation theory approach to computer simulation is valid in a given case, one must try to establish whether there is significant exchange coupling involved or not. J is known for a good many compounds, but if in a given case it is not, the temperature dependence of the EPR intensity can be used to given an indication of whether J is large. If it turns out that $|J| \gtrsim 30\ \text{cm}^{-1}$ we cannot reliably extract r from the perturbation theory approach to the problem. If $-J \gtrsim 100\ \text{cm}^{-1}$ we should expect to find a decrease in EPR signal intensity as the

temperature is lowered from room temperature to 77°K. The results which provide the strongest confirmation of the dipole-dipole model are those for which $|J| \lesssim 30\ cm^{-1}$ as determined by careful magnetic susceptibility studies at low temperatures down to 2 – 4°K.

In solution studies, it is almost invariably found that dimer spectra appear only below the freezing point of the solution. This is not understood and may involve relaxation effects. Susceptibility measurements on solutions containing dimers, especially in these cases where dimer formation is incomplete, are not thought to be very reliable. In the first place, the metal ion concentration is small, and diamagnetic corrections due to solute and solvent will be more important than diamagnetism in the pure compound. Unless J is large, we should not expect the measurements to be able to resolve monomer and dimer contributions. As has been pointed out, $D_{dip}(\text{maximum}) \approx 0.2\ cm^{-1}$ so that the dipolar interaction is *not* going to influence the value of χ unless the temperature is much less than 1°K. The limitation of magnetic susceptibility as a useful technique in solution chemistry is that it is a bulk measurement; different species can only be reliably resolved by this means when they have substantially different temperature-dependent susceptibilities.

To this point in our discussion, we have concentrated upon structural and symmetry considerations. In ideal cases, when J is small, we have stated that by means of comparisons of experimental and computer-simulated dimer spectra, one can determine r, the metal ion – metal ion separation, and other structural data. But in addition, one determines g values, hyperfine constants and linewidths. It has not been our purpose to discuss the import of these other parameters in any detail; however, it must be stated that these should all be appropriate to the type of system being studied. If g values and hyperfine constants are wildly different from those in appropriate monomeric compounds or complexes, then one's interpretation must be called into question. Nevertheless the computer simulation process is a many-parameter problem, and sometimes it is necessary to state that certain parameters were needed to produce a certain fit to the experimental results. In the absence of further guidance from other experiments, it seems wisest to reserve judgement now and then. It may genuinely happen that the symmetry model assumed is quite inadequate.

In conclusion then, we stress that the computer simulation approach to the interpretation of dimer spectra is a valid procedure provided certain safeguards and guidelines are borne in mind. It is not the only way in which metal ion dimer spectra have been interpreted, but it is the method which maximises the possible information which can be obtained from powders or frozen solutions. It has certainly been a very fruitful approach as the following pages will show.

F. COPPER(II) AND VANADYL COMPLEXES OF KNOWN STRUCTURE

The crystal structure determination of bis(pyridine N-oxide)copper(II) nitrate has revealed that in the solid state it exists in a dimeric form where each five-coordi-

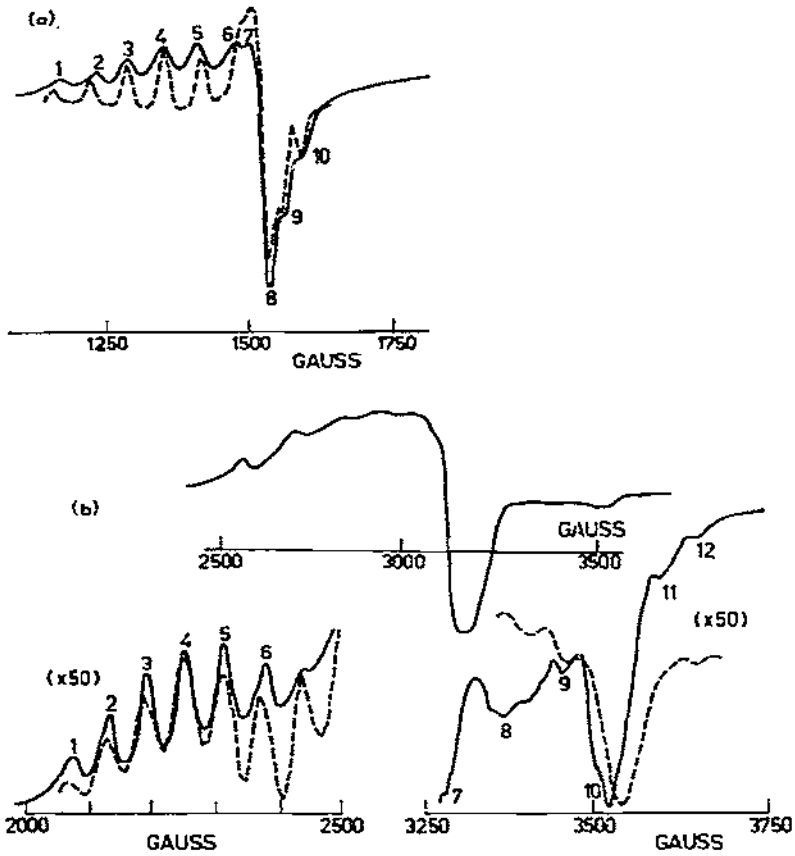

Fig. 16. X-band EPR spectrum[60] due to a powder sample of bis(pyridine *N*-oxide)copper(II) nitrate doped into the corresponding zinc salt in a 1 : 9 ratio. Microwave frequency 9140 MHz, temperature 77°K. (a) $\Delta M_s = \pm 2$ spectrum, (b) $\Delta M_s = \pm 1$ spectrum and residual monomer spectrum. Computer-simulated spectrum (- - -) obtained with following parameters: $r = 3.46 \pm 0.05$ A, $\xi = 41 \pm 1°$, $g_x = g_y = 2.040 \pm 0.005$, $g_z = 2.303 \pm 0.005$, $A_x = A_y = 0.001\ \text{cm}^{-1}$, $A_z = 0.014\ \text{cm}^{-1}$ ($\Delta M_s = 2$) and $A_z = 0.016\ \text{cm}^{-1}$ ($\Delta M_s = 1$), $W_x = W_y = W_z = 8$ gauss ($\Delta M_s = 2$) and $W_x = W_y = 24$ gauss and $W_z = 15$ gauss ($\Delta M_s = 1$), $J = +30\ \text{cm}^{-1}$.

nated copper(II) ion possesses a tetragonal pyramidal environment shown by structure I[14,15]. Magnetic susceptibility studies indicate that the molecule has a magnetic moment of 1.90 B.M. per copper(II) ion. However, the temperature dependence of the susceptibility gave a value[21] of $J \sim 30\ \text{cm}^{-1}$. The success in accounting for the X-band EPR triplet state spectra due to bis(pyridine N-oxide)copper(II) nitrates doped into the corresponding zinc salt may be judged by Fig. 16, which shows the experimental spectrum along with the computed lineshape[60a] using the parameters outlined by Table 8. Comparison of the X-ray crystallographic and EPR results as outlined by Table 8 shows excellent agreement, indicating that the copper(II) dimers

formed in the zinc complex host lattice have the same structure as the pure copper compound.

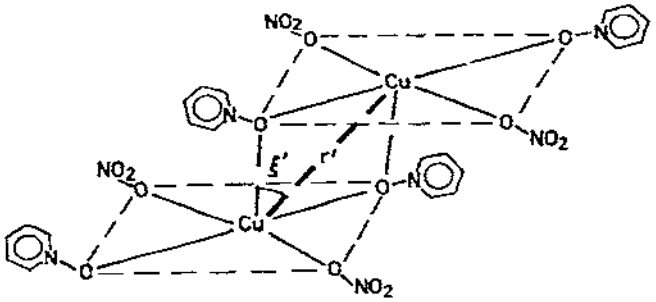

(I)

It has been suggested that other paramagnetic ions in the vicinity of a given transition metal ion can affect measured hyperfine parameters[101]. This additional contribution to the hyperfine field, produced when electrons localised primarily in the orbitals of one metal ion are transferred into the orbitals of the second transition or non-transition metal ion by a direct or indirect process, has been studied using the pyridine N-oxide copper(II) chloride complex doped into various metal chloride complexes of this ligand[102].

The crystal structure of bis-salicylaldehydato-copper(II) shows that although the coordination is basically planar, weak axial interactions with neighbouring molecules occur[16,17]. On recrystallisation from hot ethanol the modification containing the dimeric form where the bonding between neighbouring molecules occurs through the oxygen atoms is obtained. The relationship of the copper(II) ions in the dimeric complex is shown by structure II, whilst the structural parameters obtained from the triplet state EPR spectra of the complex[60a] are summarised by Table 9. It was concluded that the dimeric form of the complex which occurs in frozen solution is closely similar to that in the solid crystallised from hot ethanol solution.

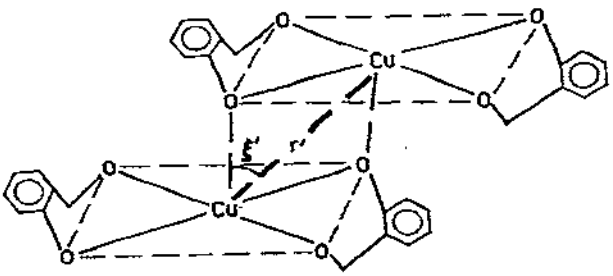

(II)

The molecular structure of crystalline copper(II) diethyldithiocarbamate may be described as a bimolecular unit in which each pair of centro-symmetrically related copper(II) ions at the rather short distance of 3.59 Å, share sulphur atoms as indicated by structure III[10b]. The geometry of the coordination of copper(II) here is closely related to a tetragonal pyramid with copper(II) having a coordination num-

System	g_x	g_y	g_z	$\cdot\cdot_x$	$\cdot\cdot_y$	$\cdot\cdot_z$					
				Units, 10^{-4} cm^{-1}			r (Å)	ξ^0	r (Å)	ξ'^0	J (cm^{-1})
Bis(pyridine-*N*-oxide)-copper(II) nitrate doped with the zinc complex at 77°K	$g_x = g_y =$ 2.040 ± 0.005		2.303 ± 0.005	$A_x = A_y = 10$ $A_x = A_y = 10$		140 (ref. 60)	3.46 + 0.05	41 ± 1 (ref. 60a)	3.46	41 (refs. 14,15)	+30 (ref. 21)
Bis (salicylaldehydato)-copper(II) in chloroform at 77°K	$g_x = g_y =$ 2.025 ± 0.005		2.265 ± 0.005	$A_x = A_y = 10$		150 ± 5	4.05 ± 0.05	30 ± 2 (ref. 60a)	4.05	28 (refs. 16, 17)	
Copper(II) diethyldithiocarbamate doped with the zinc complex at 77°K	2.020 ± 0.005	2.015 ± 0.005	2.070 ± 0.005	27	7	148	3.85 ± 0.05	42 ± 2 (ref. 60a)	3.59 3.54 (Zn complex)	41 (ref. 10b)	+24 (refs. 19, 20)
Copper(II) *d l*-tartrate in water–glycol solution at 77°K	$g_x = g_y =$ 2.060 ± 0.005		2.278 ± 0.008	$A_x = A_y = 30$		178	3.77 ± 0.05	29 ± 1 (ref. 60a)	2.99	31 (ref. 18)	−18 (ref. 18)
Copper(II) salen in chloroform–toluene solution at 77°K	$g_x = g_y =$ 2.055 ± 0.005		2.150 ± 0.005	$A_x = A_y = 20 \pm 5$		205 ± 5	4.55 ± 0.05	40 ± 5 (ref. 107)	3.18	39 (refs. 104–106)	−20 (ref. 24)
Copper(II) dimethylglyoxime in ethanol solution at 77°K	$g_x = g_y =$ 2.010 ± 0.005		2.110 ± 0.005	$A_x = A_y = 10$		175 ± 5	4.47	40 ± 1 (ref. 110)	3.88 $\eta = 23°$	50	−20 [a]
Vanadyl (++)-tartrate in 50% water–glycol solution at 77°K	1.955	1.965	1.945	$A_x = A_y = 36$		146.5	4.08	28 (ref. 113)	4.08	28 (ref. 12)	
Vanadyl (±)-tartrate in 50% water–glycol at 77°K							4.18	0–10 (ref. 113)	4.35	3 (ref. 112)	

[a] Value used in EPR simulation program.

TABLE 9

Structural data for porphyrin dimers

Porphyrin	Interplanar distance (Å)		Metal ion – metal ion separations (Å)	Method
NiDADPIXDME	ca. 3.5	(ref. 114)	3.77 (Ni–Ni)	X-ray
Porphine	3.4	(ref. 115)		X-ray
Cop. TME	7.5 – 8.5	(ref. 115)		NMR ($CHCl_3$)
M PIXDME	10	(ref. 116)		NMR ($CHCl_3$)
Ni MPIXDME	7.9	(ref. 116)		NMR ($CHCl_3$)
Cu Uro(III)			3.5 (ref. 57)	EPR (NH_3)
Cu PP			4.3 (ref. 42)	EPR (DMF)
CuDPIX DMR			3.9 (ref. 56)	EPR ($CHCl_3$)
Cu PPIX DME			3.7 (ref. 56)	EPR ($CHCl_3$)
Cu DPIX DBE			3.9 (ref. 56)	EPR ($CHCl_3$)
Cu HMPIX DME			3.9 (ref. 56)	EPR ($CHCl_3$)
Cu DBrDPIXDME			4.4 (ref. 56)	EPR ($CHCl_3$)
VO DPIX DME			3.4 (ref. 56)	EPR ($CHCl_3$)
VO DPIX DBE			3.5 (ref. 56)	EPR ($CHCl_3$)
VO PPIX DME			3.5 (ref. 56)	EPR ($CHCl_3$)

DADPIXDME = 2,4-diacetyldeuteroporphyrin IX dimethyl ester
Cop. TME = coproporphyrin tetramethyl ester
MPIXDME = *meso*-porphyrin IX dimethyl ester
Uro(III) = uroporphyrin III
DPIXDME = deuteroporphyrin IX dimethyl ester
PPIXDME = protoporphyrin IX dimethyl ester
HMPIXDME = haematoporphyrin IX dimethyl ester
DBrDPIXDME = 2,4-dibromo-deuteroporphyrin IX dimethyl ester
PP = protoporphyrin IX

ber of five with normal bonds to four sulphur atoms and a longer bond to a sulphur atom of the centrosymmetrically related molecule. On the other hand, in zinc(II) diethyldithiocarbamate (structure IV) each pair of centrosymmetrically related zinc atoms share sulphur atoms in a distorted trigonal bipyramidal environment (r' = 3.54 Å)[10c]. In addition the ligand molecule behaves in two ways in the same complex; one ligand forms a four-membered chelate ring and a second coordinates with two different zinc(II) ions while at the same time completing a chelate ring with a

long approach distance. The four shortest bonds formed by any zinc(II) ion are directed to the corners of a distorted tetrahedron with the ligand molecules planar. In the dimeric unit formed by zinc(II) dimethyldithiocarbamate the zinc(II) – zinc(II) distance[11] is 3.97 Å. The dimethyldithiocarbamate groups deviate slightly from planarity and again two types of linking are discerned. One group is chelated directly to its own zinc(II) ion tetrahedron while two of the second type act as bridging ligands between the two zinc(II) tetrahedron. Thus the structural form of the dimeric zinc(II) diethyldithiocarbamate is sufficiently different from that of the copper(II) complex to raise the possibility that doping with the zinc complex might bring about some structural modification of the copper(II) dimeric complex. The results obtained from the EPR triplet state spectra due to the copper(II) complex doped into the zinc complex are summarised in Table 8, from which it was concluded that the copper(II) ions are located in sites closely similar to the pure compound but that there is an increased copper(II)–copper(II) separation. EPR experiments on copper(II)-doped nickel(II) diethyldithiocarbamate gave no evidence of dimer spectra.

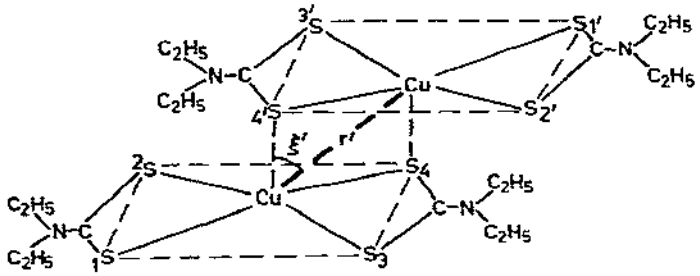

(III)

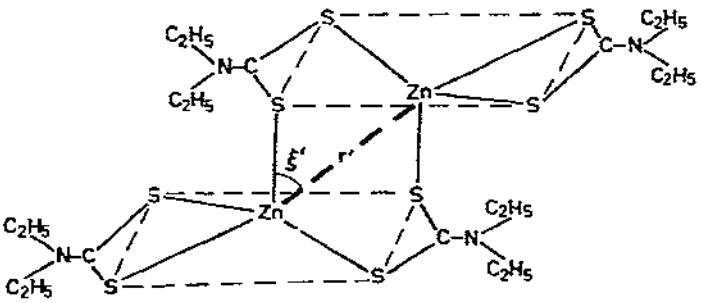

(IV)

X-ray crystal structure determination of the tartrate complex $Na_2Cu[(\pm)\text{-}C_4O_6H_2] \cdot 5H_2O$ shows that the structure exists as an assembly of centrosymmetric dimers[18]. However, X-ray structural information available on copper(II) *meso*-tartrate and copper(II) (+)-tartrate shows that the dimeric form of the complex depends markedly on the isomeric form of the ligand[11]. The complex obtained from the *meso* form is orthorhombic, involving copper(II) ions joined into chains by

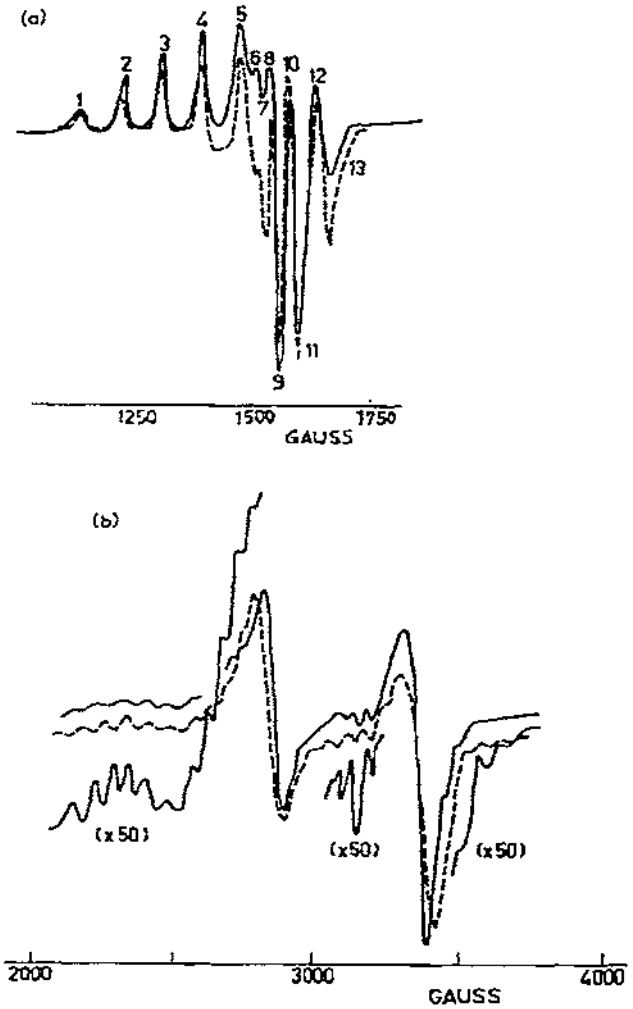

Fig. 17. X-band EPR spectrum[60] due to 0.2 *M* solution of $Na_2Cu[(\pm)C_4O_6H_2].5H_2O$ in ethylene glycol–water. Microwave frequency 9081 MHz, temperature 77°K. (a) $\Delta M_s = \pm 2$ spectrum, (b) $\Delta M_s = \pm 1$ spectrum. Computer simulated spectrum (- - -) obtained with following parameters: $r = 3.77 \pm 0.05$ Å, $\xi = 29 \pm 1°$, $g_x = g_y = 2.060 \pm 0.005$, $g_z = 2.278 \pm 0.005$, $A_x = A_y = 0.003$ cm^{-1}, $A_z = 0.0178 \pm 0.0010$ cm^{-1}, $W_x = W_y = W_z = 8$ gauss ($\Delta M_s = 2$) 18 gauss ($\Delta M_s = 1$), $J = -18$ cm^{-1}.

chelate linkages from the hydroxy and carboxyl oxygen atoms such that the internuclear copper(II)–copper(II) ion separation is 6.065 Å. For the complex synthesised from the (+)-form of the tartrate, the structure is monoclinic with two crystallographically independent copper(II) ions in an asymmetric unit linked together by two similarly independent tartrate groups to form the dimeric complex which has an internuclear separation of 5.42 Å.

The EPR spectrum of the disodium copper(II) (±)-tartrate has been reported and found to provide evidence for the presence of triplet state phenomena[61,103]. A semi-empirical approach was used to extract structural information about the dimeric species[61]. The results of a more recent treatment of the data[60a] are summarised in Table 8 and experimental and computer-simulated spectra are shown in Fig. 17.

Copper(II) Schiff-base complexes provide a further opportunity to compare structural data deduced from X-ray diffraction studies[104–106] with similar information obtained from EPR spectra by taking into account the symmetry properties of the dimer[107]. The Schiff-base complexes studied include *N*, *N'*-ethylenebis(salicylideneiminato)copper(II) (copper(II) salophen), *N*, *N'*-phenylenebis(salicylideneiminato)-copper(II) (copper(II) salen) and bis (*N*-methylsalicylaldiminato)copper(II) (copper(II) metal), whose structures have been determined by X-ray methods. The results obtained for copper(II) salen are summarised in Table 8. A crystal structure study of the chloroform adduct of copper(II) salen indicates an increase in the out-of-plane Cu—O bond to 2.79 Å, from 2.41 Å observed in copper(II) salophen[108]. In the *p*-nitrophenol adduct, the *p*-nitrophenol makes a similar, but much stronger, bond with the ligand oxygen atoms and the dimer bond is further weakened to the point where it is no longer considered to exist. Under these circumstances the chelate molecules are stacked plane-to-plane to form chains[109], successive molecules being separated by approximately 3.5 Å. The major structural effect brought about by the isolation of the dimer unit in the host lattice formed by the organic solvent is an increase in the copper(II)—copper(II) distance though the overall symmetry of the pair system is unchanged. It was proposed that in each case the dimeric unit of the Schiff-base chelates is formed by an alignment of parallel planes similar to that observed in the pure complex, but that the planes of the chelates are further apart. The faces holding the components of the dimer together were suggested to arise from π—π interactions of the multiple bond system which comprise the chelates. Such a proposal explained the following:

(1) In each case the dimer occurs only to a minor extent.

(2) The proportion of dimer formed in copper(II) salophen is greater than for copper(II) salen, the former possessing an extra π system in the bridging portion of the ligand.

(3) The distance between the copper(II) ions is insensitive to the change from phenolic oxygen to imine nitrogen.

Similar EPR studies on the dimer formed by copper(II) dimethylgloxime in ethanol showed, as indicated in Table 8, that again the effect of isolating the dimer unit in the host lattice of frozen ethanol is to increase the copper(II)—copper(II) separation[110a]. However, in this case the increase is not so great. The internuclear copper(II)—copper(II) separation observed in the dimer form in frozen ethanol is compatible with this distance estimated by means of space-filling molecular models such that it was considered that the somewhat shorter distance observed in the pure complex arises from crystal packing effects[110b,c].

The crystal structure of vanadyl *dl*-tartrate has been reported[112], while the crystal structure determination of ammonium vanadyl *dd*-tartrate has shown that the tetragonal crystals contain isolated ammonium ions, water molecules, and dimeric vanadyl tartrate units[112]. An EPR study of these complexes formed in 50% water–ethylene solution shows that the dimeric forms of these complexes persist and the parameters obtained from their triplet state spectra are summarised in Table 8, where it can be seen that the structural parameters obtained from EPR data are little different from those of X-ray diffraction data[113].

Hatfield and Lund[60b] have recently reported results for the copper(II) dimers of diethyldithiocarbamate, tartrate, dimethylglyoxime and salophen which are in marked disagreement with the work already described in this section[60a,107,110a]. In principle there is no reason why their approach to this problem, where the states are described in terms of the total electron spin, should not yield the same computer-simulated curves as those of Boyd et al.[60a]. However, for lower than axial symmetry dimers, Lund and Hatfield have ignored the $E(S_x^2-S_y^2)$ term, which must be included in the calculations at the beginning. It is not, therefore, surprising that their results not only disagree with those of Boyd et al.[60a] and Toy et al.[107,110a] in every case, but that they do not fit in with the structural information about these complexes which of course proved to be of considerable value in interpreting the EPR data for all these compounds.

It is also noted that Lund and Hatfield[60b] have assumed the general validity of Bleaney and Bowers' formula, eqn. (46), in postulating a significant contribution to D; however, this cannot influence genuine structural conclusions, but ultimately only estimates of r. As discussed by Boyd et al.[60a], eqn. (46) is certainly not correct as it based on too naive a view of the coupling of excited states of the copper(II) configurations. These pseudo-dipolar contributions are found to be unimportant in the work of Boyd et al.[60a], where the structures deduced from EPR are in agreement with those from X-ray data.

G. COPPER(II) AND VANADYL PORPHYRINS AND PHTHALOCYANINES

(i) Porphyrins

A number of investigations have revealed that the process of aggregation is ubiquitous amongst the metalloporphyrins. Crystallographic data provide important information on the mode of packing of the metalloporphyrins in the solid phase and the closest approach of the metal ions[8,114]. The formation of aggregates of the free base or metalloporphyrin in solution has been the subject of a number of investigations leading in most cases to the separation and in certain instances the relative orientation of the porphyrin molecules. Techniques involved include PMR spectroscopy[115,116], optical rotatory dispersion, circular dichroism and differential absorbance mea-

surements[116–120], circular dichroism and magnetic circular dichroism[121] and EPR spectroscopy[41,56,57,122,123]. Thus, the wealth of available information points to the fact that aggregation of porphyrin molecules and related systems when present as the free base or the chelate takes place such that the distance between the planes is variable and dependent on the nature of the substituents attached to the macrocyclic system. The metal ion—metal ion separations in some dimeric copper(II) and vanadyl porphyrins obtained from EPR data have been compared with distances obtained from X-ray and PMR techniques and the results of these comparisons are summarised in Table 9.

The distances obtained from EPR data are decidedly smaller than those obtained from PMR data, which were thought to be influenced by interactions between the side chains which allegedly prevent a closer approach than about 8 Å. Such disparity between the two sets of data is shown more clearly by consideration of the study[57] on uroporphyrin III, which is a copper(II) containing porphyrin with four acetic acid and four propionic acid substituent groups compared with four methyl and four propionic acid groups in coproporphyrin. The distance of 3.5 Å between the copper(II) ions was thus found in a case involving a greater degree of steric hindrance. It would appear that the approximations inherent in the ring current calculations involved in the PMR studies to determine the shielding of a proton on one ring due to another in close proximity on the other macrocyclic system give values of the interplanar distance which are too large by a factor of about two. The main source of error appears to arise from uncertainties concerning the values of the porphyrin ring current, especially when out-of-plane protons are being considered.

The major contribution to the binding force responsible for dimer formation in these systems is made by electrostatic dipole—dipole interactions. This was suggested for several reasons: (1) Symmetrically substituted porphyrins such as tetraphenylporphine do not form significant amounts of dimeric species; (2) the crystal structure of nickel(II) 2, 4-diacetyldeuteroporphyrin IX dimethyl ester reveals that the molecules are stacked in the head-to-tail fashion expected from the orientation of dipoles; (3) the fine structure observed in the PMR studies enables the relative configuration of the rings to be determined and in the porphyrins related to deuteroporphyrin IX dimethyl ester, such as 2-methyl-4-ethyldeuteroporphyrin IX dimethyl ester, the configuration indicated structure V is proposed[124]. Caughey et al.[125,126] have pointed out that the extent of dimer formation which is sensitive to the electron-withdrawing character of substituent groups can be explained by the concept that the stronger the electron-withdrawing character of a particular substituent group, the greater the molecular dipole will become, leading to stabler dimeric forms. In the copper(II) porphyrins, the distance between the metal ions in the dimeric species varies over a small range (ca. 3.5 – 4.5 Å). This variation may be explained by consideration of the steric repulsions between the 2,4- substituent groups on one porphyrin ring system with those of the neighbouring porphyrin rings or by a stag-

gering of one ring with respect to the other which effectively increases the distance between the metal ions. In the consideration of similar structural parameters of the vanadyl porphyrins, an additional complication arises from the fact that the vanadium atom may not be located in the plane of the ring but may lie up to about 0.4 Å out of the plane[127]. Therefore, longer intermetallic distances may be expected, such that if the ring systems were at their closest distance of approach (ca. 3.5 Å) the vanadyl–vanadyl ion separation could be ca. 4.3 Å. EPR data suggest that in the porphyrins studied the vanadium atoms lie in the plane of the porphyrin ring.

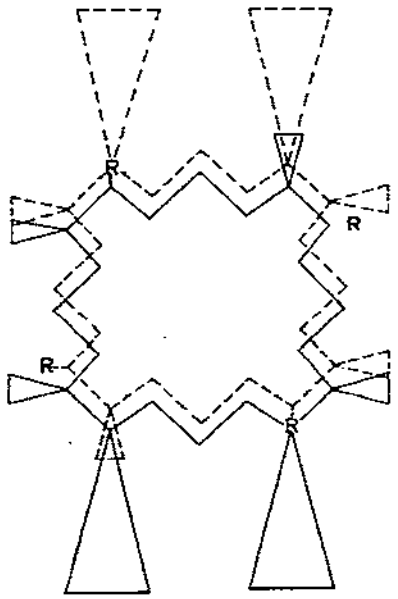

Structure V. Proposed structure of dimers formed by deuteroporphyrin IX derivatives in chloroform solution. Large triangles represent propionic acid groups and small triangles, methyl groups.

(ii) Phthalocyanines

A number of investigations have been concerned with the tendency of phthalocyanines and metallophthalocyanines to form aggregates in solution. The formation of dimeric as well as tetrameric water-soluble species by sulphonic acid derivatives of copper(II) phthalocyanine was reported by Alirens and Kuhn[128]. An EPR study of the copper(II) chelate of 3,4,4″,4‴-tetrasulphophthalocyanine did not provide definitive evidence of dimer formation, probably due to an unsuitable choice of solution condition[41]. The energetics of the dimerisation of 4,4′,4″,4‴-tetrasulphophthalocyanine (tspc) in aqueous solution has been investigated[129,130]. Dimerisation was found to be exothermic and, despite a decrease in entropy, is favoured energetically.

The dissociation process was analysed in terms of an electrostatic model involving charges separated by about 5 Å in the activated complex. This information combined with crystallographic data set the limits of separation of the planar molecules to lie between 3.38 and 5 Å in the dimer unit[130]. The visible spectra of argon matrix-isolated phthalocyanines has been studied and the results obtained from the more concentrated solid solutions were interpreted in terms of interactions in pairs[131]. The coupling of transition dipoles was involved to correlate the observed spectrum with copper(II) phthalocyanine pair configuration. Calculations with the use of non-bonded atom potentials were carried out to find the most stable relative orientation of the two molecules for various intermolecular distances. For distances between 4 and 5 Å the fully eclipsed "sandwich" configuration was most stable while at shorter distances the two planes were twisted to attain maximum stability. EPR measurements involving water–dimethylformamide solutions of the copper(II) and vanadyl chelates of 4,4′,4″,4‴-tetrasulphophthalocyanine carried out at room temperature and 77°K provide good evidence for the formation of dimers[132]. An important feature of this investigation was that it was found possible to control the amounts of mono, dimer and polymer forms of the chelates by manipulation of the relative amounts of water and dimethylformamide used as the solvent. The results of the investigation[132] are summarised by Table 10. The results indicate although copper(II) and vanadyl tspc dimeric chelates possess similar interplanar separations, their distribution of species amongst monomeric, dimeric and polymeric forms is different. Several studies of the dimeric tspc and metal chelates have been concerned with the formation of equilibrium constants for dimer formation[133]. From these studies the stability of the tspc dimers was found to be $Cu^{II} > H_2 > Fe > VO \sim Zn > Co$. The role of the metal ion in determining the instability of the dimer is thought to be due to competition between water molecules and phthalocyanine molecules for other phthalocyanine molecules such that the water molecules bond to the metal ion in the axial sites.

The nature of the forces responsible for dimerisation in planar compounds of this type has been the subject of a number of studies concerned mainly with thermodynamic considerations[134,135]. Factors contributing to the formation of aggregates in

TABLE 10

Copper(II) and vanadyl phthalocyanine dimers[32]

Chelate	$g_\parallel$	$g_\perp$	A (10^{-4} cm^{-1})	B (10^{-4} cm^{-1})	r (Å)
Cu tspc	2.20	2.04	200	20	4.3 ± 0.1
VO tspc	1.96	1.99	140	60	4.5 ± 0.1

aqueous solution include London dispersion forces between the readily polarisable aromatic systems on the phthalocyanine ring and water structure effects[135]. In the dimerisation equilibrium of the cobalt(II) tspc chelate the zero activation energy of dissociation indicates that in the course of separation of the constituents of the dimer to a distance corresponding to that in the activated complex the repelling and binding forces are approximately in balance. Using a simple electrostatic model the separation between the two parallel planes in the activated complex was estimated to be about 5 Å. This is close to the internuclear separation of 4.3 Å in the copper(II) chelate and 4.5 Å in the vanadyl chelate. The relevant distance in the dimeric cobalt(II) tspc chelate is very likely to be closely similar to these values. It seems clear that any movement of the planar molecules to the estimated separation in the activated complex would be small. This is in keeping with the findings of a zero activation energy of dissociation in the dimeric cobalt(II) tspc chelate.

H. HYDROXYCARBOXYLIC ACID CHELATES

EPR measurements have provided essential information on the structure of dimeric chelates formed by transition metal ion chelates of hydroxycarboxylic acids. The results obtained from these measurements[38,39] on the copper(II) chelates of simple aliphatic hydroxycarboxylic acids formed in both aqueous and non-aqueous solution are summarised in Table 11. The availability of information on the copper(II)–copper(II) distances in these systems immediately put in question earlier suggestions that the dimeric copper(II) citrate and malate formed in aqueous solution possessed similar structures involving the α-hydroxy group in bridging[136]. A structural formula for the malate dimer derived from molecular models and compatible with the observed 5.2 Å separation is depicted by structure VI. The hydroxy group is not ionised and the model suggests that, although long range interaction with one copper(II) ion could occur, the copper(II)–copper(II) separation is too great for the hydroxy group to play a part in the bridging. Hydrolysis of the copper(II) or ionisation of the hydroxy group on the ligand presumably generates the third proton. The important role of the hydroxy group in the structure is shown by the fact that the *O*-methyl malate copper(II) chelate is insoluble in all the solvents studied as is also the case for copper(II) tricarballylate. It is thought that the much shorter separation (3.1 Å) which occurs in aqueous solutions of the citrate can be achieved by a hydroxy group bridge as in structure VII. The dimeric form of copper(II) malate and citrate formed in non-aqueous solutions are structurally similar as shown by structure VIII.

Under conditions where all the hydrogen ions may be released from the copper(II) citrate and particularly in solvents such as propylene carbonate and trimethyl phosphate, a dimeric structure with a smaller copper(II)–copper(II) separation emerges as the main dimer form and is one in which the copper(II)–copper(II) separation is similar to that in structure VII.

TABLE 11

Magnetic and structural data for dimeric copper(II) hydroxy-carboxylates[39]

Ligand	Solvent	Triplet state transition	r (A)	$g_{\parallel}$	$g_{\perp}$
Citric acid	Water, pH 7–11 (ref. 38)	$\Delta M_S = \pm 1$	3.1	1.98	2.45
	DMF	$\Delta M_S = \pm 1$	5.2	2.00	2.20
	DMSO	$\Delta M_S = \pm 1$	5.2	2.00	2.20
	Ethanol	$\Delta M_S = \pm 1$	5.2	2.00	2.20
Malic acid	Water, pH 8.0	$\Delta M_S = \pm 1$	5.2	2.00	2.16
	DMF	$\Delta M_S = \pm 1$	5.2	2.00	2.20
	DMSO	$\Delta M_S = \pm 1$	5.2	2.00	2.20
	Ethanol	$\Delta M_S = \pm 1$	5.2	2.00	2.20
	Propylene carbonate	$\Delta M_S = \pm 1$	5.2	2.00	2.20
Mandelic acid	DMF	$\Delta M_S = \pm 1$	4.6	2.30	2.05
	DMSO	$\Delta M_S = \pm 1$	4.6	2.30	2.05
	Ethanol	$\Delta M_S = \pm 1$	3.3	2.30	2.05
Tartronic acid	Ethanol	$\Delta M_S = \pm 2$	4.5	2.30	2.05

* The value of A in each case was about 150×10^{-4} cm^{-1} and B about 20×10^{-4} cm^{-1}.

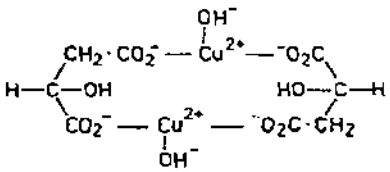

(VI)

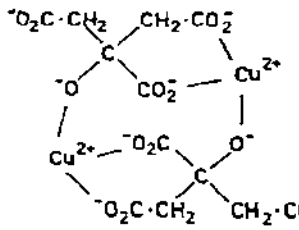

(VII)

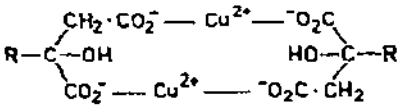

(VIII)

The structure for the copper(II) tartronate dimer formed in ethanol solution is shown by structure IX. Dimer formation by the copper(II) mandelate chelate is a

good example where two structures are possible. Thus, in ethanol the essential framework of the copper(II) mandelate dimer is shown by structure X. However, in DMF or DMSO the structure is best represented by XI. The increased separation is achieved by using one mandelate ion as a bridging group. However, with no further interactions, free rotation of the bridging group would result in a variable copper(II)–copper(II) distance. Molecular models indicate that for some orientations, other interactions involving the sharing of oxygen atoms of other ligand anions are possible. Structure XI shows one such arrangement.

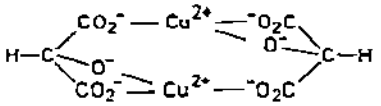

(IX)

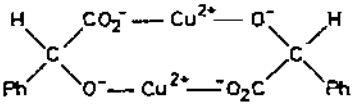

(X)

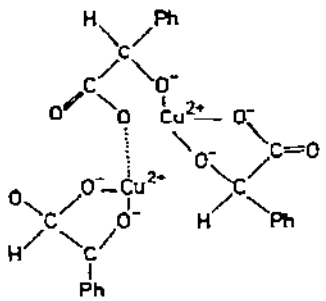

(XI)

The ability of aliphatic polyhydroxycarboxylic acids to form water-soluble complexes over a wide pH range accounts for the wide diversity of their uses and many investigations of the nature of the complexes formed in solution have been carried out. An EPR study of the copper(II) chelates formed by reaction with saccharin, lactobionic, gluconic and mucic acid[54] was made. Evidence was provided for the formation of dimeric as well as monomeric species, the relative proportions of each being dependent on pH conditions of the solution. A summary of the relevant magnetic parameters is given in Tables 12 and 13. The magnetic parameters observed for the dimeric copper(II) lactobionic acid complex suggest strongly that the individual ion site symmetry has changed from the axial symmetry observed in the monomeric form to one possibly with rhombic distortion or a tetrahedral form. The process of dimerisation also brings about a change in the parameters associated with the copper(II) gluconate chelate such that in the dimer $g_{\parallel} < g_{\perp}$ pointing to a compressed axial stereochemistry of the copper ion in the dimer[1].

A starting point for the elucidation of the structure of the dimeric species is provided by consideration of the functional groups which are common to the various

TABLE 12

Magnetic and structural data for dimeric copper (II) polyhydroxycarboxylates[54,a]

System	Transition	$g_{\parallel}$	$g_{\perp}$	A (10^{-4} cm^{-1})	B (10^{-4} cm^{-1})	r
Cu^{II} (0.1 *M*) + saccharic acid (0.1 *M*) pH 5.0	$\Delta M_S = \pm 1$	2.28 ± 0.01	2.05 ± 0.01	180 ± 20	10 ± 5	4.1 ± 0.1
	$\Delta M_S = \pm 2$	2.30 ± 0.01	2.08 ± 0.01	180 ± 20	10 ± 5	4.0 ± 0.2
Cu^{II} (0.1 *M*) + saccharic acid (0.1 *M*) pH 5.0	$\Delta M_S = \pm 2$	2.31 ± 0.005	2.06 ± 0.01	200 ± 10	6 ± 2	3.4 ± 0.1
Cu^{II} (0.1 *M*) + lactobionic acid (0.1 *M*) pH 11.1	$\Delta M_S = \pm 2$	2.09 ± 0.02	2.11 ± 0.01	40 ± 10	10 ± 5	3.9 ± 0.2
Cu^{II} (0.1 *M*) + lactobionic acid (0.1 *M*) pH 13.2	$\Delta M_S = \pm 2$	2.225 ± 0.005	2.02 ± 0.01	195 ± 5	10 ± 5	3.6 ± 0.1
Cu^{II} (0.1 *M*) + gluconic acid (0.1 *M*) pH 11.0	$\Delta M_S = \pm 2$	2.02 ± 0.01	2.11 ± 0.01	40 ± 20	10 ± 5	4.0 ± 2
Cu^{II} (0.1 *M*) + mucic acid (0.1 *M*), triethylamine (0.4 *M*) in DMF	$\Delta M_S = \pm 1$	2.24 ± 0.01	2.06 ± 0.01	200 ± 20	10 ± 5	3.9 ± 0.1
	$\Delta M_S = \pm 2$	2.29 ± 0.01	2.03 ± 0.01	200 ± 10	10 ± 5	4.0 ± 0.2

[a] Errors listed give range of parameters over which theoretical curves are compatible with the observed EPR lines.

TABLE 13

Magnetic data for monomeric copper(II) polyhydroxycarbalates

System	g values (± 0.002)	Hyperfine coupling constants $A \times 10^{-4}$ cm^{-1} ± 2 × 10^{-4} cm^{-1})
Cu^{II} (0.1 *M*) + saccharic acid	$g_z = 2.240$	$A_z^{63} = 195$ $A_z^{65} = 212$
(0.1 *M*), pH 13.3	$g_x = 2.050$	$A_x^{63} = 30$ $A_x^{65} = 32$
	$g_y = 2.054$	$A_y^{63} = 10 = A_y^{65}$
Cu^{II} (0.1 *M*) + lactobionic acid	$g_z = 2.258$	$A_z^{63} = 180$ $A_z^{65} = 192$
(0.1 *M*), pH 11.1	$g_x = 2.050$	$A_x^{63} = 30$ $A_x^{65} = 32$
	$g_y = 2.055$	$A_y^{63} = 10 = A_y^{65}$
Cu^{II} (0.1 *M*) + gluconic acid	$g_z = 2.270$	$A_z^{63} = 180$ $A_z^{65} = 192$
(0.1 *M*), pH 9.11	$g_x = 2.055$	$A_x^{63} = 20$ $A_x^{65} = 21$
	$g_y = 2.059$	$A_y^{63} = 10 = A_y^{65}$
Cu^{II} (0.1 *M*) + gluconic acid	$g_z = 2.239$	$A_z^{63} = 200$ $A_z^{65} = 214$
(0.1 *M*), pH 13.0	$g_x = 2.045$	$A_x^{63} = 35$ $A_x^{65} = 37$
	$g_y = 2.055$	$A_y^{63} = 10 = A_y^{65}$

ligands. Thus, gluconic and lactobionic acids each possess a single terminal carboxy group. Both give rise to dimeric chelates which have closely similar distances between the copper(II) ions. These distances are somewhat longer than the copper(II)—copper(II) separation of 3.1 Å observed in the dimeric form of the copper(II) complex of citric acid. A shorter separation can be achieved by a bridging structure involving the hydroxy group and carboxy group attached to the same carbon atom. The increased distance between the copper(II) ions could be accounted for by a bridging arrangement involving the terminal carboxy group and an ionised hydroxy group on the β-carbon atom. It was also found that dimer formation results from ionisation of the hydroxy groups. In some of the systems the shorter distances observed at higher pH's arise from a structural change of the dimer form, as evidenced in the case of lactobionic acid by a change in the values of $g_{\parallel}, g_{\perp}, A$ and r. Such shorter separations could also arise from an involvement of the ionised hydroxy group on the β-carbon atom.

The influence of substituent groups of the aromatic nucleus on dimer formation by copper(II) chelates of *o*-hydroxybenzoic acids has been studied by EPR measurements[49]. Ligands used include 5-sulphosalicylic acid, 5-chlorosalicylic acid, *p*-aminosalicylic acid, 2,4-, 2,5- and 2,6-dihydroxybenzoic acid. Structural variations of a different type were investigated by using 3,5-dihydroxybenzoic acid, salicylamide and *o*-phthalic acid. The results are summarised in Table 14. With 5-sulpho-

Magnetic and structural data for dimeric copper(II) chelates of hydroxy-benzoic acids[49]

System – $Cu^{II}ClO_4$ in DMF plus:	Transition	$g_{\parallel}$ ± 0.02	$g_{\perp}$ ± 0.02	A (10^{-4} cm^{-1})	B (10^{-4} cm^{-1})	r (A) ± 0.3 A	D (cm^{-1})
5-Sulphosalicylic acid, in water, pH 8.0	$\Delta M_S = \pm 1$	2.30	2.06	150	10	4.5	
5-Sulphosalicylic acid, $n = 1$	$\Delta M_S = \pm 1$	2.25	2.05	150	10	4.5	
5-Chlorosalicylic acid, $n = 1$	$\Delta M_S = \pm 1$	2.31	2.05	150	10	4.8	0.035
p-Aminosalicylic acid, $n = 1$	$\Delta M_S = \pm 2$	2.31	2.11	150	10	4.8	0.035
2,4-Dihydroxybenzoic acid, $n = 1$ or 2	$\Delta M_S = \pm 2$	2.31	2.11	150	10	4.8	0.035
2,5-Dihydroxybenzoic acid, $n = 2$	$\Delta M_S = \pm 2$	2.31	2.11	150	10	4.8	0.035
2,6-Dihydroxybenzoic acid, $n = 1$ or 2	$\Delta M_S = \pm 2$	2.31	2.11	150	10	4.8	0.035
3,5-Dihydroxybenzoic acid, $n = 1$							
species 1		2.35	2.07	*	*		0.23
species 2		2.35	2.07	*	*		0.35†
$n = 2$		2.35	2.07	*	*		0.35†
o-Phthalic acid, $n = 1$							
species 1		2.35	2.07	*	*		0.23
species 2		2.35	2.07	*	*		0.35†
$n = 2$							
species 1		2.35	2.07				0.35†
species 2	$\Delta M_S = \pm 2$	2.31	2.11	150	10	4.8	0.035
Salicylamide, $n = 1$	$\Delta M_S = \pm 2$	2.31	2.11	150	10	4.8	0.035

n = the number of moles of triethylamine added per mole of copper(II).
* Obtained by use of diagonalisation programme where hyperfine effects are not included.
† A range of values is possible here from $g_{\perp} \approx 2.03$ and $D \approx 0.32$ cm^{-1} to $g_{\perp} \approx 2.11$ and $D \approx 0.38$ cm^{-1}.

or 5-chlorosalicylic acid dimer formation takes place only in frozen solution and when one proton, presumably from the carboxyl group, has been released. With the amino group in the *para* position, dimer formation takes place at room temperature and in frozen solution with involvement of the carboxyl group and *o*-hydroxyl group. When 2,5-dihydroxybenzoic acid is used as the ligand two possibilities exist for binding of the copper(II), namely the involvement of either hydroxyl group along with the carboxyl group. The results are consistent with the view that the copper(II) is chelated by the carboxyl group and *o*-hydroxyl group. 2,6-Dihydroxybenzoic acid presents the case for two binding sites close to the carboxyl group and raises the possibility of the formation of polynuclear species where the state of aggregation would be greater than that of simple dimer formation. This possibility is realised when enough base is added to the system. When both hydroxyl groups are in the *meta* position as in 3,5-dihydroxybenzoic acid the dimer formed involves exchange coupling between the copper(II) ions.

When the binding site is provided by two carboxyl groups in close proximity as in the case of *o*-phthalic acid the monomer–dimer equilibrium mixture of copper(II) chelates is surprisingly complex and is a good example with which to illustrate the advantage offered by computer simulation techniques in locating such systems.

The formation of coordination compounds by the vanadyl ion has been the subject of many investigations which have included studies of the species formed by the interaction of the vanadyl ion with hydroxycarboxylic acids[137,138]. The identification of low-field lines occurring in the EPR spectra of vanadyl citrate provided clear evidence for the formation of dimeric species in that system. The EPR spectra of aqueous solution of vanadyl tartrate have received the attention of a number of workers with a measure of controversy as a result of their findings. A fifteen-line X-band EPR spectrum of the (±)-tartrate complex in aqueous solution at pH about 7 and a similar but more complicated X-band spectrum of the (++)-tartrate have been reported[139], the results being interpreted in terms of exchange-coupled vanadyl ion pairs. Because the fluctuations of the anisotropic component of the spin–spin interaction provide an effective spin relaxation process, the resonances of triplet states are not usually observed in solution. The observation of the EPR spectrum of an aqueous solution of vanadyl pyrophosphate at 25°C which consisted of a 22-line signal and interpreted as being due to the existence of trimeric species with a large antiferromagnetic exchange interaction has been reported[140,141]. Dunhill and Smith[71] observed the EPR spectra of vanadyl tartrates over a wide pH range and while unable to confirm the earlier results[139] noted the occurrence of satellite lines which Dunhill and Symons concluded arose from triplet state phenomena[72]. This conclusion was borne out later by calculations which indicated the presence of triplet–singlet transitions made weakly allowed due to large hyperfine coupling[73,74]. The triplet state spectra of a number of vanadyl binuclear complexes of α-hydroxycarboxylic acids had been reported, the *D* values being accounted for by simple magnetic dipole calculations[65]. A more sophisticated treatment of the

data[113], taking into account the symmetry properties of the vanadyl pair system in its tartrate chelates, has produced a set of structural parameters compatible with those derived from X-ray crystallographic data[111]. A similar treatment of the spectra obtained from the vanadyl citrate chelate at 77°K reveals that the vanadyl ion pair system in this chelate has lower than axial symmetry. An EPR study of the vanadyl ion separation in dimeric vanadyl 1-hydroxycyclohexanecarboxylate has been determined to be 3.6 Å which is comparable with that obtained[55] for similar chelates of copper(II).

Compared with copper(II) far fewer physicochemical investigations of titanium(III) chelates have been reported. Some of these studies have indicated that dimer formation takes place and magnetic susceptibility measurements have been reported in a few cases[142–144]. The EPR spectra of dimethylformamide solutions of titanium(III) complexes of a number of hydroxycarboxylic acids have shown evidence for the formation of dimeric species[53] and the results of this investigation are summarised in Table 15. The information obtained on the titanium(III)–titanium(III) separation was used to suggest possible structures for the dimeric species.

A property which is related to the ability of hydroxycarboxylic acids to form dimeric complexes is their propensity to form heterometal ion complexes[145–149]. An EPR study of the formation of heterometal ion hydroxycarboxylate chelates formed in non-aqueous solution was carried out to provide information on the structural implications involved in the formation of such complexes[50]. The solvent condi-

TABLE 15

Magnetic and structural data for dimeric titanium(III) chelates[53]

System – $TiCl_3$ (0.1 *M*) in DMF plus:	$g_{\parallel}$ ± 0.02	$g_{\perp}$ ± 0.01	r (Å)
Mandelic acid (0.3 *M*), $n = 6$	1.99	1.92	4.7
Malic acid (0.1 *M*), $n = 2$	1.99	1.92	5.6
Citric acid (0.1 *M*), $n = 3$ or 4	1.99	1.89	6.3
Cyclopentane-1,2,3,4 tetracarboxylic acid, $n = 2$ or 3	1.99	1.87	7.1
5-Chlorosalicylic acid (0.3 *M*), $n = 3$	1.97	1.92	6.5
p-Aminosalicylic acid (0.3 *M*), $n = 3$ or 6	1.99	1.92	6.5
Salicylamide, (0.3 *M*), $n = 3$	1.97	1.92	6.5
Phthalic acid (0.3 *M*), $n = 1$ or 2	1.97	1.92	6.5
8-Hydroxyquinoline (0.3 *M*), $n = 3$	1.99	1.95	8.6
5-Sulphosalicylic acid, $n = 6$	1.97	1.92	6.5
$n = 9$	1.99	1.93	5.5

n = the number of moles of triethylamine added per mole of titanium III.

tions in this study were designed to avoid complicated hydrolytic reactions in aqueous solution and to take into account the range of halide complexes which can be formed in non-aqueous solutions[150]. Thus, the possibility of heterometal ion chelate formation in dimethylformamide solution containing the ligand, copper(II), and a series of diamagnetic cations, namely aluminium(III), arsenic(III), zinc(II), cadmium(II), mercury(II) and dimethyltin(IV) was investigated. The ligands chosen were of varying complexity and included citric, malic and mandelic acid. Conditions were chosen such that the copper(II) and non-transition-metal cation competed for limited amounts of the ligand on addition of base to the system. The experiment was designed to provide answers to the following questions.

(1) In the competitive chelation of the metal ions, which will form the hydroxycarboxylate first?

(2) At what stage of base addition is each metal ion involved in chelate formation?

(3) Does the copper(II) hydroxycarboxylate at whatever stage it is formed give rise to dimeric species?

(4) If heterometal ion chelate formation takes place will this involve a simple species containing copper(II), diamagnetic cation and ligand or will more complicated species occur, possibly containing pairs of transition metal ions and diamagnetic cations?

All the evidence indicated that on addition of base the aluminium(III), antimony(III) and arsenic(III) chelates are formed first. In the remainder of the systems the copper(II) hydroxycarboxylate is formed first, except in the system involving dimethyltin(IV), where both chelates form on initial addition of base. However, in seeking the answer to the other questions it was found that the presence of the non-transition metal hydroxycarboxylate brings about an unexpected complexity in the

TABLE 16

Magnetic data for copper(II) heterometal ion hydroxycarboxylates[50]

System	$g_{\parallel}$ (± 0.01)	$g_{\perp}$ (± 0.01)	A (10^{-4} cm^{-1})	B (10^{-4} cm^{-1})
Cu^{II}, Al^{III}, citrate, n = 7 and 8	2.34	2.07	150	0
Cu^{II}, Hg^{II}, citrate, n = 7	2.34	2.07	150	0
Cu^{II}, Me_2Sn^{IV}, citrate, n = 4 to 8	2.30	2.07	160	0
Cu^{II}, Zn^{II}, mandelate, n = 4	2.37	2.06	166	0
Cu^{II}, Me_2Sn^{IV}, mandelate, n = 1—4	2.34	2.07	145	0

TABLE 17

Structural and magnetic data for heterometal ion polynuclear hydroxy-carboxylates[50]

System	Transitions observed	$g_{\parallel}$ (± 0.01)	$g_{\perp}$ (± 0.01)	A (10^{-4} cm^{-1}) (± 10)	B (10^{-4} cm^{-1}) (± 10)	r (Å) (± 0.3)
Cu^{II}, Al^{III}, citrate, $n = 6$	$\Delta M_S = \pm 1$ $\Delta M_S = \pm 2$	2.30	2.07	100	0	4.0
Cu^{II}, Al^{III}, malate, $n = 5$	$\Delta M_S = \pm 1$ $\Delta M_S = \pm 2$	2.28	2.07	120	0	4.3
Cu^{II}, As^{III}, malate, $n = 4$	$\Delta M_S = \pm 1$ $\Delta M_S = \pm 2$	2.38	2.10	150	0	3.4
Cu^{II}, Zn^{II}, mandelate, $n = 3, 4$	$\Delta M_S = \pm 1$ $\Delta M_S = \pm 2$	2.02	2.13	180	0	5.4
Cu^{II}, Me_2Sn^{IV}, mandelate	$\Delta M_S = \pm 2$	2.37	2.06 ± 0.05	140	20	2.9

distribution of chelate species. A property common to many of the systems is that the non-transition metal ion hydroxycarboxylate plays a role in the structure of the polymeric copper(II) chelates. The EPR data summarised in Tables 16 and 17 have been interpreted in terms of chelates containing uncoupled copper(II) arising from the formation of heterometal ion species and chelates containing coupled copper(II) in polymeric species[50]. Results obtained from the system containing copper(II) chloride, zinc chloride, mandelic acid and triethylamine provided clearcut evidence for a species containing both copper(II) and zinc present as their hydroxycarboxylates, and where magnetic dipole–dipole coupling between the copper(II) ions is maintained. The framework of a structure which takes into account the involvement of zinc and is compatible with the observed distance between the copper(II) ions is shown by structure XII. In this model the positioning of the zinc(II) and copper(II) in a puckered cyclic structure accounts for the copper(II)–copper(II) distance of 5.4 Å, which is a greater distance than that observed in the dimeric copper(II) mandelate above.

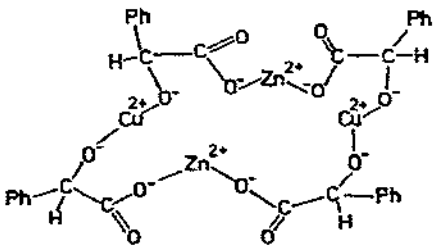

(XII)

I. AMINOPOLYCARBOXYLIC ACID CHELATES

The aminopolycarboxylic acids play an important role as reagents for metal ions in solution. Their usefulness arises from their possession of great chemical stability and their ability to convert metal ions quantitatively into their chelate forms. In this development ethylenediamine-tetraacetic acid (edta) has played a central role and stimulated interest in homologous compounds with increased affinity and selectivity for metal ions. Representative examples of these compounds are diethylenetriaminepentaacetic acid (dtpa)[151], triethylenetetraaminehexaacetic acid (ttha) and 3,6-dioxaoctane-1,8-diamine, *N*, *N*, *N'*, *N'*-tetraacetic acid (egta), where evidence has been presented for the formation of mononuclear, protonated mononuclear chelates and binuclear chelate compounds[152–157]. The structures of metal ion–polyaminocarboxylate chelates in solution and in the crystalline state have been the subject of a number of investigations[159]. A recent summary dealing with the nature and number of bonding sites in multidentate ligands reveals the general lack of information on the structures and conformations of metal complexes of multidentate ligands in solution[160]. An EPR study of the dinuclear copper(II) polyaminocarboxylate chelates formed by dtpa and ttha was undertaken to provide firm knowledge of the separation between the copper(II) ions[63], thus narrowing down the choice of possible structures. The range of values of each parameter used to achieve the fitting of the experimental curves is shown in Table 18. EPR measurements on solutions containing dtpa or ttha in 1 : 1 mole ratio showed that $\Delta M_S = \pm 2$ transitions could be observed at pH values of about 2.0 and 4.0, indicating that under these conditions some polynuclear chelate formation takes place, thus confirming the observations of the stability constant data[158].

The two major structural possibilities presented by the binding sites of ttha when forming a polynuclear complex are shown by structures XIII and XIV. In structure XIII the terminal groups bind the copper(II) ions and the ligand is an extended form

TABLE 18

Aminocarboxylic acid chelates

System	Transition	$g_\parallel$	$g_\perp$	$A \times 10^{-4}$ (cm^{-1})	$B \times 10^{-4}$ (cm^{-1})	$r \pm 0.5$ (Å)
Cu_2dtpa	$\Delta M_S = \pm 1$	2.30 ± 0.02	2.10 ± 0.02	140 ± 30	10 ± 5	5.5
	$\Delta M_S = \pm 2$	2.92 ± 0.01	2.10 ± 0.02	150 ± 30	10 ± 5	5.5
Cu_2ttha	$\Delta M_S = \pm 1$	2.42 ± 0.03	2.09 ± 0.03	150 ± 20	10 ± 5	5.5
	$\Delta M_S = \pm 2$	2.42 ± 0.02	2.09 ± 0.01	150 ± 20	10 ± 5	5.5
Cu_2egta (ref. 99)	$\xi = (77 \pm 5)°$ (dissimilar ions)	2.22 ± 0.01	2.05 + 0.01	140 ± 10	10 ± 5	4.0 ± 0.2

with free rotation about the central ethylene group and giving rise to a copper(II)–copper(II) separation larger than that found experimentally. Structure XIV, on the other hand, involves the bonding of each of the two central nitrogens to a copper(II) ion different from the one bound to the adjacent terminal nitrogen, leading to a closed form of the ligand. The more rigid framework gives rise to a separation of the copper(II) ions which is compatible with the experimentally determined distance. In a similar manner the sharing of the terminal group of dtpa by each copper(II) ion, as shown by structure XV, again places the copper(II) ions at a distance compatible with the experimental result.

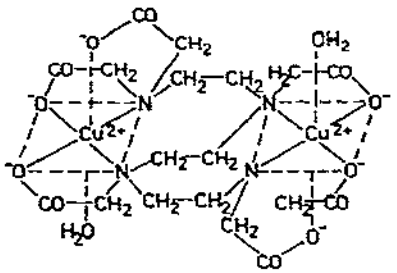

(XIII)

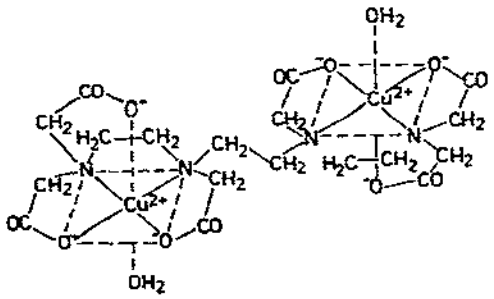

(XIV)

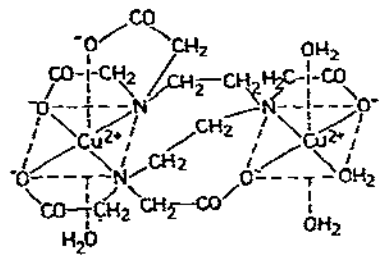

(XV)

In order to account for the salient features of the low field portion of the X-band EPR triplet state spectra due to the dinuclear copper(II) egta complex, computer line-shape simulation procedures designed to reveal the symmetry properties of the copper(II) pair system in the dinuclear complex by comparison of the experimental line-shape due to the $\Delta M_s = 2$ transitions with those computed on the basis of axial, orthorhombic or non-parallel axis symmetry of the pair system were carried out[161].

The results favoured a non-parallel axis alignment of the copper(II) ions at a separation of about 4.5 Å. A more recent theoretical development[98,99] has yielded a value of $r = 4.0 \pm 0.2$ Å. The details are given in Table 18 and the proposed structure of the dimer given by structure XVI.

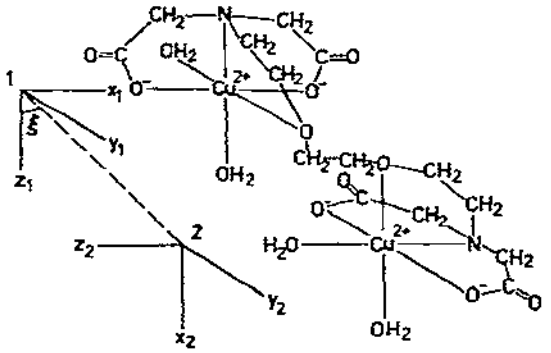

(XVI)

EPR studies[162] have proved the existence of mononuclear, dinuclear, heteronuclear and dimeric polyaminocarboxylates of titanium(III). The ligands studied include edta, egta, dtpa and ttha.

J. AMINE, AMINO-ACID AND PEPTIDE CHELATES

The X-band EPR spectra of titanium(III) trichloride in pyridine solution at room temperature and 77°K provide evidence to show that the molecular species formed in greatest amount is a dimeric form of the bis-pyridine-titanium(III) chloride complex which is characterised both in the liquid phase and at 77°K by triplet-state spectra. The observed spectra at 77°K are best accounted for by a model which takes into account the lowering of the dimer symmetry from axial. A structure XVII involving the sharing of an octahedral edge is compatible with the determination of the internuclear separation of the titanium(III) ions and their symmetry in the pair of system of the pyridine complex. Furthermore, the internuclear separation found at room temperature is closely similar to that obtained from frozen solution, indicating that the structure of the dimeric titanium(III) – pyridine complex is the same in liquid and frozen solution.

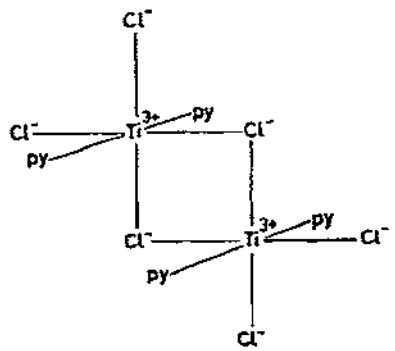

(XVII)

TABLE 19

Structural results for binuclear complexes of tetrakis (aminomethyl) methane[98,99]

Tetrakis(aminomethyl)methane complex with:	$I_1 = I_2$	r (Å)	ξ°	η°	$g_x = g_y$	g_z	$A_x = A_y$ (cm^{-1})	A_z (cm^{-1})	σ $\Delta M_s = \pm 1$ (gauss)	σ $\Delta M_s = 2$ (gauss)
Titanium (III)	0	4.5 ± 0.5			1.98 ± 0.01	1.99 ± 0.01				25 ± 5
Vanadyl	$\frac{7}{2}$	4.8 ± 0.5	50 ± 5	0	1.97 ± 0.01	1.98 ± 0.01	0.003 ± 0.001	0.014 ± 0.001		20 ± 3
Copper (II)	$\frac{3}{2}$	4.8 ± 0.5	40 ± 5	0	2.05 ± 0.01	2.27 ± 0.01	0.0010 ± 0.0005	0.014 ± 0.001	40 ± 10	17 ± 2

The EPR study of the structure of the dinuclear copper(II) complex of tetrakis (aminomethyl)methane was of particular importance in assessing the effect of a lowering of axial symmetry on the EPR triplet state spectra due to the pair system[62]. Here the spin conformation of the methylene groups ensures a fixed geometry of the terminal amino groups once they are part of the coordination sphere of each copper(II) ion. The circumstances of chemical combination allow the spatial arrangements of the two copper(II) ions to be closely defined by the molecular dimensions of the ligand, a fact which is of particular significance in helping to establish the validity of using the magnetic dipole–dipole interaction as a measure of the internuclear distance between the metal ions. The results of this investigation, along with a similar one carried out on the binuclear complexes of vanadyl and titanium(III), are summarised in Table 19. The value of r is closely similar for each dinuclear complex and is compatible with the internuclear separation of the metal ions as deduced from molecular models. Earlier results based on an incomplete theoretical model[58] have recently been superseded[98,99]. The later results are now discussed in detail.

A close inspection of molecular models of the binuclear metal ion chelates formed by tetrakis(aminomethyl)methane show there are three possible relative orientations of the metal sites. If the metal ion is considered to be a component of a six-membered ring containing it, the two nitrogen atoms, the two carbon atoms and the central carbon atoms (Fig. 18(a)), then one possible orientation of the metal ion sites with respect to the other is that for which both six-membered rings are in a chair configuration. The orientations of the axes is shown in Fig. 18(b). However, if it may be assumed that $g_x = g_y$ and $A_x = A_y$, then the x and y axes of both ions may be rotated about their respective z axes, and the symmetry reduces to the case where $\xi = 90°$ and $\eta = 0°$.

Another possible orientation of the two ions is shown in Fig. 19, where both six-membered rings take up boat configurations. If, however, we may again assume axial symmetry for each ion site, then we may rotate the x and y axes of ion 2, for example, and arrive at the monoclinic symmetry discussed in Section C.

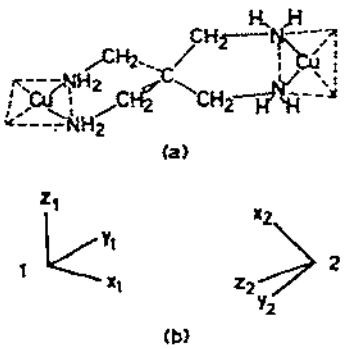

Fig. 18. (a) Possible structure of the binuclear complex of tetrakis(aminomethyl)methane and (b) related coordinates.

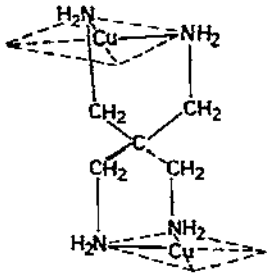

Fig. 19. Another possible structure of the binuclear complex of tetrakis(aminomethyl)methane.

The third and final arrangement is shown in Fig. 20. This arises when one six-membered ring is in a boat configuration and the other is in a chair configuration. The actual orientation of the metal ions is shown in Fig. 20(b). However, if as before we assume axial symmetry for the two ion sites, rotation of the x and y axes in each case leads to the symmetry arrangement in Fig. 20(c), which is similar to that arising from Fig. 18 except that $\xi \neq 90°$.

Computer simulation of the experimental lineshape showed that a reasonable fit to the $\Delta M_s = \pm 2$ and $\Delta M_s = \pm 1$ transitions was obtained with the parameters in Table 19 using the symmetry model in Fig. 20.

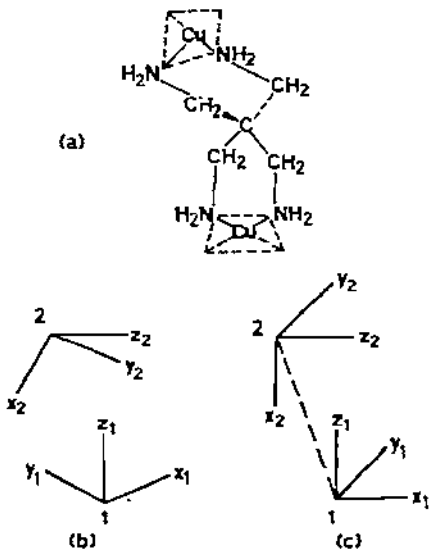

Fig. 20. (a) A further possible structure of the binuclear complex of tetrakis(aminomethyl)-methane and (b) related coordinates; (c) coordinates when copper(II) site symmetries are assumed to be axial.

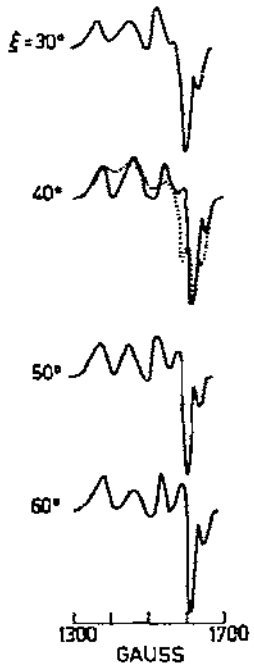

Fig. 21. $\Delta M_s = \pm 2$ spectra based on Fig. 20 symmetry to illustrate effect of variation in ξ. $r = 4.8 \pm 0.2$ Å, $g_z = 2.27 \pm 0.01$, $g_x = g_y = 2.04 \pm 0.01$, $A_z = 0.014 \pm 0.001$ cm^{-1}, $A_x = A_y = 0.0010 \pm 0.0005$ cm^{-1}, $\sigma = 17 \pm 2$ gauss, $\eta = 0°$, $\nu = 9.140$ GHz. The best fit occurs for $\xi = (40 \pm 5)°$. · · · · · ·, Experimental curve[36].

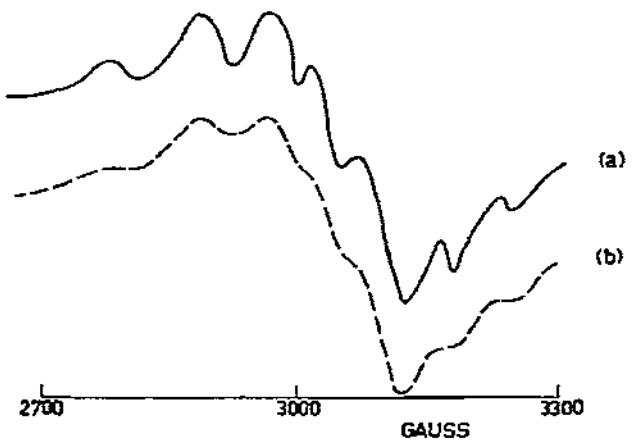

Fig. 22. (a) Computer-simulated $\Delta M_s = \pm 1$ lineshape for copper(II) binuclear complex of tetrakis(aminomethyl)methane. Parameters as in Fig. 14 with fits in range $\xi = 40 \pm 10°$, $\sigma = 40 \pm 10$ gauss. (b) Experimental spectrum.

The EPR spectra obtained from frozen solutions of the copper(II) complex of 2-hydroxy-*N*-(2-hydroxyethyl)ethylamine is consistent with the formation of dimeric species in which the copper(II)—copper(II) is about 5 Å, and where the pair system possess axial symmetry[42]. A structure for the 1 : 1 complex shown by structure XVIII shows each copper(II) bond by the terminal amino group and the oxygen of the hydroxyethyl group with the other hydroxyethyl group involved in bridging. An interesting feature of this arrangement is that the dimer structure of the *N*,*N*-bis(2-hydroxyethyl)glycinate complex can be envisaged as forming by substitution of the hydrogen on the nitrogen by the $CH_2.CO_2^-$ group which coordinates to the copper(II) ion and leaves the bridging arrangement unchanged. The EPR spectra[48] of copper(II) tris(hydroxymethyl)aminomethane complexes in aqueous and non-aqueous solution provide evidence of the formation of dimeric species in which the copper(II)—copper(II) internuclear separation is larger than anticipated from an earlier proposal of structure based on intuition rather than structural data[163]. The similarity of the spectra obtained from aqueous and non-aqueous solutions of the copper(II) complexes suggest that complexes of the same structure are formed under both circumstances. By consideration of molecular models, structures compatible with the observed distances in the 1 : 1 and 1 : 2 complexes were proposed and are shown by structures XIX and XX respectively. A survey of the EPR spectra of aqueous solutions containing the copper(II) complexes of glutamic and aspartic acids, leucine, threonine, L-histidine and tyrosine did not provide any evidence of dimer formation at room temperature or in frozen solution.

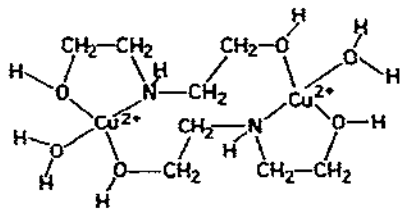

(XVIII)

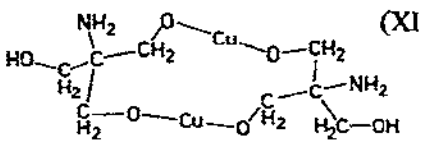

(XIX)

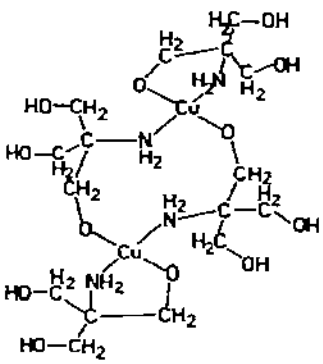

(XX)

EPR studies have been made of several copper(II) peptides[40]. In the case of the copper(II) complexes of glycylglycine, diglycylglycine and β-alanyl-L-histidine and its derivatives, dimers are observed in frozen aqueous solutions. The relevant structural and magnetic parameters are outlined by Table 20, which includes data for the 2 : 1 copper(II) L-cystinyl-bisglycinate complex. The crystal structure of the sodium salt of copper(II) diglycylglycinate monohydrate shows that the complex is dimeric with the terminal carbonyl group involved in bridging[164]. For this reason it was

TABLE 20

Magnetic and structural data for copper(II) peptide dimers[40]

Ligand	r (Å)	$g_{\parallel}$	$g_{\perp}$	$A \times 10^{-4}$ (cm^{-1})	$B \times 10^{-4}$ (cm^{-1})
Glycylglycine	5.0	2.26	2.05	160	40
Glycylglycine and imidazole	4.6 – 5.0	2.26	2.05	160	40
Diglycylglycine	4.6 – 5.5	2.19 – 2.20	2.03	160	20 – 70
β-Alanyl-L-histidine	5.0	2.20	2.05	160	30
β-Alanyl-L-3-methylhistidine	5.1 – 5.4	2.20	2.05	140	20
β-Alanyl-L-1-methylhistidine	4.6 – 5.4	2.20 – 2.24	2.03 – 2.05	160	30 – 35
L-Cystinyl-bisglycine	4.0 – 5.2	2.00	2.13	150	20

suggested that the copper(II) glycylglycine dimer formed in frozen aqueous solution involves bridging by the terminal carbonyl group with the amino and peptide nitrogen atoms in a planar arrangement around the copper(II). Even so, many conformations of the dimer are possible. The choice of a likely arrangement may be based on one which allows water molecules to occupy vacant sites unoccupied by the ligand anion and one in which additional interactions can occur, possibly by the sharing of atoms or groups already bound to one of the copper(II) ions. One such arrangement is shown by structure XXI, where the overall configuration is V-shaped.

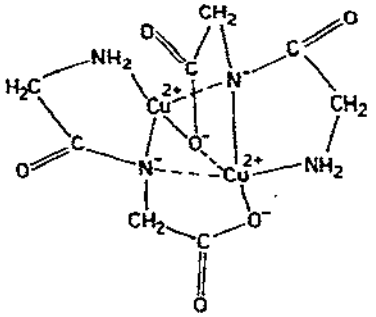

(XXI)

The copper(II) complex of glycylglycine is capable of combination with imidazole[165,166] and the EPR data are consistent with dimer formation in frozen solution under these circumstances. The copper(II)–copper(II) separation is altered little from that observed in the absence of imidazole, which presumably serves to occupy coordination positions previously taken up by water.

The X-ray structures of the copper(II) complexes of diglycylglycine depend on the pH at which they are formed[164]. For the complex formed in alkali media, dimeric units whose structure is shown by structure XXII occur. The EPR data indicate that the copper(II)–copper(II) separation in the complex formed in frozen solution would be compatible with that shown by structure XXII.

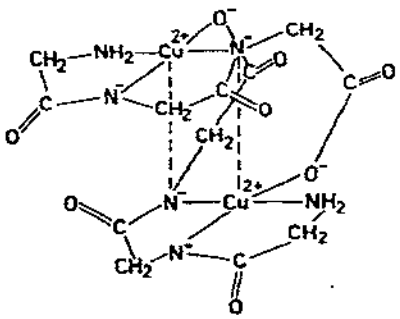

(XXII)

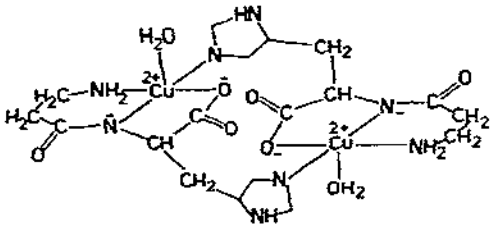

(XXIII)

The EPR spectrum of the copper(II) complex of β-alanyl-L-histidine shows that dimer formation occurs only in frozen solution and that the copper(II)—copper(II) separation is compatible with that found from X-ray structural studies, as indicated by structure XXIII[167]. A proton magnetic resonance study of the copper(II) complex of β-alanyl-L-histidine outlined the nature of the species formed at room temperature[168].

From the point of view of considering a model for copper(II)—copper(II) interactions in proteins, the EPR spectrum of the copper(II) complex of L-cystinyl-bisglycine has been studied[169]. In a re-investigation of this system it was established that the EPR data are consistent with a dipole–dipole coupling of copper(II) ions arising in structure XXIV[40]. The triplet state EPR spectrum due to a dinuclear molybdenum(V)–glutathione complex has been reported[170]. Inspection of the salient features of the spectrum in the light of the concepts put forward to discern the symmetry of the dinuclear complex from its EPR spectrum, indicated that the spectrum could arise from a lower than axial arrangement of the molybdenum(V) ion sites. A close fit to the experimental spectrum was obtained using the following values of the parameters: $g_{\parallel} = 1.97 \pm 0.005$, $g_{\perp} = 1.96 \pm 0.002$, $r = 5.0 \pm 0.2$ Å and $\xi = 70 \pm 5°$. The parameters of chief interest are ξ and r, and a structure compatible with their values is XXV.

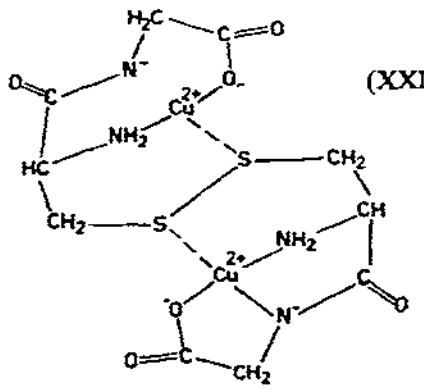

(XXIV)

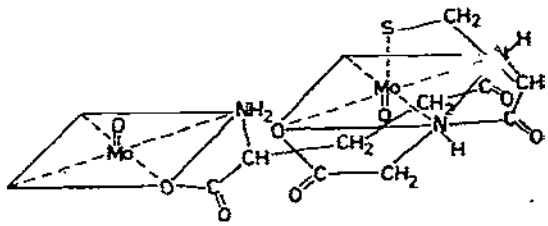

(XXV)

An EPR study of the formation of mixed-ligand chelates of copper(II) with amino acids and certain 3, 4-dihydroxyphenols showed that copper(II) forms monomeric complexes with 5, 6-dihydroxybenzene-1,3-disulphonate (Tiron) or

TABLE 21

Magnetic and structural data for copper(II) dihydroxyphenol dimers formed in aqueous solution

System	Transition	$g_{\parallel}$	$g_{\perp}$	$A \times 10^{-4}$ (cm^{-1})	$B \times 10^{-4}$ (cm^{-1})	r (Å)
Cu^{II} : Tiron, 1 : 1, pH 3.5	$\Delta M_S = \pm 1$	2.22 ± 0.02	2.12 ± 0.05	150 ± 50	10	6.0 ± 1.0
	$\Delta M_S = \pm 2$	2.20 ± 0.02	2.10 ± 0.02	150 ± 20	10	6.0 ± 1.0
Cu^{II} : Tiron: threonine, 1 : 1 : 1, pH 6.0	$\Delta M_S = \pm 1$	2.45 ± 0.03	2.11 ± 0.01	125 ± 25	10	6.0 ± 1.0
	$\Delta M_S = \pm 2$	2.45 ± 0.03	2.11 ± 0.01	150 ± 20	10	6.0 ± 1.0
Cu^{II}: Tiron: glycine, 1 : 1 : 1, pH 6.0	$\Delta M_S = \pm 1$	2.45 ± 0.03	2.11 ± 0.01	175 ± 25	10	6.0 ± 1.0
	$\Delta M_S = \pm 2$	2.46 ± 0.02	2.11 ± 0.01	175 ± 25	10	6.0 ± 0.5
Cu^{II} : adrenaline : threonine, 1 : 1 : 1, pH 6.0	$\Delta M_S = \pm 1$	2.30 ± 0.01	2.06 ± 0.01	180 ± 20	10	6.0 ± 0.5
	$\Delta M_S = \pm 2$	2.30 ± 0.05	2.07 ± 0.02	150 ± 25	10	6.0 ± 0.05
Cu^{II} : 3,4-dihydroxyphenyl-alanine:threonine, 1 : 1 : 1, pH 6.0	$\Delta M_S = \pm 1$	2.30 ± 0.01	2.06 ± 0.01	150 ± 50	10	6.0 ± 0.5
	$\Delta M_S = \pm 2$	2.30 ± 0.05	2.06 ± 0.01	150 ± 25	10	6.0 ± 0.5
Cu^{II} : noradrenaline:threonine, 1 : 1 : 1, pH 6.0	$\Delta M_S = \pm 1$	2.30 ± 0.01	2.06 ± 0.01	150 ± 50	10	6.0 ± 0.5
	$\Delta M_S = \pm 2$	2.30 ± 0.05	2.07 ± 0.01	150 ± 25	10	6.0 ± 0.5

3,4-dihydroxyphenylalanine. The addition of simple amino acids, such as glycine or threonine, to aqueous solutions containing the copper(II) chelates of 3,4-dihydroxyphenols, increases the solubility of the latter as a result of the formation of mixed-ligand complexes which are monomeric in aqueous solution. The observations of $\Delta M_s = \pm 1$ and $\Delta M_s = \pm 2$ transitions indicated the formation of dimeric species in frozen aqueous solutions of these complexes. The magnetic parameters obtained by computer lineshape simulation of the observed EPR spectra[45] are summarised in Table 21.

A structure which is compatible with a distance of about 6 Å between the copper(II) ions in the case of the copper(II)—Tiron—glycine or —threonine complex is structure XXVI. The mixed-ligand copper(II)—threonine-3,4-dihydroxyphenylalanine, —adrenaline, —*N*-noradrenaline complexes have the same basic structure, though the changes in the *g* values suggest some interaction of copper(II) with the side-chain amino or carboxy groups.

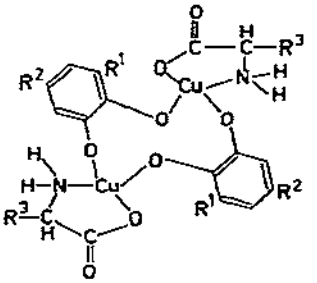

(XXVI)

$R^1 = SO_3^-, H$

$R^2 = SO_3^-, CH_2CH(NH_2)COOH, CH(OH)CH_2NHCH_3, CH(OH)CH_2NH_2$

$R^3 = H, CH_3CH(OH)$

The EPR spectra of the copper(II) chelates of L-β-(3,4-dihydroxyphenyl)-alanine (L-dopa), α-methyldopa, 3,4-dimethoxy-α-methyldopa, dopamine, dihdroxyphenylacetic acid, adrenaline, noradrenaline and catechol formed in dimethylformamide or dimethylsulphoxide have been reported[51]. At room temperature the results are consistent with the formation of monomeric chelates though in frozen solution the existence of dimeric species has been shown. The magnetic and structural parameters obtained from computer lineshape procedures are summarised in Tables 22 and 23.

A structure which is compatible with the observed copper(II)—copper(II) separation in the dimeric form of the copper(II)—dopa chelate is structure XXVII. Support for this proposed structure is supplied by the data for α-methyl-dopa, which on coordination with copper(II) gives rise to basically the same EPR signal but in order to simulate the $\Delta M_s = \pm 2$ signal an isotropic linewidth corresponding to the parallel and perpendicular directions had to be introduced. 3,4-Dimethoxy-α-methyl-

TABLE 22

Magnetic and structural data for copper(II) dihydroxyphenol dimers formed in non-aqueous solution[51]

System	Transition	$g_{\parallel}$	$g_{\perp}$	$A \times 10^{-4}$ (cm^{-1})	$B \times 10^{-4}$ (cm^{-1})	r (Å)
Cu^{II} : dopa, 1 : 1, $n = 3$	$\Delta M_S = \pm 1$	2.30 ± 0.03	2.06 ± 0.01	175 ± 25	10 ± 5	4.4 ± 0.2
	$\Delta M_S = \pm 2$	2.30 ± 0.02	2.08 ± 0.62	200 ± 10	10 ± 5	4.0 ± 0.5
Cu^{II} : dopa, 1 : 2, $n = 6$	$\Delta M_S = \pm 2$	2.31 ± 0.02	2.08 ± 0.02	190 ± 10	10 ± 5	4.0 ± 0.5
Cu^{II} : α-methyldopa 1 : 1, $n = 3$	$\Delta M_S = \pm 2$	2.29 ± 0.02	2.09 ± 0.02	160 ± 10	15 ± 5	4.5 ± 0.5
Cu^{II} : 3,4-dimethoxy-α-methyldopa, 1 : 1, $n = 0$	$\Delta M_S = \pm 2$	2.25 ± 0.02	2.11 ± 0.02	160 ± 15	10 ± 5	4.5 ± 0.5
Cu^{II} : adrenaline, 1 : 1, $n = 3$	$\Delta M_S = \pm 2$	2.40 ± 0.02	2.10 ± 0.03	60 ± 10	5 ± 3	5.5 ± 1.0
Cu^{II} : 3,4-dihydroxyphenylacetic acid, 1 : 1, $n = 3$	$\Delta M_S = \pm 2$	2.18 ± 0.02	2.08 ± 0.02	70 ± 10	10 ± 2	4.5 ± 1.0

TABLE 23

Magnetic data for copper(II) dihydroxyphenol complexes[51]

System	g_x	g_y	g_z	$A_x \times 10^{-4}$ (cm^{-1})	$A_y \times 10^{-4}$ (cm^{-1})	$A_z \times 10^{-4}$ (cm^{-1})
Cu^{II} : catechol, 1 : 1, $n = 2$	2.048 ± 0.002	2.055 ± 0.002	2.243 ± 0.002	15 ± 5	25 ± 5	195 ± 10
Cu^{II} : tiron, 1 : 1, $n = 2$	2.047 ± 0.002	2.055 ± 0.002	2.243 ± 0.002	15 ± 5	27 ± 5	180 ± 5
Cu^{II} : adrenaline, 1 : 1, $n = 3$	2.048 ± 0.002	2.056 ± 0.002	2.241 ± 0.002	16 ± 4	28 ± 5	185 ± 5
Cu^{II} : noradrenaline, 1 : 1, $n = 3$	2.047 ± 0.002	2.054 ± 0.002	2.242 ± 0.004	16 ± 4	29 ± 5	185 ± 6
Cu^{II} : dopamine, 1 : 1, $n = 2$	2.048 ± 0.002	2.056 ± 0.002	2.241 ± 0.002	16 ± 4	28 ± 5	185 ± 5
Cu^{II} : 3,4-dihydroxyphenyl-acetic acid, 1 : 1, $n = 3$	2.046 ± 0.002	2.054 ± 0.002	2.243 ± 0.002	16 ± 4	28 ± 5	185 ± 6

dopa with copper(II) also give rise to a $\Delta M_s = \pm 2$ signal similar to that given by the dopa complex, and in this instance the 1,2-dihydroxy group is not available for coordination to the copper(II) ion.

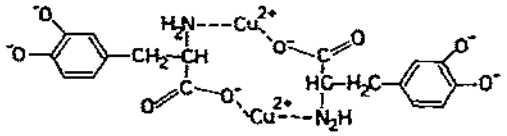

(XXVII)

K. CHELATES OF THIO LIGANDS

The introduction of sulphur atoms into the structure of organic chelating agents often results in important changes in their ability to combine with metal ions. EPR techniques have often provided useful information about the nature of the metal–ligand bonding situation in these chelates[171]. In order to explore the role played by sulphur when present as a linking atom in the ligand structure, or as part of a cyclic system, or as the terminal group combining with copper(II), an EPR study of the copper(II) chelates of certain thio ligands was undertaken[47]. The ligands studied include *o*-methylmercaptobenzoic acid[172], *S*-carboxydiethyldithiocarbamic acid, thiazolidine-4-carboxylic acid, 5-hydroxy-1,3-benzoxathiol-2-one and diacetylbisthiosemicarbazone[173]. The EPR spectra of dimethylformamide solutions of the chelates were interpreted in terms of dimeric species which exist at room temperature as well as in frozen solutions in the case of *o*-methylmercaptobenzoic acid, *S*-carboxydiethyldithiocarbamic acid and 5-hydroxy-1,3-benzoxathiol-2-one, whereas the dimeric forms of the remaining chelates are formed solely in frozen solution. Table 24 summarises the magnetic parameters obtained from a computer lineshape simulation procedure involving the assumption of axial symmetry of the copper(II) pair system in each case.

The structural forms of the dimeric species are shown by structures XXVIII–XXXIV, which depict the essential framework required for dimer formation and where the internuclear distances between the copper(II) ions are compatible with molecular models.

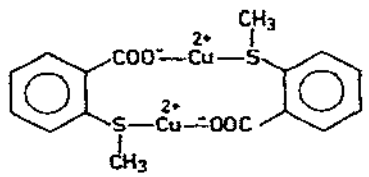

(XXVIII)

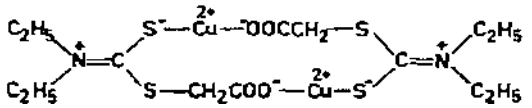

(XXIX)

TABLE 24

Magnetic and structural data for copper(II) thio-ligand dimers[47]

Ligand	Transition	$g_{\parallel}$	$g_{\perp}$	$A \times 10^{-4}$ (cm^{-1})	$B \times 10^{-4}$ (cm^{-1})	r (Å)
o-Methylmercaptobenzoic acid	$\Delta M_S = \pm 1$	2.15	2.05	170 ± 20	10 ± 5	4.2 ± 0.5
S-Carboxydithyldithiocarbamic acid	$\Delta M_S = \pm 1$	2.15	2.05	170 ± 20	10 ± 5	4.2 ± 0.5
Thiazolidine-4-carboxylic acid	$\Delta M_S = \pm 1$	2.26	2.07	130 ± 10	20 ± 5	6.0 ± 0.3
	$\Delta M_S = \pm 2$	2.26	2.07	120 ± 10	20 ± 5	6.0 ± 0.4
Diacetylbisthiosemicarbazone	$\Delta M_S = \pm 1$[a]					
	$\Delta M_S = \pm 2$	2.20	2.02	190 ± 10	10 ± 5	5.6 ± 0.5
Diacetylbisthiosemicarbazone, copper(II)–zinc chelate, $n = 0$	$\Delta M_S = \pm 1$[a]					
	$\Delta M_S = \pm 2$	2.20	2.02	190 ± 10	10 ± 5	5.6 ± 0.5
Diacetylbisthiosemicarbazone, copper(II)–zinc chelate, $n = 2$	$\Delta M_S = \pm 1$[a]					
	$\Delta M_S = \pm 2$	2.34	2.06	220 ± 10	20 ± 5	6.4 ± 0.2

[a] Line simulation not carried out because of superposition of signal due to monomeric species.

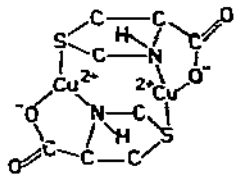

(XXX)

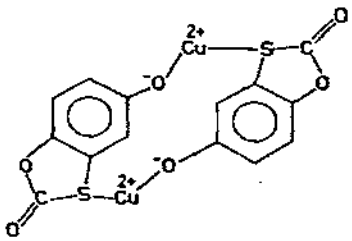

(XXXI)

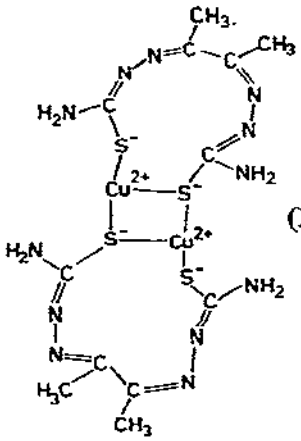

(XXXII)

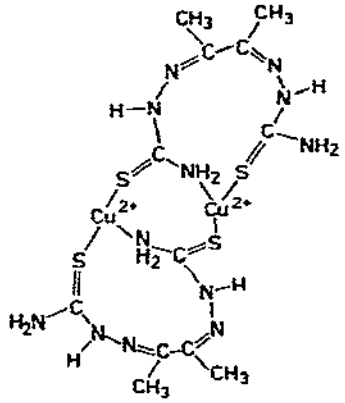

(XXXIII)

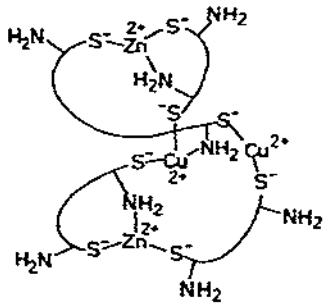

(XXXIV)

The possibility of replacement of a copper(II) ion in the copper(II)–copper(II) pairs by a diamagnetic cation was investigated by the introduction of zinc chloride into the copper(II) ligand mixtures. Of the systems studies the reaction mixture containing copper(II) chloride (0.1 *M*), zinc chloride (0.1 *M*) and diacetylbisthiosemicarbazone (0.2 *M*) provided the most interesting results. Thus at room temperature little change in the signal could be observed when compared with those obtained using copper(II) alone. However, at 77°K the mixture gave a spectrum which was similar to that obtained in the absence of zinc chloride except that the intensity of the $\Delta M_s = \pm 2$ transition increased fourfold. Addition of triethylamine

resulted in little change of the room temperature spectrum but at 77°K, where previously a very broad signal was obtained, a well resolved $\Delta M_s = \pm 2$ signal was observed indicating the presence of a species depicted by structure XXXIV. The introduction of zinc chloride into the other copper(II) ligand mixtures leads to the formation of heterometal chelates though the addition of zinc chloride to a dimethylformamide solution of the copper(II)–5-hydroxy-1,3-benzoxathiol-2-one chelate did not result in a modification of the dimeric form of the copper(II) chelate.

The structure of the dimeric forms of the copper(II) chelate of 3-ethoxy-2-oxobutyraldehyde bisthiosemicarbazone, which is structurally similar to the diacetylbisthiosemicarbazone, has been reported[174]. In acid solution the formation of a dimeric species was recognised, which it was suggested might persist at higher pH values and would involve a large exchange coupling between the copper(II) ions. The structure put forward involved an interaction of the copper(II) with the fully protonated form of the ligand in an extended configuration in which the copper(II) ions must be at least 6–7 Å apart. It is not clear from these results whether or not the copper(II) chelate is dimeric in solution at room temperature. The results obtained for the copper(II) chelate of diacetylbisthiosemicarbazone in dimethylsulphoxide indicate that monomeric species are formed at room temperature. The extreme line broadening at 77°K is interpreted as arising from a magnetic dipole–dipole interaction of a pair of copper(II) ions as represented by structure XXXII, which may be compared with the copper–copper distance of 3.8 Å in the structurally related copper(II) chelate of 3-ethoxy-2-oxobutyraldehyde bisthiosemicarbazone[175]. An arrangement of bonding groups compatible with the longer distance of 6 Å is shown by structure XXXIII, where the ligand is in a protonated form.

The EPR spectra of copper(II) chelates of the monothio-β-diketones of the type $R_1C(SH)=CHCOR_2$, where $R_1 \equiv$ phenyl and $R_2 \equiv$ phenyl, and where $R_1 \equiv$ α-thienyl and $R_2 \equiv$ perfluoromethyl, have been studied in a range of frozen solvents[52]. The chemical stability of these compounds has been described in terms of the delocalization of charge within the chelate ring resulting in a greater charge density on the oxygen atom, thus stabilising the copper(II) state[176]. Other monothio-β-diketones which have electron-attracting groups bound to the carbon atom of the carbonyl group, e.g. OC_2H_5 or CF_3, reduce copper(II) to copper(I)[177]. Thus enough information is available to indicate that stabilisation of the copper(II) in these chelates is strongly influenced by the nature of the substituent attached to the carbon atoms bonded to the oxygen and sulphur atoms.

An EPR study of these chelates was undertaken to provide more precise information about the electronic environment of the copper(II) in the monothio-β-diketonate chelates. The magnetic parameters associated with the spectra due to monomeric species observed at g ca. 2 were determined by consideration of axial and orthorhombic spin Hamiltonians and compared with those obtained from the spectra of copper(II) diethyldithiocarbamate under similar circumstances. The EPR spectrum of the copper(II) chelate of 1,1,1-trifluoro-4-mercapto-4-(2-thienyl)-but-3-en-2-one

(ttmb) in pyridine or petroleum-ether containing pyridine at 77°K can be accounted for by an axial spin Hamiltonian, the relevant magnetic parameters being listed in Table 25. On the other hand, the EPR spectra of the chelates of 3-mercapto-1, 3-diphenyl-prop-2-en-1-one (dpmb), ttmb and diethyldithiocarbamate at 77°K in the other solvents used, are best accounted for by an orthorhombic spin Hamiltonian. The parameters of copper(II) diethyldithiocarbamate have been determined previously using an axial spin Hamiltonian[178]. However, such a treatment does not account for all the lines present in the spectrum and the subtle difference between the experimental lineshape and that calculated on the basis of an axial spin Hamiltonian is explained by the introduction of rhombic terms. The values of the magnetic parameters obtained from the spectra of the $Cu(dpmb)_2$ and $Cu(ttmb)_2$ chelates are close to those obtained for β-diketone chelates, indicating that the binding site is dominated by binding to oxygen.

For each copper(II) monothio-β-diketone chelate, low field lines were observed at 77°K which were attributed to $\Delta M_s = \pm 2$ transitions arising from the presence of dimeric species in frozen solvent. With the assumption of axial symmetry of the pair

TABLE 25

Magnetic data for copper(II) thioligand complexes

Chelate	g values (± 0.001)	Hyperfine constants $\times 10^{-4}$ (cm^{-1})	
$Cu(dpmb)_2$ in pyridine	$g_z = 2.180$ $g_x = 2.040$ $g_y = 2.050$	$A_z = 163 \pm 2$ $A_x = 20 \pm 2$ $A_y = 20 \pm 2$	
$Cu(dpmb)_2$ in dimethylsulphoxide	$g_z = 2.180$ $g_x = 2.020$ $g_y = 2.040$	$A_z = 170 \pm 2$ $A_x = 30 \pm 2$ $A_y = 30 \pm 2$	
$Cu(ttmb)_2$ in dimethylsulphoxide containing 20% chloroform	$g_z = 2.189$ $g_x = 2.044$ $g_y = 2.052$	$A_z = 165 \pm 2$ $A_x = 20 \pm 2$ $A_y = 20 \pm 2$	
Cu^{II} diethyldithiocarbamate in chloroform containing 60% toluene	$g_z = 2.008$ $g_x = 2.009$ $g_y = 2.021$	$^{63}A_z = 164 \pm 1$ $^{63}A_x = 30 \pm 1$ $^{63}A_y = 48 \pm 1$	$^{65}A_z = 175 \pm 1$ $^{65}A_x = 32 \pm 1$ $^{65}A_y = 51 \pm 1$
Cu^{II} diethyldithiocarbamate in chloroform containing 60% pyridine	$g_z = 2.120$ $g_x = 2.029$ $g_y = 2.017$	$^{63}A_z = 140 \pm 1$ $^{63}A_x = 24 \pm 1$ $^{63}A_y = 20 \pm 1$	$^{65}A_z = 149 \pm 1$ $^{65}A_x = 25 \pm 1$ $^{65}A_y = 21 \pm 1$
$Cu(ttmb)_2$ in pyridine	$g_\parallel = 2.204$ $g_\perp = 2.046$	$A = 155 \pm 5$ $B = 5 \pm 5$	
$Cu(ttmb)_2$ in petroleum ether containing 20% pyridine	$g_\parallel = 2.200$ $g_\perp = 2.046$	$A = 155 \pm 5$ $B = 5 \pm 5$	

TABLE 26
Magnetic and structural data for copper(II) thio-ligand dimers

Chelate	$g_{\parallel}$	$g_{\perp}$	$A \times 10^{-4}$ (cm^{-1})	$B \times 10^{-4}$ (cm^{-1})	r(Å)
Cu(dpmb)$_2$	2.34	2.05	220 ± 10	10 ± 5	3.9 ± 0.2
Cu(ttmb)$_2$	2.21	2.03	190 ± 10	10 ± 5	4.2 ± 0.2

systems, the application of computer simulation of the lineshapes enabled the distanc of about 4 Å between the copper(II) ions in the dimeric species to be determined. The other parameters are outlined by Table 26. A possible arrangement of the dimeric species which is compatible with this distance is shown by structure XXXV[179].

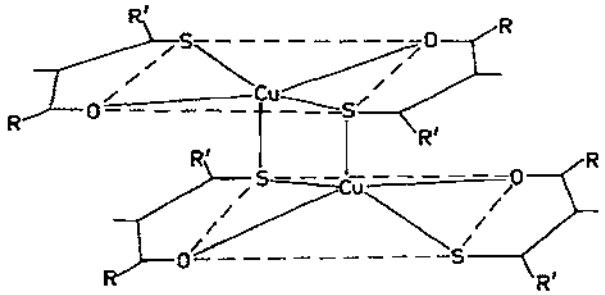

(XXV)

The EPR spectra of copper(II) dialkyldithiocarbamates in frozen solutions of chloroform, containing small amounts of other solvent, have been shown to give well resolved signals at g ca. 2 and 77°K superimposed on a broader line, while at the same instrumental gain a low field signal is observed[44]. The broad signal at g ca. 2, and the lines at half-field, have been interpreted as arising from triplet state phenomena occurring as the result of dimer formation. The lineshapes of the $\Delta M_s = \pm 1$ and $\Delta M_s = \pm 2$ transitions are accounted for by consideration of a spin Hamiltonian involving axial symmetry of the pair system. Application of computer simulation of the lineshapes enabled the distance of 4.7 ± 0.4 Å between the copper(II) ions in the dimer to be determined. It is likely that the planar symmetry of the copper(II) ion with respect to the sulphur atoms of the ligand anion is maintained. However, the positioning of two planes containing the copper(II) ions, as occurs in the crystalline state of the pure complex, or doped into the corresponding zinc chelate, leads to a distance shorter than that observed in the host lattice provided by the frozen organic solvent. If, as in the molecular structure of zinc dimethyldithiocarbamate, the ligand anion is in some way shared between two copper(II) ions, and if an essentially planar symmetry about each copper(II) ion is maintained, the distance between the copper(II) ions is determined by the dimensions of the terminal C(S)S$^-$ group. Such an arrangement is shown by structure XXXVI for the extreme case where all the dialkyldithio-

carbamate anions are involved in bridging, though a similar copper(II)–copper(II) distance could be achieved by a structure involving two bridging anions. The planar symmetry of each copper(II) ion is maintained such that the dimeric unit forms a square antiprism. Quite large groups can be accomodated in the volume of space around these planes, and this explains the observation that the EPR spectrum of the dimer molecule is little influenced by the nature of the alkyl or aryl groups attached to the nitrogen atom of the ligand. In this system the formation of dimeric units in mainly chloroform solution is critically dependent on the addition of small amounts of other solvents. It is difficult to describe the causes of dimer formation under these circumstances, though it may be speculated that their role is one of a specific type of solvation.

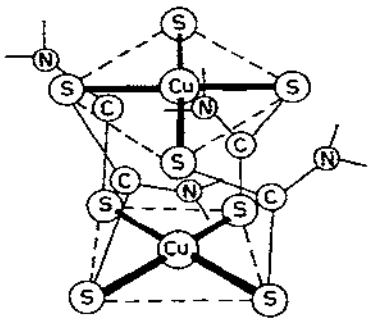

(XXXVI)

The mixed-valence copper complexes formed by reaction of copper(II) with certain thiols have been reported[180]. Polarographic and optical titration showed that the intense violet colour obtained in the case of the interaction of mercaptosuccinic acid with copper(II) was due to the formation of a complex which contained copper in two valence states. The EPR spectra of the violet solution at various values of pH have been studied[43]. At 77°K the main feature of the spectrum between pH 1.9 and 9.8 is a broad resonance which extends over 2,500 gauss at $g \sim 2$. The origin of the EPR signals was clarified by studies of the copper(II) chelates of mercaptosuccinic acid formed in *N*,*N*'-dimethylformamide or dimethylsulphoxide, where formation of a mixed valency complex does not occur and the results can be explained in terms of a monomer–dimer equilibrium similar to that observed in the copper(II) hydroxycarboxylate chelates. The most reasonable explanation for the broad signal observed for the violet mixed-valency state complex formed in aqueous solution, is that it is due to delocalisation of the unpaired electron. This situation could be described as copper of indeterminate valence as discussed by Hemmerich[43]. However, Hemmerich's contention that copper of indeterminate valence does not give an EPR signal in the cases he considered is erroneous since the resonance is so broad that it would not have been observed at the millimolar concentrations which he used.

L. COPPER(II) IN NATURAL PRODUCTS

EPR studies on naturally occurring compounds which fulfil some vital role in biochemical reactions, and which contain a paramagnetic ion giving rise to a detectable signal, have proved to be valuable in a number of respects. Thus such studies have rendered assistance in establishing (1) the role of the metal ion in chemical change, (2) the nature of the binding site of the metal ion, (3) the possible relationship between the amount of the metal ion detectable by EPR to the total metal ion content not detectable, and (4) the presence of any spin interactions between various metal ions sites or attached molecules.

An important approach involves the study of model systems which have a relatively simple molecular structure, but which possess one or more of the attributes of the invariably far more complex material of natural occurrence. This has often been used to good effect. From a consideration of the spectra obtained in these model systems, some of the difficulties involved in the interpretation of the spectra due to the materials of natural occurrence may be resolved[43]. A study of this type has been carried out on haemocyanin, which is a copper-containing protein which functions as the oxygen carrier in the blood of some species of invertebrates. It has been shown that the binding of oxygen takes place in the ratio of *one* oxygen molecule to *two* copper atoms present[181]. The results of an electron microscopy investigation dealing with the structure of haemocyanin were recently reported[182]. It was found there that gastropod haemocyanin consists of a cylindrical wall structure whose ends possess a fivefold collar and a central cap. The cylindrical wall consists of sixty dimers which may be correlated with 120 oxygen binding sites. However, no evidence has been found for any coupling between pairs of copper(II) ions in this or any other system involving pairs of paramagnetic ions in molecular oxygen binding. A new development in the field is the discovery that treatment of the α-haemocyanin of *Helix pomatia* with nitric oxide produces a triplet state spectrum due to copper(II) pairs which can be accounted for on the basis of dipolar coupling[183,184]. The spectrum near $g \approx 2$ shows a monomer signal which corresponds to about 20% of the copper in the protein. In addition, there is also a broad signal at $g \approx 2$ as well as the $\Delta M_s = \pm 2$ spectrum at $g \approx 4$.

A further development in this field stems from an EPR study of nitric-oxide-treated reduced ceruloplasmin[185]. Here the EPR-inactive reduced ceruloplasmin reacts reversibly with nitric oxide to form paramagnetic Cu^{II}–NO^- complexes which show EPR signals centred around $g = 2$ and $g = 4$. The EPR absorption around $g = 4$ is attributed to $\Delta M_s = \pm 2$ transitions arising from magnetic dipolar coupling in copper(II) pair systems occurring in the product. From the reported spectrum it can be seen that this is one of the rare cases where the $\Delta M_s = \pm 2$ signal is observed at the same instrumental gain as the high field portion of the spectra, implying a very good conversion of the copper(II) sites to conformations in which the copper(II) ions may interact in pair systems. A cursory inspection of the spectra indicates that the

copper(II) pair systems may possess lower than axial symmetry with metal ion separations of about 4.7 Å. The magnetic parameters are likely to be quite different from those due to copper(II) in ceruloplasmin itself[43].

M. DIMERIC CHELATES WITH SIGNIFICANT EXCHANGE

An EPR study of exchange and dipole–dipole coupling in copper(II) chelates of cyclopentanetetracarboxylic acid and related systems showed that an easy transformation from exchange-coupled copper(II) to essentially magnetic dipole–dipole may occur[46]. The EPR spectra were often complex in nature arising from subtle structural differences brought about by variation of solvent composition, counter-anion and metal : ligand ratio. Exchange coupling in dimeric species was observed in the copper(II) chelates of *m*- and *p*-hydroxybenzoic acids and in the copper(II) complexes of adenine formed in both aqueous and non-aqueous solution.

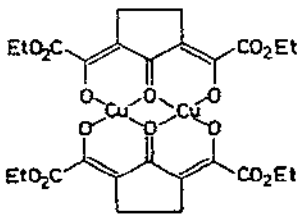

(XXXVII)

An EPR spectra study of the copper(II) chelate of 2,5-diethoxalyl-cyclopentanone supports the conclusions that dimeric species are formed in which exchange coupling takes place[186] (structure XXXVII). In dimethylformamide the introduction of zinc(II) results in the replacement of copper(II) in the copper(II) pairs, thus forming a hetero-ion chelate. In trimethylphosphate the same process leads to a novel species involving both copper(II) and zinc(II) ions in which exchange coupling persists between the copper(II)–copper(II) pairs. Structure XXXVIII represents the essential framework of the structure of this polynuclear heterometal ion chelate. The structure involves the assumption of tetrahedral symmetry about each zinc ion.

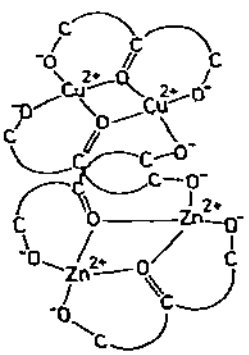

(XXXVIII)

ACKNOWLEDGEMENT

Much of the work described herein was made possible through financial support from the Australian Research Grants Committee.

APPENDIX

Dissimilar ion dimers – transition probability calculations[99]

Transition probabilities

The transition probabilities must be calculated with care in view of the fact the two ion sites are, in general, rotated with respect to one another. The following calculations are valid only within the Zeeman, or high field, limit and should not be taken as being of general applicability in all cases. There are some aspects of the discussion which are independent of the present model, for example the correlation of the coordinates of the two sites, a factor which will be more obvious when the averaged probabilities are calculated later. In principle, the discussion follows closely the work of one of the authors in connection with anisotropic probabilities for monomers[93] and the notation here is the same as used in that paper.

Since most experiments are performed in resonant cavities in which the microwave magnetic field is polarised linearly in a vertical direction, while the d.c. magnetic field is always horizontal, and therefore $\mathbf{H} \perp \mathbf{H}_{rf}$ at all times, the calculations which follow are based on this assumption.

Let us define the direction cosines of the r.f. magnetic field, H_{rf}, with respect to the x_i, y_i, z_i axes (Figs. 23 and 24). Then from the definitions of angles in Fig. 23, we have that

$$\begin{aligned} l'_{ix_i} &= \cos\phi_i \cos\theta_i \sin\eta_i - \sin\phi_i \cos\eta_i \\ l'_{iy_i} &= \sin\phi_i \cos\theta_i \sin\eta_i + \cos\phi_i \cos\eta_i \\ l'_{iz_i} &= -\sin\eta_i \sin\theta_i, \quad i = 1, 2 \end{aligned} \tag{A1}$$

In Figs. 23(a) and 23(b), OP_i and OQ_i lie in the $x_i y_i$ plane and OQ_i is normal to the $z_i OH_i P_i$ plane. The expressions (A1) were calculated assuming that $\theta'_i - \theta_i = \frac{\pi}{2}$, which is a direct consequence of the choice $\mathbf{H} \perp \mathbf{H}_{rf}$. More general expressions for eqns. (A1) would be required for an experimental set-up in which H was not perpendicular to H_{rf}.

The "oscillatory Hamiltonian" is then expressed as

$$\mathcal{H}_{rf} = \beta H_{rf} \cos\omega t \, [g_{x_i} l'_{ix_i} S_{ix} + g_{y_i} l'_{iy_i} S_{iy} + g_{z_i} l'_{iz_i} S_{iz}] \quad i = 1, 2 \tag{A2}$$

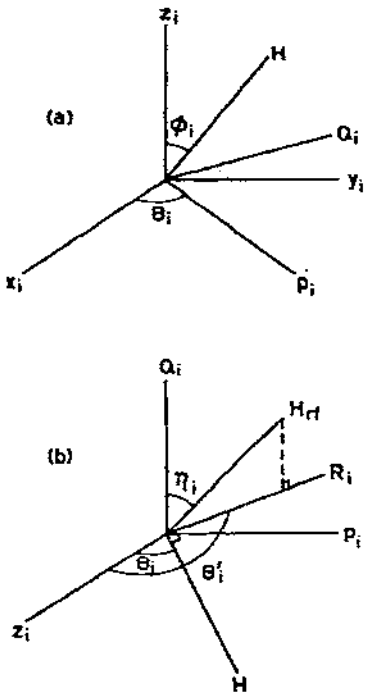

Fig. 23. Polar coordinates for (a) H and (b) H_{rf} for ion *i*. Notation as in ref. 93 except for subscripts.

This expression is then transformed into the Zeeman representation, that in which the $\mathcal{H}_1$ (Zeeman) and $\mathcal{H}_2$ (Zeeman) are separately diagonal, whence

$$\begin{aligned}\mathcal{H}_{irf} = \beta H_{rf} \cos \omega t \; [&g_{x_i} l'_{ix_i} (l^i_{xx} S'_{ix} + l^i_{xy} S'_{iy} + l^i_{xz} S'_{iz})] \\ &+ g_{y_i} l'_{iy_i} (l^i_{yx} S'_{ix} + l^i_{yy} S'_{iy} + l^i_{yz} S'_{iz}) \\ &+ g_{z_i} l'_{iz_i} (l^i_{zx} S'_{ix} + l^i_{iz} S'_{iy} + l^i_{zz} S'_{iz})] \qquad (i = 1, 2) \end{aligned} \tag{A3}$$

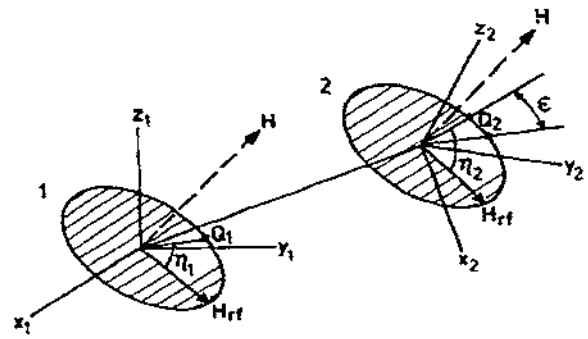

Fig. 24. General representation as in Fig. 1 to illustrate orientations of r.f. field plane and the result $\eta_2 = \eta_1 + \epsilon$.

The oscillatory Hamiltonian, eqn. (A3), is used to evaluate the basic transition matrix elements for ion i.

$$\begin{aligned}\langle \pm_i|\mathcal{H}_{irf}|\mp_i\rangle &= \tfrac{1}{2}\left[g_{x_i} I'_{ix_i} I^i_{xx} + g_{y_i} I'_{iy_i} I^i_{yz} + g_{z_i} I'_{iz_i} I^i_{zx}\right] \\ &\quad \mp \frac{i}{2}\left[g_{x_i} I'_{ix_i} I^i_{xy} + g_{y_i} I'_{iy_i} I^i_{yy} + g_{z_i} I'_{iz_i} I^i_{zy}\right] \\ &= P_{i1} \mp iP_{i2} \quad i = 1, 2\end{aligned} \tag{A4}$$

In the derivation of eqn. (A4), only terms in S'_{ix} and S'_{iy} have been considered since magnetic dipole transitions involve coupling between states whose spin quantum numbers differ by 1. Of course when the states contain mixtures, as in eqn. (28), not only will correction terms become apparent in first order, but also "forbidden" or $\Delta M_s = \pm 2$ transitions may occur. In passing we note that contributions from S'_z terms in eqn. (A3) do not affect the calculated $\Delta M_s = \pm 1$ probabilities up to first order, so they will not be considered further. To proceed with the calculations, we first determine the matrix elements of

$$\mathcal{H}_{rf} = \mathcal{H}_{1rf} + \mathcal{H}_{2rf} \tag{A5}$$

in the coupled representation, the $|\psi_i>$ (eqn. (25)), and then finally in terms of the corrected wavefunctions, the $|\psi_i>'$, which are given in eqn. (28) modified by eqns. (56) – (58). Let us define

$$\alpha_{ij} = \langle \psi_j|\mathcal{H}_{rf}|\psi_j\rangle \tag{A6a}$$

Now

$$\begin{aligned}\alpha_{12} &= \langle ++|\mathcal{H}_{1rf}|-+\rangle\, b + \langle ++|\mathcal{H}_{2rf}|+-\rangle\,(U+iV) \\ &= (U+iV)\,(P_{21} - iP_{22}) + b\,(P_{11} - P_{12}) \\ &= \alpha^*_{21}\end{aligned} \tag{A6b}$$

Similarly the other combinations of states yield

$$\begin{aligned}\alpha_{23} &= (U-iV)\,(P_{11} - iP_{12}) + b\,(P_{21} - iP_{22}) = \alpha^*_{32} \\ \alpha_{14} &= (W-iX)\,(P_{21} - iP_{22}) + d\,(P_{11} - iP_{12}) = \alpha^*_{41} \\ \alpha_{43} &= (W-iX)\,(P_{11} - iP_{12}) + d\,(P_{21} - iP_{22}) = \alpha^*_{34} \\ \alpha_{13} &\equiv \alpha_{31} \equiv \alpha_{24} \equiv \alpha_{42} \equiv 0\end{aligned} \tag{A6c}$$

Then we may define

$$\alpha'_{ij} = \langle \psi'_i|\mathcal{H}_{rf}|\psi'_j\rangle \tag{A7a}$$

where $|\psi_j'\rangle \equiv |\psi_j\rangle'$. Thus for a magnetic dipole transition between states 1 and 2,

$$\alpha'_{12} = \alpha_{12} + \frac{S_3 + iS_4}{2W_0}\,\alpha_{32} + \text{higher order terms} \tag{A7b}$$

Expressed in terms of the P_{12}, etc., then

$$\begin{aligned}\alpha'_{12} = {} & U\left(P_{21} + \frac{S_3P_{11} - S_4P_{12}}{2W_0}\right) - V\left(-P_{22} + \frac{S_3P_{12} + S_4P_{11}}{2W_0}\right) \\ & + b\left(P_{11} + \frac{S_3P_{21} - S_4P_{22}}{2W_0}\right) + i\left\{V\left(P_{21} + \frac{S_3P_{11} - S_4P_{21}}{2W_0}\right)\right. \\ & \left. + U\left(-P_{22} + \frac{S_3P_{12} + S_4P_{11}}{2W_0}\right) + b\left(-P_{21} + \frac{S_4P_{21} + S_3P_{22}}{2W_0}\right)\right\}\end{aligned} \tag{A7c}$$

and the relative transition probability is

$$P_{\psi'_1\psi'_2} = |\alpha'_{12}|^2 \tag{A8}$$

The results for the relative probabilities, $P_{\psi'_i\psi'_j}$, are given later in this Appendix, eqns. (A14)–(A17) to first order for $\Delta M_j = \pm 1$ transitions, and in eqn. (A18) for the $\Delta M_s = \pm 2$ transition to second order in the perturbations.

The expressions for the $P_{\psi'_i\psi'_j}$ apply to a dimer in a particular spatial relationship both to the d.c. field, **H**, and also to $\mathbf{H}_{rf}$. Therefore they apply for specific pairs of values of η_1 and η_2. It is important to remember that transition positions (and energy levels) are determined by the d.c. field direction, i.e. upon the specific pairs of θ_i and ϕ_i values ($i = 1, 2$). Intensities depend in addition upon η_1 and η_2.

In the simulation of ESR spectra from randomly oriented dimers, one considers a particular orientation of H (θ_1 and ϕ_1) at a time for which *all* possible values of η_1 are likely. Thus one must average over all values of η_1 in the appropriate expressions. First, however, the relationship between η_1 and η_2 must be investigated. By means of Fig. 24, which is related to the definitions in Fig. 23, it can easily be seen that

$$\eta_2 = \eta_1 + \epsilon \tag{A9}$$

i.e. that there is a 1 : 1 correspondence and a simple relationship between η_1 and η_2. Therefore, when averaging over η_1 values, one automatically averages over the corresponding η_2 values provided ϵ is introduced, or vice versa. The proof of eqn. (A9) depends on the realisation that since $\mathbf{H}_{rf} \perp \mathbf{H}$, $\mathbf{H}_{rf}$ therefore lies somewhere in the plane perpendicular to H, and these perpendicular planes for each ion must of course be parallel to one another! The orientation of OQ_i (Figs. 23 and 24) is different for each ion so that there is a unique value of ϵ for each pair of values of θ_1 and ϕ_1. Of course θ_1 and ϕ_1 fix the values of θ_2 and ϕ_2. The value of ϵ may be determined by means of the orthogonal transformation between the l'_{2j_2} and l'_{1j_1} ($j = x$,

y, z). This is the same transformation as given in eqn. (60) for the l_{i_2} and l_{j_1}. We can substitute $\eta_1 + \epsilon$ for η_2 and then solve for ϵ. This information is used to determine the average values of the various quantities in the $P_{\psi_i'\psi_j'}$ by means of the results in eqn. (A10).

$$\begin{aligned}
&\overline{\sin^2\eta_1} = \overline{\cos^2\eta_1} = \overline{\cos^2\eta_2} = \overline{\sin^2\eta_2} = \tfrac{1}{2} \\
&\overline{\sin\eta_1 \sin\eta_2} = \overline{\sin^2\eta_1 \cos\epsilon} = \tfrac{1}{2}\cos\epsilon \\
&\overline{\sin\eta_1 \cos\eta_2} = \overline{-\sin^2\eta_1 \sin\epsilon} = -\tfrac{1}{2}\sin\epsilon \\
&\overline{\cos\eta_1 \sin\eta_2} = \overline{\cos^2\eta_1 \sin\epsilon} = \tfrac{1}{2}\sin\epsilon \\
&\overline{\cos\eta_1 \cos\eta_2} = \overline{\cos^2\eta_1 \cos\epsilon} = \tfrac{1}{2}\cos\epsilon
\end{aligned} \tag{A10}$$

Products of the type $\overline{\sin\eta_i \cos\eta_i}$ average to zero. In calculating the average probabilities, quantities of the form

$$\overline{P_{ik}P_{jl}} = \sum_{P,R=x,y,z} g_{P_i}\, l^i_{iPK'}\, g_{R_j}\, l^j_{jRL'}\, \overline{l'_{iP_i}\, l'_{jR_j}} \tag{A11}$$

must be evaluated. Equation (A11) follows immediately from eqn. (A4) where the P_{ik} are defined; i, j, k and l all take the values 1 or 2. When $k = 1, K' = x$; when $k = 2, K' = y$; when $l = 1, L' = x$ and when $l = 2, L' = y$. The averaged values of the $\overline{l'_{iP_i}\, l'_{jR_j}}$ are given by eqn. (A19). Finally, to obtain the averaged values $\overline{P_{\psi_i'\psi_j'}}$ we must simply average the $\overline{P_{ik}P_{jl}}$ terms in eqns. (A14) – (A17) for $\Delta M_s = \pm 1$ transitions using the results above, eqn. (A11), and the $\overline{l'_{iP_i}\, l'_{iR_j}}$, (A19). For $\Delta M_s = \pm 2$ transitions, $\overline{P_{\psi_1'\psi_3'}}$ is given in eqn. (A20). In the similar ion limit where the principal axes of the g tensor of each ion are parallel to one another, $P_{11} \mp iP_{12} = P_{21} \mp iP_{22}$ so that $P_{11} = P_{21}$ and $P_{12} = P_{22}$. If these conditions are applied to the transition probabilities then, for example,

$$\overline{P_{\psi_1'\psi_2'}} = [(U+b)^2 + V^2]\ [\overline{P_{11}^2} + \overline{P_{22}^2} + \{S_3(\overline{P_{11}^2} - \overline{P_{22}^2}) - 2S_4\overline{P_{22}P_{11}}\}/W_0] \tag{A12}$$

The result within eqns. (30) for similar ion dimers in the S_x' part of H_{ff}, shows that

$$\overline{P_{\psi_1'\psi_2'}} = [(U+b)^2 + V^2]\ [\overline{P_{11}^2} + \overline{P_{22}^2}]\ \left[1 + \frac{S_3}{W_0}\right] \tag{A13}$$

The term $(\overline{P_{11}^2} + \overline{P_{22}^2})$ represents the angular dependent term in the transition probability which is called g_1^2 in ref. 93. It can be seen that the first order terms in eqns. (A12) and (A13) disagree. To establish whether this disagreement makes any difference in practice, a test for similar ion dimers was carried out using the program

GNDIMER and that developed for similar ion dimers ALLSYM. No difference was found, from which it was concluded that first order terms are not of paramount importance in the case of $\Delta M_s = \pm 1$ transitions.

Single crystal transition probabilities

$$\begin{aligned}
P_{\psi'_1\psi'_2} &= (U^2+V^2)\,[P_{21}^2+P_{22}^2+(S_3\,(P_{11}P_{21}-P_{12}P_{22})-S_4\,(P_{12}P_{21}+P_{11}P_{22}))/W_0] \\
&+ b^2\,[P_{11}^2+P_{12}^2+(S_3\,(P_{21}P_{11}-P_{22}P_{12})-S_4\,(P_{22}P_{11}+P_{21}P_{12}))/W_0] \\
&+ 2Ub\,[P_{11}P_{21}+P_{12}P_{22}+(S_3\,(P_{11}^2+P_{21}^2-P_{12}^2-P_{22}^2)-S_4 \\
&\quad \times (2P_{11}P_{12}+2P_{21}P_{22}))/2W_0] \\
&+ 2Vb\,[P_{11}P_{22}-P_{21}P_{12}+(S_3(2P_{21}P_{22}-2P_{11}P_{12})+S_4\,(P_{21}^2-P_{22}^2+P_{12}^2-P_{11}^2))/2W_0
\end{aligned} \tag{A14}$$

Similarly

$$\begin{aligned}
P_{\psi'_1\psi'_4} &= (W^2+X^2)\,[P_{21}^2+P_{22}^2+(S_3\,(P_{11}P_{21}-P_{12}P_{22})-S_4\,(P_{21}P_{12}+P_{11}P_{22}))/W_0] \\
&+ d^2\,[P_{11}^2+P_{12}^2+(S_3\,(P_{11}P_{21}-P_{12}P_{22})-S_4\,(P_{11}P_{22}+P_{12}P_{21}))/W_0] \\
&+ 2Xd\,[P_{22}P_{11}-P_{21}P_{12}+(S_3(2P_{22}P_{21}-2P_{11}P_{12})+S_4 \\
&\quad \times (-P_{22}^2-P_{11}^2+P_{21}^2+P_{12}^2))/2W_0] \\
&+ 2Wd\,[P_{11}P_{21}+P_{12}P_{22}+(S_3\,(P_{21}^2+P_{11}^2-P_{12}^2-P_{22}^2)-S_4 \\
&\quad \times (2P_{21}P_{22}+2P_{11}P_{12}))/2W_0]
\end{aligned} \tag{A15}$$

$$\begin{aligned}
P_{\psi'_4\psi'_3} &= (W^2+X^2)\,[P_{11}^2+P_{12}^2+(S_3\,(P_{11}P_{21}+P_{12}P_{22})-S_4\,(P_{11}P_{22}-P_{12}P_{21}))/W_0] \\
&+ d^2\,[P_{21}^2+P_{22}^2+(S_3\,(P_{12}P_{22}-P_{11}P_{21})+S_4\,(P_{21}P_{12}+P_{22}P_{11}))/W_0] \\
&+ 2Wd\,[P_{11}P_{21}+P_{12}P_{22}+(S_3\,(P_{22}^2+P_{12}^2-P_{11}^2-P_{21}^2)+S_4 \\
&\quad \times (2P_{21}P_{22}+2P_{11}P_{12}))/2W_0] \\
&+ 2Xd\,[P_{11}P_{22}-P_{12}P_{21}+(S_3\,(2P_{11}P_{12}-2P_{21}P_{22})+S_4 \\
&\quad \times (P_{22}^2+P_{11}^2-P_{21}^2-P_{12}^2))/2W_0]
\end{aligned} \tag{A16}$$

$$P_{\psi'_2\psi'_3} = = (U^2+V^2)[P_{11}^2+P_{12}^2+(S_3(P_{22}P_{12}-P_{11}P_{21})+S_4(P_{21}P_{12}+P_{11}P_{22}))/W_0]$$
$$+b^2[P_{21}^2+P_{22}^2+(S_3(P_{22}P_{12}-P_{11}P_{21})+S_4(P_{21}P_{12}+P_{22}P_{11}))/W_0]$$
$$+2Ub[P_{11}P_{21}+P_{12}P_{22}+(S_3(P_{12}^2+P_{22}^2-P_{21}^2-P_{11}^2)+S_4$$
$$\times(2P_{11}P_{12}+2P_{21}P_{22}))/2W_0]$$
$$+2Vb[P_{11}P_{22}-P_{12}P_{21}+(S_3(2P_{11}P_{12}-2P_{22}P_{21})+S_4$$
$$\times(P_{11}^2+P_{22}^2-P_{12}^2-P_{21}^2))/2W_0]$$

and for the $\Delta M_s = \pm 2$ transition, to second order

$$P_{\psi'_1\psi'_3} = \left\{\frac{2}{W_0}[S_1(UP_{11}-VP_{12}+bP_{21})+S_2(VP_{11}+UP_{12}+bP_{22})-S_5(UP_{21}+VP_{22}+bP_{\blacksquare}\right.$$
$$+S_6(VP_{21}-UP_{22}-bP_{12})+S_7(WP_{11}-XP_{12}+dP_{21})+S_8(XP_{11}+WP_{12}+dP_{22})$$
$$\left.-S_9(WP_{21}+XP_{22}+dP_{11})-S_{10}(XP_{21}-WP_{22}-dP_{12})]\right\}^2$$
$$+\left\{\frac{2}{W_0}[-S_1(VP_{11}+UP_{12}+bP_{22})+S_2(UP_{11}-VP_{12}+bP_{21})-S_5(VP_{21}-UP_{22}-bP_{12})\right.$$
$$-S_6(UP_{21}-VP_{22}+bP_{11})-S_7(XP_{11}+WP_{12}+dP_{22})+S_8(WP_{11}-XP_{12}+dP_{21})$$
$$\left.-S_9(XP_{21}-WP_{22}-dP_{12})+S_{10}(WP_{21}+XP_{22}+dP_{11})]\right\}^2 \qquad \text{(A18)}$$

Powder average values of $\overline{l'_{iP_i}l'_{jR_j}}$

$$\overline{l'_{ix_i}l'_{ix_i}} = \tfrac{1}{2}[\cos^2\phi_i\cos^2\theta_i+\sin^2\phi_i] \qquad \text{(A19a)}$$
$$\overline{l'_{iy_i}l'_{iy_i}} = \tfrac{1}{2}[\sin^2\phi_i\cos^2\theta_i+\cos^2\phi_i] \qquad \text{(A19b)}$$
$$\overline{l'_{iz_i}l'_{iz_i}} = \tfrac{1}{2}\sin^2\theta_i \qquad \text{(A19c)}$$
$$\overline{l'_{ix_i}l'_{iy_i}} = \overline{l'_{iy_i}l'_{ix_i}} = \tfrac{1}{2}[\cos^2\theta_i\sin\phi_i\cos\phi_i-\sin\phi_i\cos\phi_i] \qquad \text{(A19d)}$$
$$\overline{l'_{iy_i}l'_{iz_i}} = \overline{l'_{iz_i}l'_{iy_i}} = \tfrac{1}{2}[-\sin\phi\cos\theta_i\sin\theta_i] \qquad \text{(A19e)}$$

$i = 1, 2$

$$\overline{l'_{1x_1}l'_{2x_2}} = \tfrac{1}{2}[\cos\phi_1\cos\theta_1\cos\phi_2\cos\theta_2\cos\epsilon+\sin\phi_1\sin\phi_2\cos\epsilon \qquad \text{(A19f)}$$

$$+\cos\theta_1\cos\phi_1\sin\phi_2\sin\epsilon-\cos\phi_2\cos\theta_2\sin\phi_1\sin\epsilon]$$

$$\overline{l'_{1y_1}l'_{2y_2}}=\tfrac{1}{2}[\sin\phi_1\cos\theta_1\sin\phi_2\cos\theta_2\cos\epsilon+\cos\phi_1\cos\phi_2\cos\epsilon \quad \text{(A19g)}$$
$$-\sin\phi_1\cos\phi_2\cos\theta_1\sin\epsilon+\sin\phi_2\cos\theta_2\cos\phi_1\sin\epsilon]$$

$$\overline{l'_{1z_1}l'_{2z_2}}=\tfrac{1}{2}\sin\theta_1\sin\theta_2\cos\epsilon \quad \text{(A19h)}$$

$$\overline{l'_{1x_1}l'_{2y_2}}=\tfrac{1}{2}[\cos\phi_1\cos\theta_1\sin\phi_2\cos\theta_2\cos\epsilon-\sin\phi_1\sin\phi_2\cos\theta_2\sin\epsilon \quad \text{(A19i)}$$
$$-\cos\phi_1\cos\theta_1\cos\phi_2\sin\epsilon-\sin\phi_1\cos\phi_2\cos\epsilon]$$

$$\overline{l'_{1y_1}l'_{2x_2}}=\tfrac{1}{2}[\sin\phi_1\cos\theta_1\cos\phi_2\cos\theta_2\cos\epsilon+\sin\phi_1\cos\theta_1\sin\phi_2\sin\epsilon \quad \text{(A19j)}$$
$$+\cos\phi_2\cos\theta_2\cos\phi_1\sin\epsilon-\sin\phi_2\cos\phi_2\cos\epsilon]$$

$$\overline{l'_{1y_1}l'_{2z_2}}=-\tfrac{1}{2}[\sin\phi_1\cos\theta_1\sin\theta_1\cos\epsilon+\cos\phi_2\sin\theta_2\sin\epsilon] \quad \text{(A19k)}$$

$$\overline{l'_{1z_1}l'_{2x_2}}=-\tfrac{1}{2}[\sin\theta_1\cos\phi_2\cos\theta_2\cos\epsilon+\sin\phi_2\sin\theta_1\sin\epsilon] \quad \text{(A19l)}$$

and

$$\overline{l'_{1z_1}l'_{2y_2}}=\tfrac{1}{2}[\sin\phi_2\cos\theta_2\sin\theta_1\cos\epsilon+\cos\phi_2\sin\theta_1\sin\epsilon] \quad \text{(A19m)}$$

Powder-averaged $\Delta M_s = \pm 2$ transition probability

$$\begin{aligned}\overline{P_{\psi_1'\psi_3'}} &= \left[\frac{4}{W_0}\right]^2[\overline{P_{11}^2}(\Gamma_{11}^2+t_{11}^2)+\overline{P_{21}^2}(\Gamma_{21}^2+t_{21}^2)+\overline{P_{12}^2}(\Gamma_{12}^2+t_{12}^2)\\ &+\overline{P_{22}^2}(\Gamma_{22}^2+t_{22}^2)+\overline{2P_{11}P_{12}}(\Gamma_{11}\Gamma_{12}+t_{11}t_{12})\\ &+\overline{2P_{12}P_{21}}(\Gamma_{12}\Gamma_{21}+t_{12}t_{21})+\overline{2P_{21}P_{22}}(\Gamma_{21}\Gamma_{22}+t_{21}t_{22})\\ &+\overline{2P_{22}P_{11}}(\Gamma_{22}\Gamma_{11}+t_{22}t_{11})+\overline{2P_{11}P_{21}}(\Gamma_{11}\Gamma_{21}+t_{11}t_{21})\\ &+\overline{2P_{12}P_{22}}(\Gamma_{12}\Gamma_{22}+t_{12}t_{22})] \quad \text{(A20)}\end{aligned}$$

where

$$\begin{aligned}\Gamma_{11}&=(S_1U-S_2V-S_5b+S_7W+S_8X-S_9d)\\ \Gamma_{12}&=(-S_1V+S_2U-S_6b-S_7X+S_8W+S_{10}d)\\ \Gamma_{21}&=(S_1b-S_5U+S_6V+S_7d-S_9W-S_{10}X)\\ \Gamma_{22}&=(S_2b-S_5V-S_6U+S_8d-S_9X+S_{10}W) \quad \text{(A21)}\end{aligned}$$

and

$$t_{11} = (-S_1 V + S_2 U - S_6 b - S_7 X + S_8 W + S_{10} d)$$

$$t_{12} = (-S_1 U - S_2 V + S_5 b - S_7 W - S_8 X + S_9 d)$$

$$t_{21} = (-S_2 b - S_5 V - S_6 U + S_8 d - S_9 X + S_{10} W)$$

$$t_{22} = (-S_1 b + S_5 U - S_6 V - S_7 d + S_9 W + S_{10} X) \qquad \text{(A22)}$$

REFERENCES

1 M. Kato, H.B. Jonassen and J.C. Fanning, *Chem. Rev.*, 64 (1964) 99, and references therein.
2 R.L. Martin, in E.A.V. Ebsworth, A.G. Maddock and A.G. Sharpe (Eds.), *New Pathways in Inorganic Chemistry*, Cambridge University Press, Cambridge, 1968, Chap. 9, and references therein.
3 E. Sinn, *Coordin. Chem. Rev.*, 4 (1969) 313.
4 R.E. Tapscott, R.L. Belford and I.C. Paul, *Coordin. Chem. Rev.*, 4 (1969) 323.
5 P.W. Ball, *Coordin. Chem. Rev.*, 4 (1969) 361.
6 G.F. Kokoszka and R.W. Duerst, *Coordin. Chem. Rev.*, 5 (1970) 209, and references therein.
7 G.F. Kokoszka and G. Gordon, *Transition Metal Chem.*, 5 (1969) 181, and references therein.
8 E.B. Fleischer, *Accounts Chem. Res.*, 3 (1970) 105.
9 (a) H.C. Freeman, *The Biochemistry of Copper*, in J. Peisach, P. Aisen and W.E. Blumberg (Eds.), Academic Press, New York, 1966, p. 35.
9 (b) H.C. Freeman and J.T. Szymanski, *Acta Crystallogr.*, 22 (1967) 406.
10 (a) M. Bonamico, G. Dessy, M. Mariani, A. Vaciago and L. Zambonelli, *Acta Crystallogr.*, 19 (1965) 619.
10 (b) M. Bonamico, G. Dessy, A. Mugnoli, A. Vaciago and L. Zambonelli, *Acta Crystallogr.*, 19 (1965) 886.
10 (c) M. Bonamico, G. Massone and L. Zambonelli, *Acta Crystallogr.*, 19 (1965) 899.
11 H.P. Klug, *Acta Crystallogr.*, 21 (1966) 536.
12 E. Sletten, *Acta Crystallogr., Sect. B*, 25 (1969) 1480.
13 E. Sletten, *Acta Crystallogr., Sect. B*, 26 (1970) 1609.
14 S. Scarnicar and B. Matkovic, *Chem. Commun.*, (1967) 297.
15 S. Scarnicar and B. Matkovic, *Acta Crystallogr., Sect. B*, 25 (1969) 2046.
16 D. Hall, A.J. McKinnon and T.N. Waters, *J. Chem. Soc. A*, (1964) 3290.
17 D. Hall, A.J. McKinnon and T.N. Waters, *J. Chem. Soc. A*, (1965) 425.
18 R.L. Belford, R.J. Missavage, I.C. Paul, N.D. Chasteen, W.E. Hatfield and J. Villa, *Chem. Commun.*, (1971) 508.
19 J.F. Villa and W.E. Hatfield, *Inorg. Chim. Acta*, 5 (1971) 145.
20 J.F. Villa and W.E. Hatfield, *Inorg. Chem.*, 10 (1971) 2038.
21 W.E. Hatfield, J.A. Barnes, D.Y. Jeter, R. Whyman and E.R. Jones, *J. Amer. Chem. Soc.*, 92 (1970) 4982.
22 J.F. Villa and W.E. Hatfield, *Inorg. Nucl. Chem. Lett.*, 6 (1970) 511.
23 D.J. Hodgson, P.K. Hale, J.A. Barnes and W.E. Hatfield, *Chem. Commun.*, (1970) 786.
24 G.O. Carlisle and W.E. Hatfield, *Inorg. Nucl. Chem. Lett.*, 6 (1970) 633.
25 L.E. Warren and W.E. Hatfield, *Chem. Phys. Lett.*, 7 (1970) 371.
26 J.A. Barnes, W.E. Hatfield and D.J. Hodgson, *Chem. Phys. Lett.*, 7 (1970) 374.
27 J.F. Villa, J.M. Flowers and W.E. Hatfield, *Spectrosc. Lett.*, 3 (1970) 201.

28 J.F. Villa and W.E. Hatfield, *Chem. Commun.*, (1971) 101.
29 J.F. Villa, M.M. Bursey and W.E. Hatfield, *Chem. Commun.*, (1971) 307.
30 D.Y. Jeter, W.E. Hatfield and D.J. Hodgson, *Inorg. Chim. Acta*, 5 (1971) 257.
31 J.A. Barnes, W.C. Barnes and W.E. Hatfield, *Inorg. Chim. Acta*, 5 (1971) 276.
32 D.J. Hodgson, P.K. Hale and W.E. Hatfield, *Inorg. Chem.*, 10 (1971) 1061.
33 N.T. Watkins, S.M. Horner, D.Y. Jeter and W.E. Hatfield, *Trans. Faraday Soc.*, 67 (1971) 2431.
34 J.F. Villa and W.E. Hatfield, *Chem. Phys. Lett.*, 9 (1971) 568.
35 W.E. Hatfield, *Inorg. Chem.*, 11 (1972) 216, and references therein.
36 W.E. Hatfield and J. Villa, *Inorg. Chem.*, 11 (1972) 1331.
37 B. Bleaney and K.D. Bowers, *Proc. Roy. Soc., Ser. A*, 214 (1952) 451.
38 R.H. Dunhill, J.R. Pilbrow and T.D. Smith, *J. Chem. Phys.*, 45 (1966) 1474.
39 J.F. Boas, R.H. Dunhill, J.R. Pilbrow, R.C. Srivastava and T.D. Smith, *J. Chem. Soc. A*, (1969) 94.
40 J.F. Boas, J.R. Pilbrow, C.R. Hartzell and T.D. Smith, *J. Chem. Soc. A*, (1969) 572.
41 J.F. Boas, J.R. Pilbrow and T.D. Smith, *J. Chem. Soc. A*, (1969) 721.
42 J.F. Boas, J.R. Pilbrow and T.D. Smith, *J. Chem. Soc. A*, (1969) 723.
43 J.F. Boas, J.R. Pilbrow, G.J. Troup, C. Moore and T.D. Smith, *J. Chem. Soc. A*, (1969) 965.
44 J.R. Pilbrow, A.D. Toy and T.D. Smith, *J. Chem. Soc. A*, (1969) 1029.
45 J.R. Pilbrow, S.G. Carr and T.D. Smith, *J. Chem. Soc. A*, (1970) 723.
46 J.H. Price, J.R. Pilbrow, K.S. Murray and T.D. Smith, *J. Chem. Soc. A*, (1970) 968.
47 J.R. Pilbrow, A.D. Toy and T.D. Smith, *Aust. J. Chem.*, 23 (1970) 2287.
48 P.D.W. Boyd, J.R. Pilbrow and T.D. Smith, *Aust. J. Chem.*, 24 (1971) 59.
49 T. Lund, J.R. Pilbrow and T.D. Smith, *J. Chem. Soc. A*, (1971) 2251.
50 R.C. Srivastava, T.D. Smith, J.F. Boas, T. Lund, J.H. Price and J.R. Pilbrow, *J. Chem. Soc. A*, (1971) 2538.
51 S.G. Carr, T.D. Smith and J.R. Pilbrow, *J. Chem. Soc. A*, (1971) 2569.
52 A.D. Toy, S.H.H. Chaston, J.R. Pilbrow and T.D. Smith, *Inorg. Chem.*, 10 (1971) 2219.
53 T. Lund, J.R. Pilbrow and T.D. Smith, *J. Chem. Soc. A*, (1971) 2786.
54 A.D. Toy, T.D. Smith and J.R. Pilbrow, *J. Chem. Soc. A*, (1971) 2925.
55 T.D. Smith, T. Lund, J.R. Pilbrow and J.H. Price, *J. Chem. Soc. A*, (1971) 2936.
56 P.D.W. Boyd, T.D. Smith, J.H. Price and J.R. Pilbrow, *J. Chem. Phys.*, 56 (1972) 1253.
57 W.E. Blumberg and J. Peisach, *J. Biol. Chem.*, 240 (1965) 870.
58 S.G. Carr, P.D.W. Boyd and T.D. Smith, *J. Chem. Soc. Dalton*, (1972) 1491.
59 A.D. Toy and T.D. Smith, *J. Amer. Chem. Soc.*, 93 (1971) 3049.
60 (a) P.D.W. Boyd, A.D. Toy, T.D. Smith and J.R. Pilbrow, *J. Chem. Soc. Dalton*, (1973) 1549.
60 (b) W.E. Hatfield and T. Lund, *J. Chem. Phys.* 59, (1973) 885.
61 N.D. Chasteen and R.L. Belford, *Inorg. Chem.*, 9 (1970) 169 (see also correction ibid. p. 2805).
62 A.E. Martell and T.D. Smith, *J. Amer. Chem. Soc.*, 94 (1972) 3029.
63 A.E. Martell and T.D. Smith, *J. Amer. Chem. Soc.*, 94 (1972) 4123.
64 A.J. Fatiadi, *J. Res. Nat. Bur. Stand., Sect. A*, 74 (1970) 723.
65 R.L. Belford, N.D. Chasteen, H. So and R.E. Tapscott, *J. Amer. Chem. Soc.*, 91 (1969) 4675.
66 J.H. van der Waals and M.S. de Groot, *Mol. Phys.*, 2 (1959) 333.
67 J.H. van der Waals and M.S. de Groot, *Mol. Phys.*, 3 (1960) 190.
68 P. Kottis and R. Lefebvre, *J. Chem. Phys.*, 39 (1963) 393.
69 P. Kottis and R. Lefebvre, *J. Chem. Phys.*, 41 (1964) 379.
70 E. Wasserman, L.C. Snyder and W.A. Yager, *J. Chem. Phys.*, 41 (1964) 1763.
71 R.H. Dunhill and T.D. Smith, *J. Chem. Soc. A*, (1969) 2189.
72 R.H. Dunhill and M.C.R. Symons, *Mol. Phys.*, 16 (1968) 105.
73 L.C. Dickinson, R.H. Dunhill and M.C.R. Symons, *J. Chem. Soc. A*, (1970) 922.
74 P.G. James and G.R. Luckhurst, *Mol. Phys.*, 18 (1970) 141.

75 D.M.S. Bagguley and J.H.E. Griffiths, *Nature (London)*, 162 (1948) 538.
76 D.M.S. Bagguley and J.H.E. Griffiths, *Proc. Roy. Soc. Ser. A*, 201 (1950) 366.
77 M.H.L. Pryce, *Nature (London)*, 162 (1948) 539.
78 K. Ono and M. Ohtsuka, *J. Phys. Soc. Jap.*, 13 (1958) 206.
79 A. Abragam and B. Bleaney, *Electron Paramagnetic Resonance of Transition Ions*, Oxford University Press, London, 1970, p. 9.6.
80 J.S. Leigh, *J. Chem. Phys.*, 52 (1970) 2608.
81 P. Erdös, *J. Phys. Chem. Solids*, 27 (1966) 1705.
82 H.P. Baltes, J.-F. Moser and F.K. Kneubühl, *Phys. Lett. A*, 24 (1967) 314.
83 H.P. Baltes, J.-F. Moser and F.K. Kneubühl, *J. Phys. Chem. Solids*, 28 (1967) 2635.
84 I.C. Ross, *Trans. Faraday Soc.*, 55 (1959) 1057.
85 I.G. Ross and J. Yates, *Trans. Faraday Soc.*, 55 (1959) 1064.
86 A. Abragam and B. Bleaney, *Electron Paramagnetic Resonance of Transition Ions*, Oxford University Press, London, 1970, p. 494.
87 J.M. Baker, *Rep. Progr. Phys.*, 34 (1971) 109.
88 R.K. Cowsik, G. Rangarajan and R. Srinivasan, *Chem. Phys. Lett.*, 8 (1971) 136.
89 E. Buluggiu, G. Dascola, D.C. Giori and V. Varacca, *Phys. Status Solidi B*, 45 (1971) 217.
90 J.H. Price, *Ph. D. Thesis*, Monash University, 1970.
91 P.D.W. Boyd, *Ph. D. Thesis*, Monash University, 1972.
92 J.R. Pilbrow and M.E. Winfield, *Mol. Phys.*, 25 (1973) 1073.
93 J.R. Pilbrow, *Mol. Phys.*, 16 (1969) 307.
94 F.D. Tsay, H.B. Gray and J. Danon, *J. Chem. Phys.*, 54 (1971) 3760.
95 L.D. Rollman and S.I. Chan, *J. Chem. Phys.*, 50 (1969) 3416.
96 J.N. van Niekerk and F.R.L. Shoening, *Acta Crystallogr.*, 6 (1953) 227.
97 B. Bleaney, *Rev. Mod. Phys.*, 25 (1953) 161.
98 S.G. Carr, *Ph. D. Thesis*, Monash University, 1973.
99 S.G. Carr, T.D. Smith and J.R. Pilbrow, *J. Chem. Soc. Faraday II*, (1974) 497.
100 J.R. Pilbrow, unpublished calculations.
101 N.L. Huang, R. Orbach, E. Simanek, J Owen and D.R. Taylor, *Phys. Rev.*, 156 (1967) 383.
102 R.W. Duerst and G.K. Kokoszka, *J. Chem. Phys.*, 51 (1969) 1673.
103 C.K. Prout, J.R. Carruthers and F.J.C. Rossotti, *J. Chem. Soc. A*, (1971) 3336.
104 D. Hall and T.N. Waters, *J. Chem. Soc.*, (1960) 2644.
105 H. Montgomery and B. Morosin, *Acta Crystallogr.*, 14 (1961) 551.
106 E.C. Lingafelter, G.L. Simmons, B. Morosin, C. Scheringer and C. Freiburg, *Acta Crystallogr.*, 14 (1961) 1222.
107 A.D. Toy, M.D. Hobday, P.D.W. Boyd, T.D. Smith and J.R. Pilbrow, *J. Chem. Soc. Dalton*, (1973) 1259.
108 E.N. Baker, D. Hall and T.N. Waters, *J. Chem. Soc. A*, (1970) 406.
109 E.N. Baker, D. Hall and T.N. Waters, *J. Chem. Soc. A*, (1970) 450.
110 (a) A.D. Toy, T.D. Smith and J.R. Pilbrow, *Aust. J. Chem.*, 26 (1973) 2349.
110 (b) E. Frasson, R. Bardi and S. Bezzi, *Acta Crystallogr.*, 12 (1959) 201.
110 (c) A. Vaciago and L. Zambonelli, *J. Chem. Soc. A*, (1970) 218.
111 R.E. Tapscott, R.L. Belford and I.C. Paul, *Inorg. Chem.*, 7 (1968) 356.
112 J.C. Forrest and C.K. Prout, *J. Chem. Soc. A*, (1967) 1312.
113 A.D. Toy, T.D. Smith and J.R. Pilbrow, *Aust. J. Chem.*, 27 (1974) 1.
114 T.A. Hamor, W.S. Caughey and J.L. Hoard, *J. Amer. Chem. Soc.*, 87 (1965) 2305.
115 R.J. Abraham, P.A. Burbridge, A.H. Jackson and D.B. MacDonald, *J. Chem. Soc. B*, (1966) 620.
116 D.A. Doughty and C.W. Dwiggins, *J. Phys. Chem.*, 73 (1969) 423.
117 (a) D.W. Urry, *J. Amer. Chem. Soc.*, 89 (1967) 4190.
117 (b) D.W. Urry, in B. Chance, R.W. Estabrook and T. Yonetani (eds.), *Hemes and Hemoproteins*, Academic Press, New York, 1966.
118 I. Tinoco, *J. Amer. Chem. Soc.*, 82 (1960) 4785; *J. Chem. Phys.*, 34 (1961) 1067.

119 W. Rhodes, *J. Amer. Chem. Soc.*, 83 (1961) 3609.
120 D.W. Urry and J.W. Pettegrew, *J. Amer. Chem. Soc.*, 89 (1967) 5276.
121 C. Houssier and K. Sauer, *J. Amer. Chem. Soc.*, 92 (1970) 779.
122 P.A. Loach and M. Calvin, *Biochemistry*, 2 (1963) 362.
123 A. MacCragh, C.B. Storm and W.S. Koski, *J. Amer. Chem. Soc.*, 87 (1965) 1470.
124 A.H. Jackson, G.W. Kenner and G.S. Sach, *J. Chem. Soc. C*, (1965) 2045.
125 W.S. Caughey, J.L. York and P.K. Iber, in A. Ehrenberg, B.C. Malmström and T. Vangard (Eds.), *Magnetic Resonance in Biological Systems*, Pergamon Press, Oxford, 1967.
126 W.S. Caughey, H. Eberspaecher, W.H. Fuchsman, S. McCoy and J.O. Alben, *Ann. N.Y. Acad. Sci.*, 153 (1969) 722.
127 R. Peterson and L. Alexander, *J. Amer. Chem. Soc.*, 90 (1968) 3873.
128 U. Ahrens and H. Kuhn, *Z. Phys. Chem. (Frankfurt am Main)*, 37 (1963) 1.
129 Z.A. Schelly, R.D. Farina and E.M. Eyring, *J. Phys. Chem.*, 74 (1970) 617.
130 Z.A. Schelly, D.J. Harward, P. Hemmes and E.M. Eyring, *J. Phys. Chem.*, 74 (1970) 3040.
131 E.A. Lucai, F.D. Verderane and G. Taddei, *J. Chem. Phys.*, 52 (1970) 2307.
132 P.D.W. Boyd and T.D. Smith, *J. Chem. Soc. A*, (1972) 839.
133 H. Sigel, P. Waldmeier and B. Prijs, *Inorg. Nucl. Chem. Lett.*, 7 (1971) 161.
134 K.K. Rohatgi and G.S. Singhai, *J. Phys. Chem.*, 70 (1966) 1695.
135 P. Mukerjee and A.K. Ghosh, *J. Amer. Chem. Soc.*, 92 (1970) 6419.
136 K.S. Rajan and A.E. Martell, *J. Inorg. Nucl. Chem.*, 29 (1967) 463.
137 J. Selbin, *Chem. Rev.*, 65 (1965) 153; *Coord. Chem. Rev.*, 1 (1966) 293.
138 B.M. Niklova and G.St. Nikolov, *J. Inorg. Nucl. Chem.*, 29 (1967) 1013.
139 R.E. Tapscott and R.L. Belford, *Inorg. Chem.*, 6 (1967) 735.
140 A. Hasegawa, Y. Yamata and M. Miuva, *Bull. Chem. Soc. Jap.*, 42 (1969) 846.
141 C.C. Parker, R.R. Reeder, L.B. Richards and P.H. Lieger, *J. Amer. Chem. Soc.*, 92 (1970) 5230.
142 R.S.P. Coutts and P.C. Wailes, *Advan. Organometal. Chem.*, 9 (1970) 135.
143 G.S. Kyker and E.P. Schraur, *Inorg. Chem.*, 8 (1969) 2306.
144 R.L. Martin and G. Winter, *J. Chem. Soc.*, (1965) 4709.
145 T.D. Smith, *J. Chem. Soc.*, (1965) 2145.
146 R.C. Srivastava and T.D. Smith, *J. Chem. Soc. A*, (1968) 2192.
147 T.W. Gilbert, L. Newman and P. Kolotz, *Anal. Chem.*, 45 (1966) 1474.
148 H.M.N. Irving and W.R. Tomlinson, *Chem. Commun.*, 9 (1968) 497.
149 W.W. Schultz, J.E. Wendel and J.F. Phillips, *J. Inorg. Nucl. Chem.*, 28 (1966) 2399.
150 B.S. Magor and T.D. Smith, *J. Chem. Soc. A*, (1968) 1753.
151 E.J. Durham and D.P. Ryskiewick, *J. Amer. Chem. Soc.*, 80 (1958) 4812.
152 J.H. Grimes, A.J. Huggerd and S.P. Wilford, *J. Inorg. Nucl. Chem.*, 25 (1963) 1225.
153 T.A. Bohigian and A.E. Martell, *Inorg. Chem.*, 4 (1965) 1264.
154 T.A. Bohigian and A.E. Martell, *J. Amer. Chem. Soc.*, 89 (1967) 832.
155 A. Yingst and A.E. Martell, *J. Amer. Chem. Soc.*, 91 (1969) 6927.
156 K.H. Schroder, *Acta Chem. Scand.*, 17 (1963) 1087; 19 (1965) 1347.
157 E. Jacobsen and E. Saetic, *Acta Chem. Scand.*, 19 (1965) 2291.
158 L. Harja, *Anal. Chim. Acta*, 50 (1970) 475.
159 B. Lee, *Inorg. Chem.*, 11 (1972) 1072.
160 R.G. Wilkins and R.E. Yelin, *J. Amer. Chem. Soc.*, 92 (1970) 1191.
161 S.G. Carr, P.D.W. Boyd and T.D. Smith, *J. Chem. Soc. Dalton*, (1972) 907.
162 D.J. Cookson, T.D. Smith and J.R. Pilbrow, *J. Chem. Soc. Dalton*, in press.
163 K.S. Bai and A.E. Martell, *J. Inorg. Nucl. Chem.*, 31 (1969) 1697.
164 H.C. Freeman, in J. Peisach, P. Aisen and W.E. Blumberg (Eds.), *The Biochemistry of Copper*, Academic Press, New York, 1966, p. 77.
165 W.L. Koltun, M. Fried and F.R.N. Gurd, *J. Amer. Chem. Soc.*, 82 (1960) 233.
166 H. Driver and W.R. Walker, *Aust. J. Chem.*, 21 (1968) 671.
167 H.C. Freeman and J.T. Szymanski, *Acta Crystallogr.*, 22 (1967) 406.

168 M. Ihnat and R. Bersohn, *Biochemistry*, 9 (1970) 4555.
169 A. Zuberbuhler and H.S. Mason, *Transition Metal Chem.*, 5 (1969) 187.
170 T. Huang and G.P. Haight, *J. Amer. Chem. Soc.*, 93 (1971) 611.
171 H.A. Kuska and M.T. Rogers, in E.T. Kaizer and L. Kevan (Eds.), *Radical Ions*, John Wiley, New York, 1968, p. 694.
172 S.E. Livingstone and R.S. Plowman, *J. Proc. Roy. Soc. N.S.W.*, 83 (1951) 116.
173 H. Petering and G.J. Geissen, in J. Peisach, P. Aisen and W.E. Blumberg (Eds.), *The Biochemistry of Copper*, Academic Press, New York, 1966, p. 197.
174 W.E. Blumberg and J. Peisach, *J. Chem. Phys.*, 49 (1968) 1793.
175 M.R. Taylor, E.J. Gabe, J.P. Glusker, J.A. Minkin and A.L. Patterson, *J. Amer. Chem. Soc.*, 88 (1966) 1945.
176 S.H.H. Chaston and S.E. Livingstone, *Aust. J. Chem.*, 20 (1967) 1065.
177 R.K.Y. Ho, S.E. Livingstone and T.N. Lockyer, *Aust. J. Chem.*, 19 (1966) 1179.
178 H. Gersmann and J.D. Swalen, *J. Chem. Phys.*, 36 (1962) 3221.
179 E.S. Shygam, L.M. Shkol'nikova and S.E. Livingstone, *J. Struct. Chem. (USSR)* 8 (1967) 490.
180 I.M. Klotz, G.H. Czerlinski and H.A. Fiess, *J. Amer. Chem. Soc.*, 80 (1958) 2920.
181 F. Ghivetti, in O. Hayaishi (Ed.), *Oxygenases*, Academic Press, New York, 1962, p. 137.
182 J.E. Mellema and A. Klug, *Nature (London)*, 239 (1972) 146.
183 A.J.M. Schoot Uiterkamp, *FEBS Lett.*, 20 (1972) 93.
184 A.J.M. Schoot Uiterkamp and H.S. Mason, *Proc. Nat. Acad. Sci. U.S.A.*, 70 (1973) 993.
185 F.X.R. van Leeuwen, R. Wever and B.F. van Gelde, *Biochim. Biophys. Acta*, 315 (1973) 200.
186 A.D. Toy, T.D. Smith and J.R. Pilbrow, *J. Chem. Soc. A*, (1970) 2600.